50272-101

REPORT DOCUMENTATION PAGE	1. REPORT NO. NCEER-94-0013	2.	PB95-181806

4. Title and Subtitle
Seismic Energy Based Fatigue Damage Analysis of Bridge Columns: Part II - Evaluation of Seismic Demand

5. Report Date
June 1, 1994

6.

7. Author(s)
G.A. Chang and J.B. Mander

8. Performing Organization Rept. No.

9. Performing Organization Name and Address
State University of New York at Buffalo
Department of Civil Engineering
Buffalo, New York 14260

10. Project/Task/Work Unit No.

11. Contract(C) or Grant(G) No.
(C) BCS 90-25010
NEC-91029
(G) DTFH61-92-C-00106

12. Sponsoring Organization Name and Address
National Center for Earthquake Engineering Research
State University of New York at Buffalo
Red Jacket Quadrangle
Buffalo, New York 14261

13. Type of Report & Period Covered
Technical Report

14.

15. Supplementary Notes
This research was conducted at the State University of New York at Buffalo and was partially supported by the Federal Highway Administration under contract number DTFH61-92-C-00106, the National Science Foundation under Grant No. BCS 90-25010 and the New York State Science and Technology Foundation under Grant No. NEC-91029.

16. Abstract (Limit: 200 words)
This is the second part of a two-part series on the Seismic Energy Based Fatigue Damage Analysis of Bridge Piers. This second part deals with the determination of energy and fatigue demands on bridge columns. A smooth asymmetric degrading hysteretic model is presented, capable of accurately simulating the behavior of bridge piers. The model parameters are determined automatically by using a system identification routine integrated into a computer program OPTIMA. The program can use either real experimental data or simulated experiment results from a reversed cyclic loading Fiber Element analysis. A SDOF inelastic dynamic analysis program was implemented capable of using different hysteretic models. Spectral results were produced by using the smooth model presented which had been calibrated with full-size bridge column experimental data to determine global parameters to simulate column behavior. Design recommendations regarding the assessment of fatigue energy are made based on the results obtained through the nonlinear dynamic analysis. A complete methodology of seismic evaluation of existing bridge structures is proposed, which incorporated the traditional strength and ductility aspects plus the fatigue energy demand. The relevance of fatigue aspects for the seismic design of new bridge structures is also demonstrated. It is shown that the present code use of force reduction factors, that are independent of natural period, are unconservative for short period stiff structures. Recommendations are made for force reduction factors to be used in fatigue resistant design.

17. Document Analysis a. Descriptors

b. Identifiers/Open-Ended Terms
Earthquake engineering. Reinforced concrete columns. Bridge piers. Energy demand. Fatigue damage analysis. Parametric identification. Fiber element analysis. Tension. Macroscopic models. Low cycle fatigue. Damage assessment. Cyclic strut-tie models. Reinforcing steel. Fracture models. Confined concrete. Unconfined concrete. Cyclic loads. Compression. Bilinear hysteretic models.

c. COSATI Field/Group

18. Availability Statement	19. Security Class (This Report)	21. No. of Pages
Release Unlimited	Unclassified	164
	20. Security Class (This Page)	22. Price
	Unclassified	

(See ANSI-Z39.18) See Instructions on Reverse OPTIONAL FORM 272 (4-77) (Formerly NTIS-35)

NATIONAL CENTER FOR EARTHQUAKE ENGINEERING RESEARCH

State University of New York at Buffalo

PB95-181806

Seismic Energy Based Fatigue Damage Analysis of Bridge Columns: Part II—Evaluation of Seismic Demand

by

G.A. Chang and J.B. Mander

State University of New York at Buffalo
Department of Civil Engineering
Buffalo, New York 14260

Technical Report NCEER-94-0013

June 1, 1994

This research was conducted at the State University of New York at Buffalo and was partially supported by the Federal Highway Administration under contract number DTFH61-92-C-00106, the National Science Foundation under Grant No. BCS 90-25010 and the New York State Science and Technology Foundation under Grant No. NEC-91029.

NOTICE

Seismic Energy Based Fatigue Damage Analysis of Bridge Columns: Part II - Evaluation of Seismic Demand

by

G.A. Chang[1] and J.B. Mander[2]

June 1, 1994

Technical Report NCEER-94-0013

NCEER Task Numbers 91-3412 and 10693-E-5.2

FHWA Contract Number DTFH61-92-C-00106

NSF Master Contract Number BCS 90-25010
and
NYSSTF Grant Number NEC-91029

1 Teaching Staff Professor, Department of Civil Engineering, Universidad Tecnológica de Panamá. Former Fullbright-LASPAU Scholar, Department of Civil Engineering, State University of New York at Buffalo
2 Assistant Professor, Department of Civil Engineering, State University of New York at Buffalo

NATIONAL CENTER FOR EARTHQUAKE ENGINEERING RESEARCH
State University of New York at Buffalo
Red Jacket Quadrangle, Buffalo, NY 14261

PREFACE

The National Center for Earthquake Engineering Research (NCEER) was established to expand and disseminate knowledge about earthquakes, improve earthquake-resistant design, and implement seismic hazard mitigation procedures to minimize loss of lives and property. The emphasis is on structures in the eastern and central United States and lifelines throughout the country that are found in zones of low, moderate, and high seismicity.

NCEER's research and implementation plan in years six through ten (1991-1996) comprises four interlocked elements, as shown in the figure below. Element I, Basic Research, is carried out to support projects in the Applied Research area. Element II, Applied Research, is the major focus of work for years six through ten. Element III, Demonstration Projects, have been planned to support Applied Research projects, and will be either case studies or regional studies. Element IV, Implementation, will result from activity in the four Applied Research projects, and from Demonstration Projects.

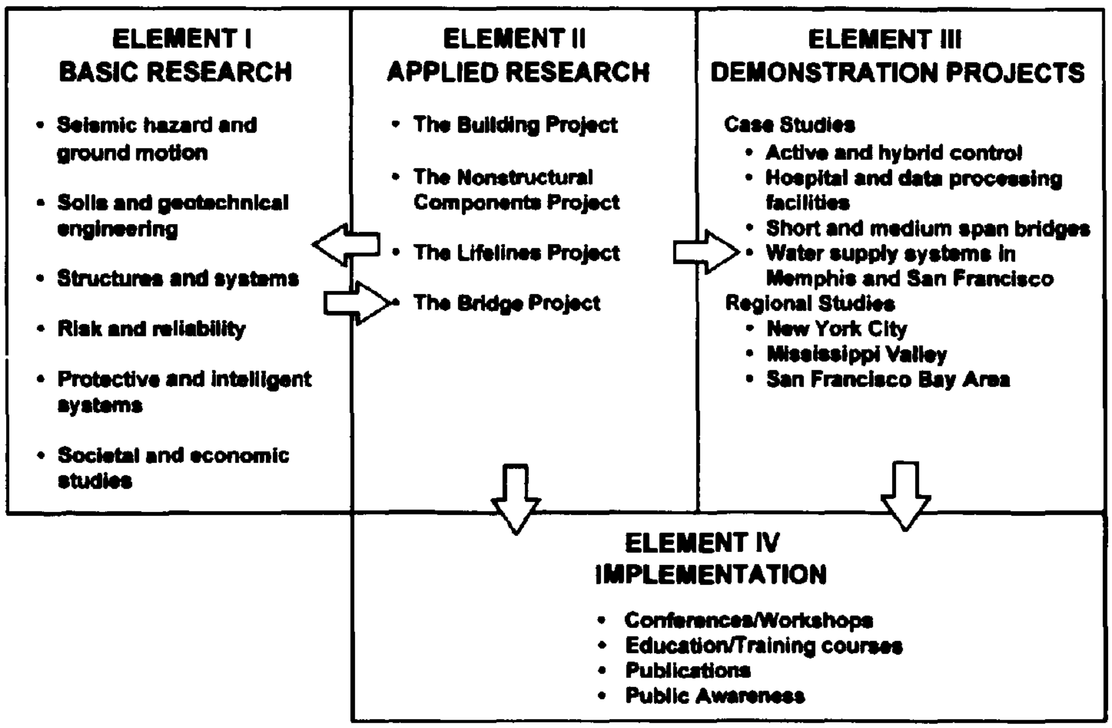

Research tasks in the **Bridge Project** expand current work in the retrofit of existing bridges and develop basic seismic design criteria for eastern bridges in low-to-moderate risk zones. This research parallels an extensive multi-year research program on the evaluation of gravity-load design concrete buildings. Specifically, tasks are being performed to:

Abstract

This is the second part of a two-part series on the Seismic Energy Based Fatigue Damage Analysis of Bridge Piers. The complete analysis methodology for determining the capacity bridge columns was developed starting from basic principles and presented in Part I. This second part deals with the determination of energy and fatigue demands on bridge columns.

A smooth asymmetric degrading hysteretic model is presented, capable of accurately simulating the behavior of bridge piers. The model parameters are determined automatically by using a system identification routine integrated into a computer program OPTIMA. The program can use either real experimental data or simulated experiment results from a reversed cyclic loading Fiber Element analysis.

A SDOF inelastic dynamic analysis program was implemented capable of using different hysteretic models. Spectral results were produced by using the smooth model presented which had been calibrated with full-size bridge column experimental data to determine global parameters to simulate column behavior. More traditional models were also used and some conclusions are presented regarding the significance of the analysis.

Design recommendations regarding the assessment of fatigue energy are made based on the results obtained through the nonlinear dynamic analysis. A complete methodology of seismic evaluation of existing bridge structures is proposed, which incorporated the traditional strength and ductility aspects plus the fatigue energy demand. The relevance of fatigue aspects for the seismic design of new bridge structures is also demonstrated. It is shown that the present code use of force reduction factors, that are independent of natural period, are unconservative for short period stiff structures. Recommendations are made for force reduction factors to be used in fatigue resistant design.

Acknowledgments

This research was conducted at the department of Civil Engineering of the State University of New York at Buffalo.

Special thanks to Professors Andrei M., Reinhorn, Ian G. Buckle and Peter Gergely.

The financial support of LASPAU and the Universidad Tecnológica de Panamá is deeply appreciated. The financial support of the National Center for Earthquake Engineering Research is also appreciated.

Table of Contents

List of Figures

List of Figures (cont'd)

List of Figures (cont'd)

Figure	Title	Page

Section 1

Introduction

1.1 Background

This is the second part of a two-part series on the Seismic Energy Based Fatigue Damage Analysis of Bridge Columns. Part I dealt with Evaluation of Seismic Capacity where constitutive models for concrete and steel were developed and integrated into a Fiber Element procedure to predict the hysteretic behavior of reinforced concrete columns. The Fiber Element program UB-COLA can also be used to determine quantitatively the amount of damage in both the confining steel and the longitudinal reinforcement. This quantitative evaluation of the amount of damage can be used as a post-processor to assess member suitability to a predefined time history.

This second part is concerned with the Evaluation of Seismic Demand. A comprehensive macro model is advanced, in which the hysteretic behavior of bridge columns is closely captured. This macro model is the basis for the formation of reliable inelastic energy and fatigue demands of bridge piers.

The *demand* on a structure can be of two types: displacement ductility demand and energy demand. The former dictates bearing set width requirements and secondary P-Δ load effects, while the latter leads to failure of the constituent materials, steel and concrete, through low cycle fatigue. It will subsequently be shown that the two are also interrelated. Much of the research effort had been concentrated on the ductility demand, although energy demand research is gaining popularity among researchers. The *capacity* of structural elements is, of course, a fundamental problem.

SEISMIC EVALUATION METHODOLOGY

Step 1. Strength Demand, C(d)

Step 2. Strength Capacity C(c) (Limit Analysis)

Step 3. $r_{ec} = \dfrac{C(c)}{C(d)} = \dfrac{1}{R_\mu}$ [If $r_{ec} \geq 1.5$ STOP]

↓

1st Order Ductility Based Analysis (SDOF)

Step 4.1 Ductility Demand $\mu(d)$

Step 5.1 Ductility Capacity $\mu(c)$ per ATC 6-2

Step 6.1 $r_\mu = \dfrac{\mu(c)}{\mu(d)}$ [If $r_\mu \geq 1.5$ STOP]

↓

2nd Order Energy Based Damage Analysis (SDOF)

Step 4.2 Rotational Demand *Section 4*

$\theta_p(d), N(d) = f(R_\mu, EQ, Hyst.model)$

Step 5.2 Rotational Capacity $\theta_p(c), N(c)$

Step 6.2 $r_N = \dfrac{N(c)}{N(d)}$ [If $r_N \geq 1.5$ STOP]

↓

3rd Order Time History Damage Analysis (MDOF)

Step 7. Generate Member Specific Hysteretic Models (From Steps 4.2 and 5.2) *Section 4*

Step 8. Perform Time History Analysis (IDARC or DRAIN-2DX)

Step 9. Examine Critical Members Performance. Use Fiber-Element to predict detailed behavior based on member time-history.

Fig. 1-1 Summary of Research Significance of this Study in the Context of a Seismic Evaluation Methodology.

1.4 Scope of Present Investigation

Firstly, this investigation deals with the modeling of the hysteretic and fracture characteristics of reinforcing steel (Part I, section 2). The low cycle fatigue behavior of steel is modeled based on experimental data. The importance of this modeling is that it allows the prediction of the fatigue life of longitudinal bars in the context of a reinforced concrete member subjected to cyclic loading. Such modeling will thus allow the prediction of failure of a structural concrete member due to low cycle fatigue, which is predominant on well detailed beams and columns with low levels of axial load. Numerous examples are presented to show the capacity of the model to simulate both the stress-strain cyclic behavior and the fatigue fracture.

Secondly, this investigation incorporates the modeling of the behavior of both confined and unconfined concrete subjected to cyclic compression and tension (Part I, section 3). This is the first time any model have attempted to model cyclic behavior of concrete in both tension and compression. The need for such model is more obvious when considering shear deformations where the tension capacity of reinforced steel plays an important role, as in the Modified Compression Field Theory (Collins and Mitchell, 1991), and the Softened Truss Model (Hsu, 1993).

Part I, Section 4 deals with the Fiber Elements modeling of the moment-curvature behavior of a concrete section and with the assessment of deformations. A cyclic strut-tie model is developed to assess shear deformations. This cyclic strut-tie model for shear deformation, which makes good use of the comprehensive constitutive models developed in sections 2 and 3 of Part I, allows to simulate the behavior of shear dominated members.

In this second part, Section 2 presents a modified bilinear version of the Takeda model which is employed to generate spectral responses. This model can simulate some other models commonly used, specifically: the elastic-perfectly plastic model, the bilinear model, the degrading Clough's model and the Q-hyst model (Saiidi, 1982). By using different parameters, the sensitivity of the hysteretic model may be studied.

In Section 3, a smooth rule-based hysteretic model is advanced which can accurately simulate cyclic behavior of bridge columns. An automated system identification technique is used to determine the most suitable set of parameters to simulate a given hysteretic behavior.

The model can used either experimental data or simulated results from the Fiber Element program to calibrate its parameters. It is shown that by using a Fiber Element simulation a good agreement is achieved with actual experimental data. In this approach the need for an experiment is eliminated, as well as the guessing of parameters, while a very close resemblance of actual member behavior is maintained.

Section 4 develops an inelastic SDOF dynamic analysis program to generate energy and fatigue demand. Spectra generated through the proposed procedure is believed to be a reliable assessment of energy demands on bridges.

Section 5 presents some design recommendations and shows the relevance of low cycle fatigue considerations in seismic design.

Finally, some general conclusions are drawn. Future research needs are also suggested. By using this rational approach some additional insight into the expected ductility and energy demands is gained.

Section 2

Piecewise Linear Hysteretic Models

2.1 Introduction

Early hysteretic models were generally in the form of rule-based piecewise linear models. Starting with the simplest form is the elastic-perfectly plastic model. The next level of sophistication is the bilinear model. Both of these models are unable to reflect either the Bauschinger effect in steel or softening in cracked reinforced concrete. Thus more sophisticated models were invented to reflect such behavior such as the smooth Ramberg-Osgood model (1943) and Clough's (1966) degrading stiffness model, respectively. These models, although somewhat more accurate than either the elastic-perfectly plastic or bilinear models, lacked the refinement necessary to capture the idiosyncrasies of steel and/or structural cracked behavior.

Takeda et al. (1970) proposed a trilinear model to simulate the behavior of reinforced concrete members under cyclic loading. This model, which is capable of modeling quite well the nonlinear behavior of reinforced concrete, has become one of the most popular piecewise linear models in use. Mander et al. (1984) introduced a modified bilinear version of this model that for certain values of its parameters could emulate some other known models, specifically: the elasto-perfectly plastic model, the bilinear model, Clough's degrading stiffness model (1966) and the Q-hyst model (Saiidi, 1982). In this section further modifications will be introduced to give it a better capability to represent local cyclic behavior.

2.2 Description of the Model

The model used herein is symmetric for the purpose of developing inelastic response spectra, thus the strength characteristics are defined by the yield point. The model has only three control parameters α, β and γ. This makes 5 the total number of parameters that define the behavior of the whole hysteretic behavior of the model.

The parameter α is related to the unloading stiffness which is defined as:

$$K_{un} = K_e\left(\frac{X_{max}}{x_y}\right)^{\alpha} \quad \textbf{(2-1)}$$

in which

$$X_{max} = \max\{|x_{max}|, |x_{min}|\} \geq x_y \quad \textbf{(2-2)}$$

where K_{un} = unloading stiffness, K_e = elastic stiffness, x_{max} = maximum excursion into the positive yielded zone, x_{min} = maximum excursion into the negative yielded zone and x_y = yield deformation.

The parameter β controls the reloading point, which in turn controls the size of the hysteretic loops, this is shown in Fig. 2-1a. This reloading point is a function of the maximum deformation so that,

$$x_{re}^{+} = x_{max}(1-\beta) \quad \textbf{(2-3a)}$$

or

$$x_{re}^{-} = x_{min}(1-\beta) \quad \textbf{(2-3b)}$$

Finally, the parameter γ controls the post yielding stiffness which is given by,

$$K_{py} = \gamma K_e \quad \textbf{(2-4)}$$

2.2.1 Envelope Curves

The positive envelope curve is a bilinear function composed of two rules: rule 1 and rule 3. Similarly the negative envelope curve is composed of rules 2 and 4 as shown in Fig. 2-1a.

Rule 1 : is the elastic loading rule, which changes to rule 3 when reaches the yielding point or to rule 2 when a reversal occurs. In this model a unique rule number was chosen to make the description of the rules unambiguous. The number of rules might look overwhelming, but at the time of implementation it makes it very simple to have unique rule definitions for every situation.

Rule 3 : is the post-yielding loading rule, which has the post-yielding stiffness given by Eq. 2-4.

Rules 2 and 4 : are analogous to rules 1 and 3 for the negative envelope curve. In general, every rule definition has an analogous counterpart for the opposite direction. The numbering was defined in such a way that every odd number rule has a complementary even number rule defined by adding one, this means the complementary rule for rule 13 is rule 14.

The rule system is illustrated in Fig. 2-1 and 2-2, and the whole rule flow is pictured in Fig. 2-3.

2.2.2 Connecting Curves

The negative connecting curve is composed of three rules: rule 5, rule 7 and rule 11. Similarly, the positive connecting curve is composed of rules 6, 8 and 12, as shown in Fig. 2-1a.

Rule 5 : when a reversal from rule 3 takes place from point ***M*** as shown in Fig. 2-1a, point ***P*** is targeted with and unloading stiffness as given by Eq. 2-1.

Rule 7 : when point ***P*** has been reached, rule 5 changes to rule 7 with a target point ***Q***, as shown in Fig. 2-1a, which is computed by Eq. 2-3.

Rule 9 : in the case of an incomplete unloading in rule 5, point ***M*** is targeted again and rule 5 changes to rule 9. The rule flow given in Fig. 2-3 shows that a reversal from rule 5 goes to rule 9 and a change in rule by passing the target point goes to rule 7; this is illustrated graphically in Fig. 2-1a.

Rule 11 : once the point ***Q*** has been reached, rule 7 changes to rule 11. Although rule 11 has the same properties of rule 4, it is called a different number because the cycle is not complete until it reaches point ***N***, as shown in Fig. 2-1a.

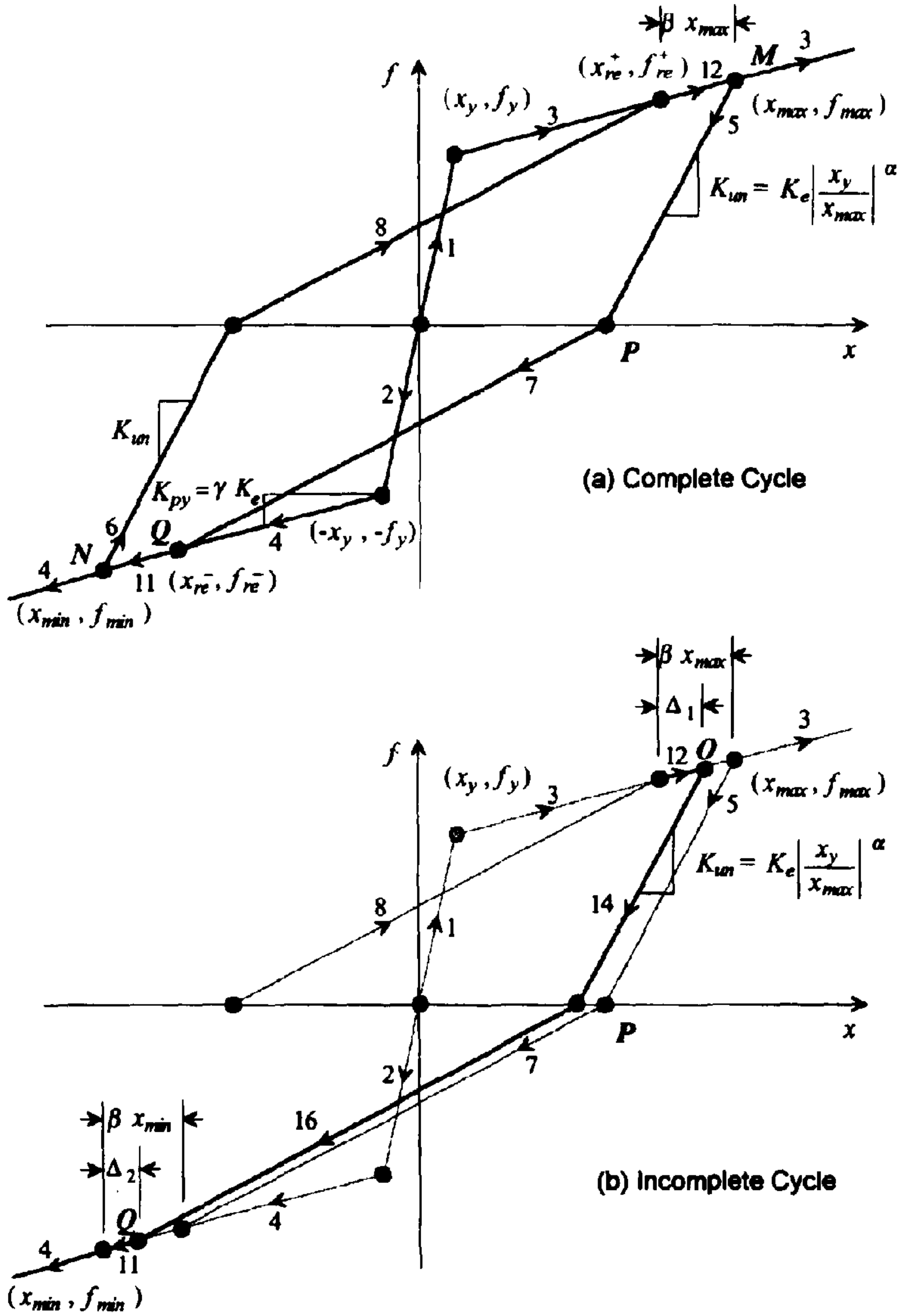

Fig. 2-1 Modified Takeda Model Under Complete and Incomplete Cycling

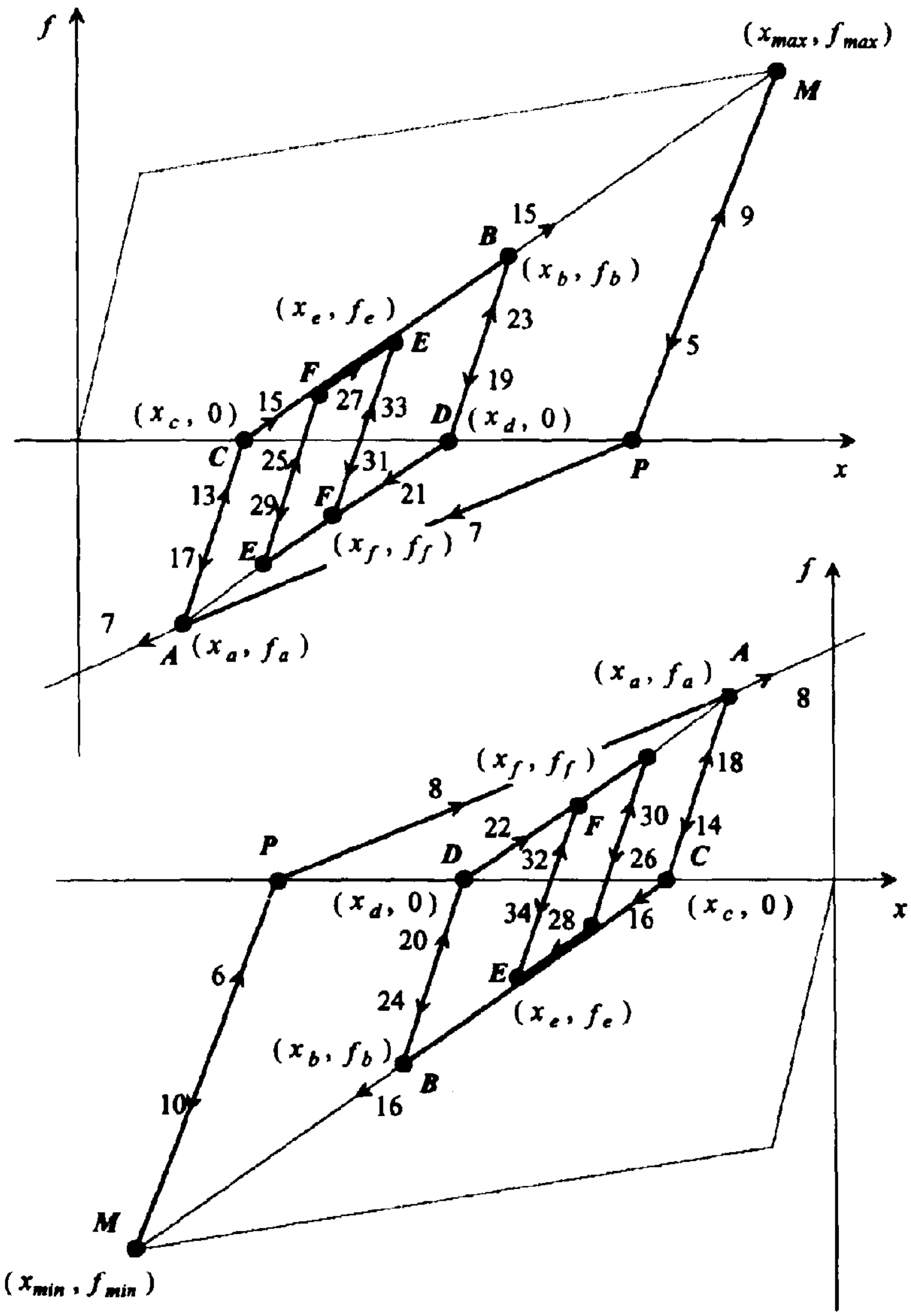

Fig. 2-2 Modifications for Local Cycling

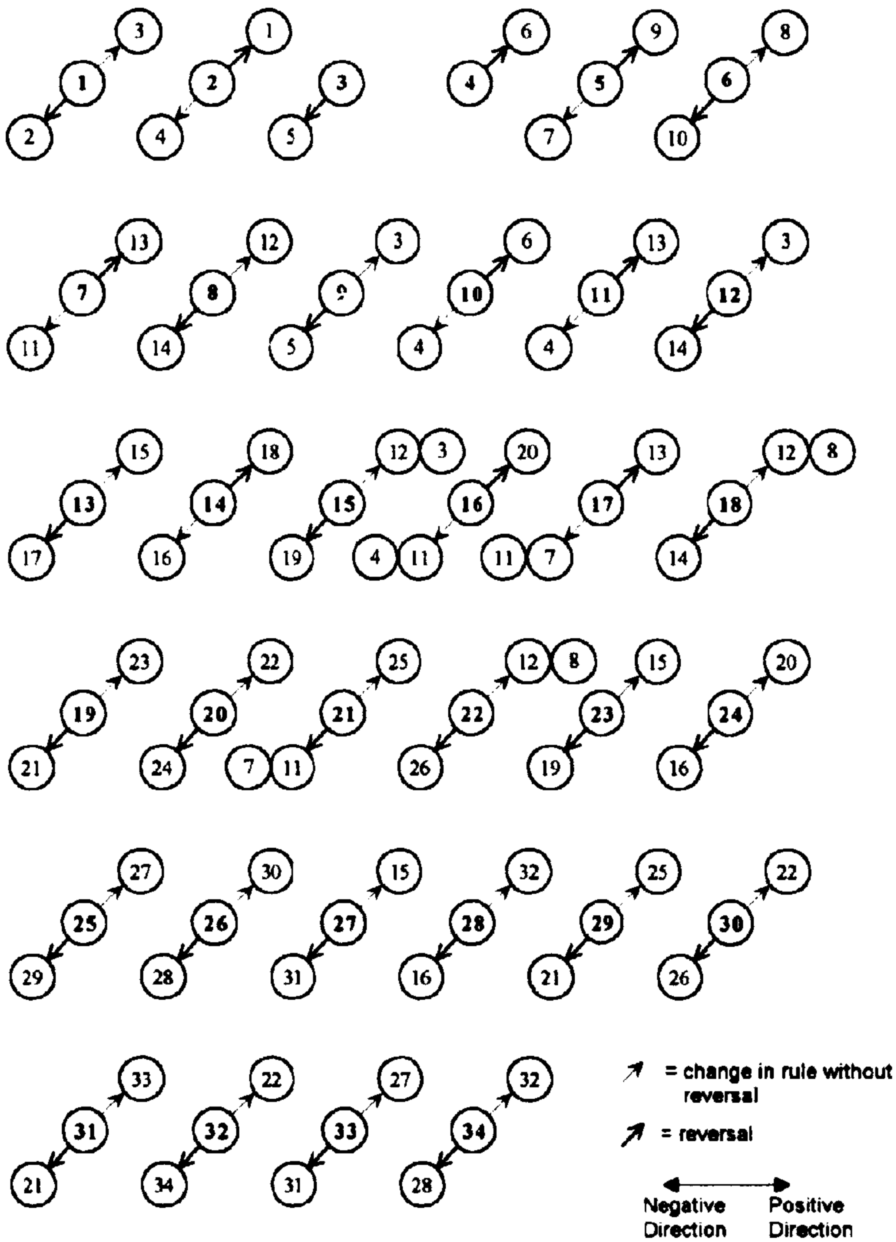

Fig. 2-3 Rule Flow Diagram for the Modified Takeda Model

2.2.3 Incomplete Cycles

If the maximum point (x_{max}, f_{max}) is not reached while in rule 12, and a reversal takes place, rule 12 changes to rule 14, as illustrated in Fig. 2-1b. In this case an incomplete cycle has occurred and point Q needs to be located between the returning point (x_{re}^{-}, f_{re}^{-}) and the minimum point (x_{min}, f_{min}). Should the reversal have taken place at the maximum point, point Q coincides with the returning point. While at the other extreme, should the reversal take place from the positive returning point (x_{re}^{+}, f_{re}^{+}), the target point Q is the minimum point (x_{min}, f_{min}). Any case in between, can be modeled by a proportion as:

$$\Delta_2 = \Delta_1 \frac{x_{min}}{x_{max}} \tag{2-5}$$

where Δ_1 and Δ_2 are shown in Fig. 2-2.

2.2.4 Local Cycling

Local cycling is not a secondary phenomena. During the random excitations of an earthquake motion, a hysteretic model needs to cater for all kinds of reversals. Normally an earthquake input increases in magnitude until it reaches a maximum. Following the time when the maximum response has been achieved, the structure continues vibrating mostly on smaller cycles that constitute local cycling. If a good estimate is to be made of the hysteretic energy, the local cycling behavior becomes a relevant issue. Most experiments are performed at increasingly levels of ductility, and the hysteretic behavior for complete cycles can be successfully modeled, as in the previous section. The nature of local cycling is based, nevertheless, on speculative basis to make it compatible with the overall hysteretic behavior. A deeper study into the nature of local cycling is needed to base its modeling on a more experimental basis.

Fig. 2-2 illustrates the modeling of local cycling behavior. At the reversal from rule 7, point A is defined. This point also defines point C, as the unloading is done with the unloading stiffness K_{un} given by Eq. 2-3. The unloading is represented by rule 13, and when point C is reached it changes to rule 15 which targets the maximum point. A reversal on rule

15 defines point ***B*** and therefore point ***D*** and thus every local cycling is performed within the boundaries defined by points ***A***, ***C***, ***B*** and ***D***, as shown in Fig. 2-2.

2.3 Model Parameters

This model can be used to represent the behavior of some well known models.

(a) Elasto-Perfectly Plastic Model	$\alpha = 0$	$\beta = 1$	$\gamma = 0$
(b) Bilinear Model	$\alpha = 0$	$\beta = 1$	$\gamma \neq 0$
(c) Clough's Degrading Stiffness Model	$\alpha = 0$	$\beta = 0$	$\gamma = 0$
(d) Q-hyst Model (Saiidi, 1982)	$\alpha = 0.5$	$\beta = 0$	$\gamma = 0.1$

Mander et al. (1984) found that values of $\alpha = 0.5$, $\beta = 0.3$ and $\gamma = 0.03$ provided the best overall fit to the experimental hysteresis loops of circular, square and hollow bridge columns. These values will be adopted in the Section 4 as typical values for bridge columns for the purpose of generating inelastic response spectra.

2.4 Conclusions

In this section a modified version of the Takeda model has been presented, with further modifications for local cycling. Typical model parameters calibrated with full-size column experiments by Mander et al. (1984) were adopted.

Section 3

Smooth Assymetric Degrading Hysteretic Model with Parameter Identification

3.1 Introduction

The analytical description of the behavior of reinforced concrete structural elements subjected to inelastic cyclic behavior usually requires lengthy computations. Both the steel and the concrete have non-linear hysteretic behavior, so the behavior of structural reinforced and prestressed concrete elements will reflect the non-linearities of the constituent materials. In the context of dynamic time-history analysis programs, macro-models tend to be the preferred approach used to simulate the hysteretic behavior of individual elements. These models try to simulate a hysteretic behavior, without the more cumbersome calculations that might be involved in modeling this behavior through either a finite element or a fiber model approach. Most macro models use one of two methods to simulate a hysteretic response: (1) Differential Equations, such as the Bouc-Wen Model, Wen (1975); (2) Piecewise linear rules, such as the well known elasto-perfectly plastic, bilinear, Clough's degrading stiffness model and various forms of the Takeda model (Saiidi, 1982). The first class of macro model is relatively easy to implement, but may require the identification of a number of hysteretic and monotonic control parameters. However, such models also tend to show instabilities under certain partial reversal situations. The second class of models that are based on piecewise linear rules may be harder to implement and maintain the bookkeeping controls, but they can be designed to be stable and flexible. The model presented herein belongs to this second category, but has been enhanced by using continuous smooth curves. This is to more realistically reflect real behavior of structural concrete elements. The approach also has the advantage of minimizing numerical overshoot, because the stiffness is changing gradually rather than suddenly as for linearized models.

In what follows, a smooth macro model is presented for the mathematical simulation of hysteretic behavior of structural concrete elements. This macro model is based on the Three Parameter Model suggested by Park et al. (1987), which has been further refined to better simulate experimental hysteretic behavior. A FORTRAN subroutine (DICHMDL) for displacement controlled input is developed. An optimization routine for the identification of the model's control parameters which may use experimental or fiber-element analyses input is also presented in this chapter. Finally, a FORTRAN program (OPTIMA) which implements the optimization routine (based on Press et al., 1992) and the macro model was implemented.

3.2 A Smooth Curve to Fit Two Tangents

It is necessary to adopt a suitable function which can be used to smooth a piecewise linear system. Herein the modified Menegotto and Pinto relation (Mander et al., 1984), described below is used in the model to simulate a smooth behavior. This curve essentially joins two tangents together with the curve radii controlled by a single parameter, *R*. At every change in rule three points are identified and a smooth curve is used to make the transition from the starting point to the ending point. The middle point represents the intersection of the tangents at the initial and ending point.

3.2.1 The Menegotto-Pinto Equation

The Menegotto-Pinto equation is expressed in terms of general coordinates and its shown in Fig. 3-1 as:

$$F = F_o + S_o(u - u_o)\left\{ Q + \frac{1-Q}{\left[1 + \left|S_o \frac{u-u_o}{F_{ch}-F_o}\right|^R\right]^{\frac{1}{R}}} \right\} \qquad \textbf{(3-1)}$$

The tangent at any point is given by:

$$S_t = \frac{\partial F}{\partial u} = S_o \left\{ Q - \frac{1-Q}{\left[1 + \left| S_o \frac{u - u_o}{F_{ch} - F_o} \right|^R \right]^{\frac{R+1}{R}}} \right\} \tag{3-2}$$

where F = ordinate, u = abscissa, F_o = initial ordinate, u_o = origin abscissa, S_o = initial slope, F_{ch} = characteristic (yield) ordinate, Q = the post-yielding slope ratio and R = radius of curvature parameter.

It should be noted that for computational tractability R has to be limited to about 25. This essentially represents a bilinear curve given by a single equation. To use this equation it is necessary to develop an algorithm to compute the parameters Q, F_{ch} and R. A procedure to compute these parameters is presented in the next section.

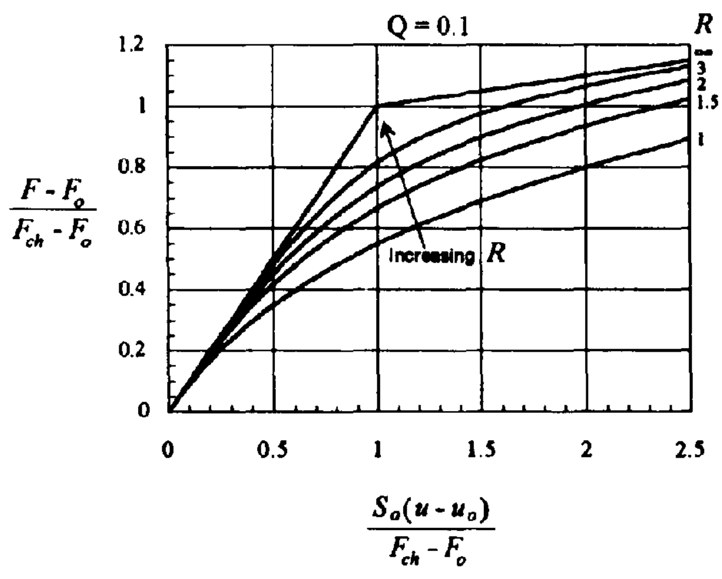

Fig. 3-1 The Menegotto-Pinto Equation

3.2.2 Computation of parameters Q, F_{ch} and R.

By taking A as:

$$A = \left[1 + \left| S_o \frac{u - u_o}{F_{ch} - F_o} \right|^R \right]^{\frac{1}{R}} \tag{3-3}$$

The derivative of A can be found to be:

$$\frac{dA}{du} = \frac{A(1 - A^{-R})}{u - u_o} \tag{3-4}$$

Equation (3-1) can be expressed in terms of A as:

$$F = F_o + S_o(u - u_o)\left(Q + \frac{1-Q}{A}\right) \tag{3-5}$$

with the derivative of F respect to u being:

$$S_t = \frac{dF}{du} = S_o\left(Q + \frac{1-Q}{A}\right) - S_o\frac{1-Q}{A}\left(\frac{u-u_o}{A}\frac{dA}{du}\right) \tag{3-6}$$

By substituting equations (3-4) into (3-6) and rearranging:

$$\frac{S_t}{S_o} = Q + \frac{(1-Q)}{A^{R+1}} \tag{3-7}$$

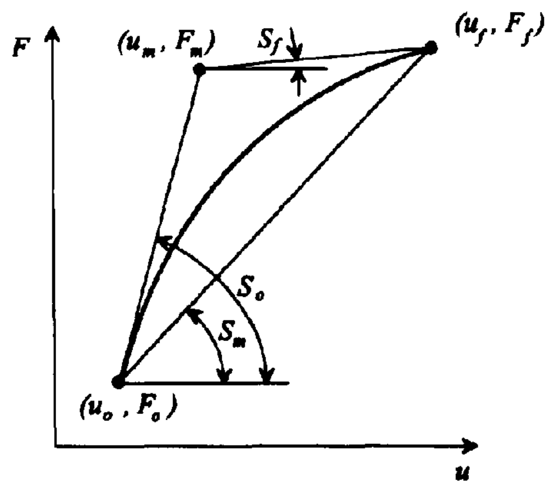

Fig. 3-2 Computation of Parameters for the M-P equation

By evaluating equation (3-7) at $u = u_f$, and solving for Q,

$$Q = \frac{\frac{S_f}{S_o} - A^{-(R+1)}}{1 - A^{-(R+1)}} \tag{3-8}$$

Solving for Q in equation (3-5),

$$Q = \frac{\frac{S_{sec}}{S_o} - A^{-1}}{1 - A^{-1}} \tag{3-9}$$

where:

$$S_{sec} = \frac{F_f - F_o}{u_f - u_o} \tag{3-10}$$

Equation (3-8) was obtained from an equation related to the final slope (S_f), thus this equation guarantees that at the final point the slope condition is met $S(u_f) = S_f$. Equation (3-9) was derived from an ordinate equation, thus by satisfying this equation, the ordinate condition is met $F(u_f) = F_f$. To satisfy both conditions, it is needed to equate both equations.

$$S_f - S_{sec}\frac{1 - a^{R+1}}{1 - a} + S_o\frac{a(1 - a^R)}{1 - a} = 0 \tag{3-11}$$

where $a = A^{-1}$.

Suppose that the three points (u_o, F_o), (u_m, F_m) and (u_f, F_f) are given, it is necessary to compute the values of Q, f_{ch} and R so that the M-P equation passes through the point (u_f, F_f) and that the initial and ending tangents intersect at (u_m, F_m) as shown in Fig. 3-2. The solution procedure is as follows:

(1) Compute the initial slope $S_o = \dfrac{F_m - F_o}{u_m - u_o}$

(2) Compute the final slope $S_f = \dfrac{F_f - F_m}{u_f - u_m}$

(3) Compute the secant slope $S_m = \dfrac{F_f - F_o}{u_f - u_o}$

(4) Compute the critical value of R as, $R_{min} = \dfrac{S_f - S_m}{S_m - S_o}$

(5) If $R_{min} = 0$, it means that the three points are aligned, thus take $Q = 1$, $S_o = S_m$ and $F_{ch} = F_f$. The value of R need not to be modified.

(6) If $R \le R_{\min}$ then take $R = R_{\min} + 0.01$

(7) Solve for the value of a in the following expression:

$$S_f - S_{sec}\frac{1-a^{R+1}}{1-a} + S_o\frac{a(1-a^R)}{1-a} = 0 \qquad \textbf{(3-12)}$$

To find the value of a the following procedure is used:

(a) Define a function $f(a)$ as:

$$f(a) = S_f - S_{sec}\frac{1-a^{R+1}}{1-a} + S_o\frac{a(1-a^R)}{1-a} \qquad \textbf{(3-13)}$$

(b) Evaluate $f(1\text{-}\varepsilon)$ and $f(\varepsilon)$, where ε is a small value (≈ 0.01).

(c) If $f(1\text{-}\varepsilon) * f(\varepsilon) > 0$, decrease the value of e and repeat step (b).

(d) If $f(1\text{-}\varepsilon)*f(\varepsilon) \le 0$ then a solution is found in this interval. The quadratically converging Newton-Raphson procedure will be used to find the solution.

(e) Take as an initial estimate:

$$a_o = \frac{R_{\min}}{R} \qquad \textbf{(3-14)}$$

(f) If $f(a_o) * f(1-\varepsilon) < 0$ then replace a_o by $\sqrt{a_o}$ until inequality is false. This is to ensure proper convergence, if this condition is not met the algorithm will find a solution outside the meaningful range.

(g) With a_o as an initial estimate the following recursive expression should be applied until convergence is met. It is important to note that the function $f(a)$ has a singularity at a = 1, so the value of Δa should be the smaller of $0.5(1 - a_o)$ and 0.001.

$$a_{i+1} = a_i - \frac{2f(a_i)\Delta a}{f(a_i+\Delta a) - f(a_i - \Delta a)} \qquad \textbf{(3-15)}$$

(8) After the value of a has been defined then,

$$b = \frac{(1-a^R)^{\frac{1}{R}}}{a} \qquad \textbf{(3-16)}$$

(9) The values of f_{ch} and Q are then calculated as:

$$f_{ch} = f_o + \frac{E_o}{b}(\varepsilon_f - \varepsilon_o) \qquad \textbf{(3-17)}$$

$$Q = \frac{\frac{S_m}{S_o} - a}{1-a} \qquad \textbf{(3-18)}$$

3.3 Description of Smooth Hysteretic Model

The model has 32 control parameters that completely defines a general asymmetric response. For a system with equal forward and reverse strengths only 18 control parameters are needed (eight of which are for monotonic, the rest for cyclic control), because most of the parameters defined for the positive side have a counterpart in the negative side. The model has either loading or unloading curves composed of three basic types: (1) envelope curves, (2) reverse curves and (3) transition curves. Each of these curves is defined in the following sections.

3.3.1 Monotonic Envelope Curves

Forward Monotonic Envelope Curve

The forward monotonic envelope curve is composed of branches 1 and 2 as shown in Fig. 3-3. Branch 1 begins at the origin, ends at (u_{o2}, F_{o2}) and its middle point is (u_c^+, F_c^+). Any branch is defined by three points: a starting point, an ending point and a middle point that represent the intersection of the initial and ending tangents.

The point (u_{o2}, F_{o2}) is defined through the proportionality factor k_1^+ in the following way:

$$u_{o2} = (1 - k_1^+)u_c^+ + k_1^+ u_y^+ \qquad \textbf{(3-19)}$$

$$F_{o2} = (1 - k_1^+)F_c^+ + k_1^+ F_y^+ \qquad \textbf{(3-20)}$$

Branch 2 starts at (u_{o2}, F_{o2}), ends at (u_u^+, F_u^+) and its middle point is (u_y^+, F_y^+). The initial envelope loading curve stiffness is calculated as:

$$S_1^+ = \frac{F_c^+}{u_c^+} \qquad \textbf{(3-21)}$$

The model parameters related to the envelope loading curve are seven: u_c^+, F_c^+, u_y^+, F_y^+, u_u^+, F_u^+ and k_1^+. Here u and F are displacement and force with subscripts c, y and u denoting cracking, yield and ultimate points respectively.

Reverse Monotonic Envelope Curve

Similarly, the reverse monotonic envelope curve is formed by branches 1 and 3 (Fig. 3-3). Branch 1 starts at the origin, ends at (u_{o3}, F_{o3}) and its middle point is (u_c^-, F_c^-).

The proportionality factor k_1^- is used to locate the point (u_{o3}, F_{o3}) between (u_c^-, F_c^-) and (u_y^-, F_y^-).

$$u_{o3} = (1 - k_1^-)u_c^- + k_1^- u_y^- \quad \textbf{(3-22)}$$

$$F_{o3} = (1 - k_1^-)F_c^- + k_1^- F_y^- \quad \textbf{(3-23)}$$

Branch 3 starts at (u_{o3}, F_{o3}), ends at (u_u^-, F_u^-) and its middle point is (u_y^-, F_y^-). The initial stiffness for the unloading curve is then:

$$S_1^- = \frac{F_c^-}{u_c^-} \quad \textbf{(3-24)}$$

The model parameters related to the reverse monotonic envelope curve are seven: u_c^-, F_c^-, u_y^-, F_y^-, u_u^-, F_u^- and k_1^-.

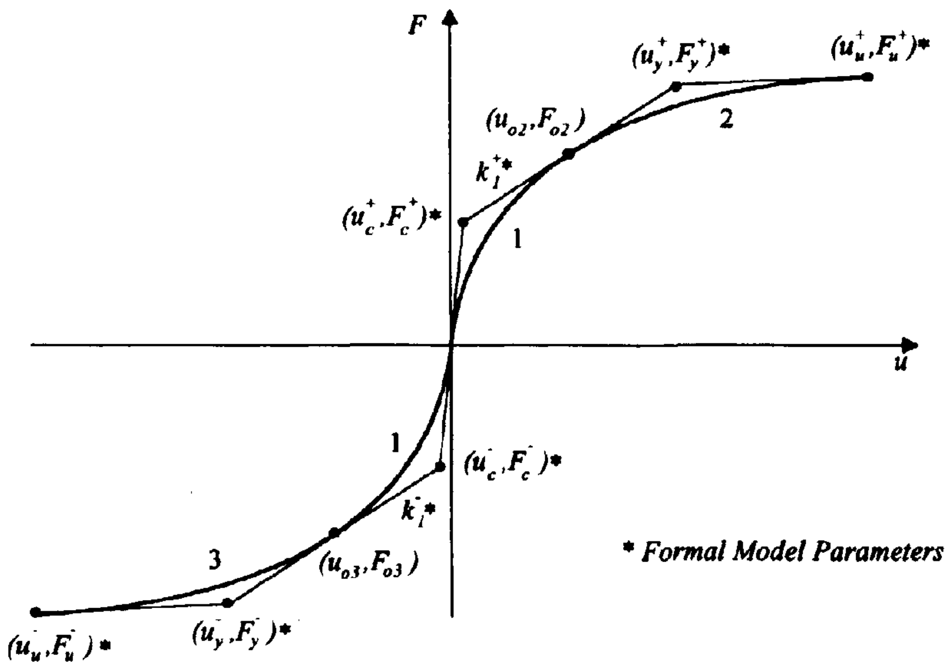

Fig. 3-3 Monotonic Envelope Curves

3.3.2 Reverse Curves

Reverse Loading Curve

The reverse loading curve is composed of three branches 5, 13 and 9 (Fig. 3-4). Curve **5** is formed by the points A, B and C. Point **A** is the point of reversal on the envelope unloading curve, and it defines the minimum or most negative excursion. Point **h** is a fixed point defined over the projection of the initial positive elastic tangent with coordinate $(\alpha^+ u_c^+, \alpha^+ F_c^+)$. Point **B** is defined by the intersection of the line joining points A and h with a line which slope is $\beta^- S_1^-$ and passes through the origin.

The reverse loading initial stiffness is:

$$S_R^+ = \frac{\alpha^+ F_c^+ - F_A^+}{\alpha^+ u_c^+ - u_A^+} \tag{3-25}$$

$$u_B^+ = u_s^- = \frac{S_R^+ u_A^+ - F_A^+}{S_R^+ - \beta^- S_1^-} \tag{3-26}$$

$$F_B^+ = \beta^- S_1^- u_B^+ \tag{3-27}$$

Point i has a fixed coordinate $(\gamma^+ u_c^+, \gamma^+ F_c^+)$ while point j has a variable coordinate $(u_s^+, \gamma^+ F_c^+)$, where u_s^+ is calculated from the last reverse unloading curve. Point **D** is located through the proportionality factor k_3^+ between points i and j.

$$u_D^+ = u_i^+(1 - k_3^+) + u_j^+ k_3^+ = \gamma^+ u_c^+(1 - k_3^+) + u_s^+ k_3^+ \tag{3-28}$$

Point **C** is located through the proportionality factor k_2^+ between points B and D. There are eight proportionality factors used in the model, four for the forward direction and four for the reverse direction.

$$u_C^+ = u_B^+(1 - k_2^+) + u_D^+ k_2^+ \tag{3-29}$$

$$F_C^+ = F_B^+(1 - k_2^+) + \gamma^+ F_c^+ k_2^+ \tag{3-30}$$

Point F is located on the envelope loading curve and it has a value that depends on the maximum positive excursion and a degrading factor k_5^+. Point **E** is then placed between points D and F by using the proportionality factor k_4^+. Finally, point G is calculated by amplifying the degrading factor k_5^+ by a factor r_{jn}.

$$u_F^+ = u_{\max}^+\left(1 + k_5^+\frac{D_u^+}{u_c^+ - u_c^-}\right) \tag{3-31}$$

$$u_E^+ = (1 - k_4^+)u_D^+ + k_4^+u_F^+ \tag{3-32}$$

$$F_E^+ = (1 - k_4^+)F_D^+ + k_4^+F_F^+ \tag{3-33}$$

$$u_G^+ = u_{\max}\left(1 + r_{jn}k_5^+\frac{D_u^+}{u_c^+ - u_c^-}\right) \tag{3-34}$$

where D_u^+ is the total unloading displacement since the last reversal from the envelope loading curve. Branch 9 is then formed by the points E, F and G. The ordinate for both

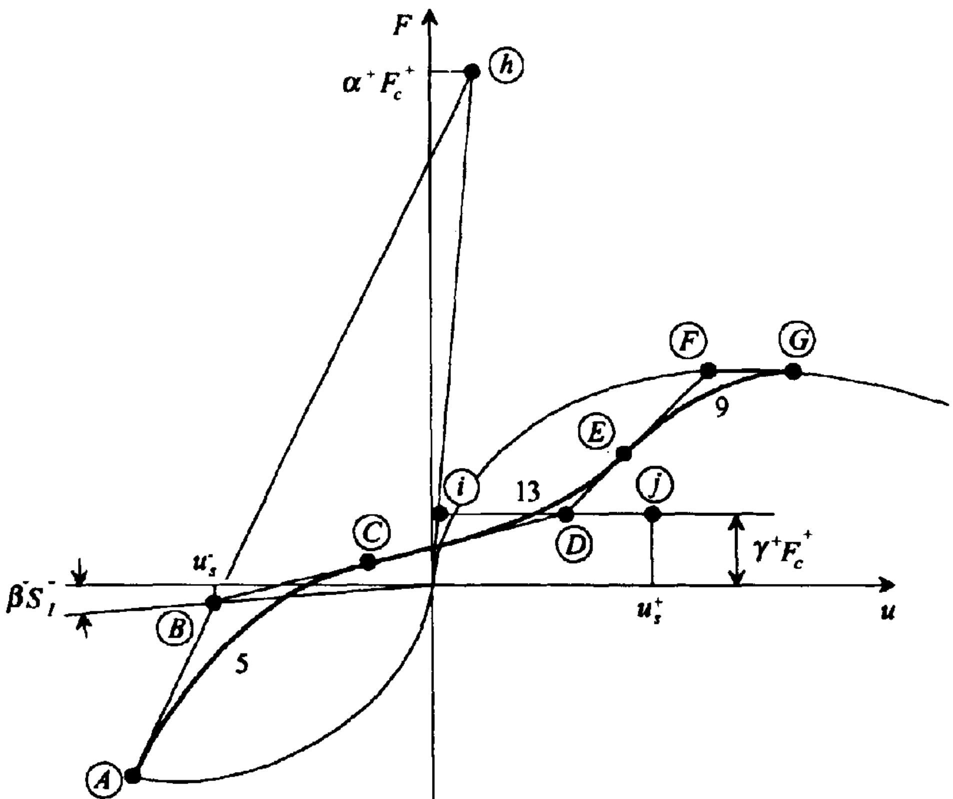

Fig. 3-4 Reverse Loading Curve

point F and G is calculated by evaluating the envelope loading curve for the corresponding abscissa value.

If the maximum loading excursion $u^{+}_{\max}$ has not exceeded the yield value u_{o2} then point D is taken at the location of point i and the reverse loading curve is formed by branches 5 and 7. Branch 7 connects points i and (u_{o2}, F_{o2}), and makes the transition directly to the envelope loading curve (branch 2).

The model parameters related to the reverse loading curve are eight: α^{+}, β^{-}, γ^{+}, k_2^{+}, k_3^{+}, k_4^{+}, k_5^{+}, r_{jn}.

Reverse Unloading Curve

Similarly the reverse unloading curve is formed by branches 4, 12 and 8 (Fig. 3-5). Curve **4** starts at point A, ends at point C and its middle point is B. Point **A** is the point of reversal on the envelope loading curve and defines the maximum positive excursion. Point **h** is a fixed point on the projection of the initial envelope unloading tangent with coordinate $(\alpha^{-}u_c^{-}, \alpha^{-}F_c^{-})$. Point **B** is the intersection of the line that goes through A and h with the line that passes through the origin with slope $\beta^{+}S_1^{+}$, where S_1^{+} is defined in Eq. (3-12). The reverse unloading initial stiffness is given by:

$$S_R^{-} = \frac{\alpha^{-}F_c^{-} - F_A^{-}}{\alpha^{-}u_c^{-} - u_A^{-}} \tag{3-35}$$

The coordinate of B can be calculated by:

$$u_B^{-} = u_s^{-} = \frac{S_R^{-}u_A^{-} - F_A^{-}}{S_R^{-} - \beta^{+}S_1^{+}} \tag{3-36}$$

$$F_B^{-} = \beta^{+}S_1^{+}u_B^{-} \tag{3-37}$$

Point **i** has a fixed coordinate $(\gamma^{-}u_c^{-}, \gamma^{-}F_c^{-})$ and point **j** has a coordinate $(u_s^{-}, \gamma^{-}F_c^{-})$, where u_s^{-} is calculated from the last loading reverse curve. Point **D** is located by the proportionality factor k_3^{-} between points i and j.

$$u_D^{-} = u_i^{-}(1-k_3^{-}) + u_j^{-}k_3^{-} = \gamma^{-}u_c^{-}(1-k_3^{-}) + u_s^{-}k_3^{-} \tag{3-38}$$

Point **C** is located by the proportionality factor k_2^{-} between points B and D.

$$u_C^- = u_B^-(1-k_2^-) + u_D^- k_2^- \tag{3-39}$$

$$F_C^- = F_B^-(1-k_2^-) + \gamma^- F_C^- k_2^- \tag{3-40}$$

Point **F** is located on the envelope unloading curve and it has a value that depends on the maximum negative excursion u_{min} and the degrading factor k_5^-. Point **E** is then placed between points D and F by using the proportionality factor k_4^-. Point **G** is then calculated by increasing the degrading factor k_5^- by a factor r_{jn}.

$$u_F^- = u_{\min}\left(1 + k_5^- \frac{D_u^-}{u_c^+ - u_c^-}\right) \tag{3-41}$$

$$u_E^- = (1-k_4^-)u_D^- + k_4^- u_F^- \tag{3-42}$$

$$F_E^- = (1-k_4^-)F_D^- + k_4^- F_F^- \tag{3-43}$$

$$u_G^- = u_{\min}\left(1 + r_{jn} k_5^- \frac{D_u^-}{u_c^+ - u_c^-}\right) \tag{3-44}$$

where D_u^- is the total unloading displacement since the last reversal from the envelope unloading curve. Branch 8 is then formed by the points E, F and G. The ordinate for both point F and G is calculated by evaluating the envelope unloading curve for the corresponding abscissa value.

If the maximum loading excursion u_{min} has not exceeded the yield value u_{o3} then point D is taken at the location of point i and the reverse loading curve is formed by branches 4 and 6. Branch 6 connects points i and (u_{o3}, F_{o3}), and makes the transition directly to the envelope unloading curve (branch 3).

The model parameters related to the reverse loading curve are seven: α^-, β^+, γ^-, k_2^-, k_3^-, k_4^-, k_5^-. The factor r_{jn} is used by both the loading and unloading reverse curves.

3.3.3 Transition Curves

Transition Loading Curve

When a reversal occurs from a point outside the envelope, a transition curve is used as shown in Fig. 3-6. The loading transition curve will connect the current position with the reverse loading curve or with the envelope loading curve. This curve is branch 10 in the model.

The initial stiffness of the transition loading curve is calculated as:

$$S_o^+ = \frac{S + s_{lp} S_s^+}{1 + s_{lp}} \tag{3-45}$$

where

$$S_s^+ = \begin{cases} S_1^+ & ; u_o \geq \dfrac{F_o}{S_1^+} \\ \dfrac{F_o - \alpha^+ F_c^+}{u_o - \alpha^+ u_c^+} & ; u_o < \dfrac{F_o}{S_1^+} \end{cases} \tag{3-46}$$

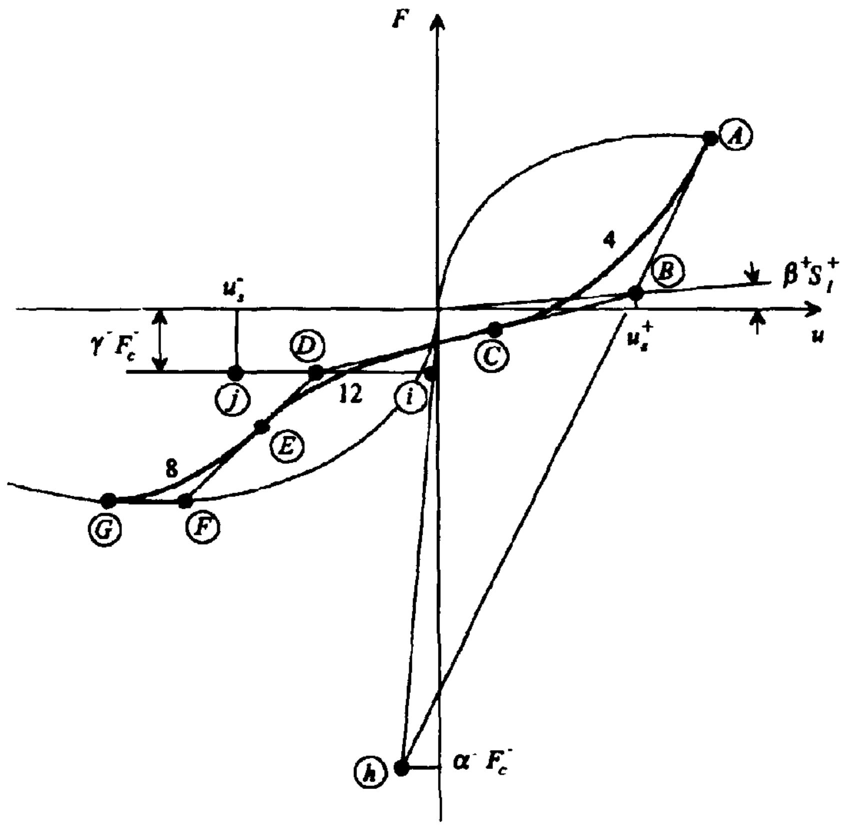

Fig. 3-5 Reverse Unloading Curve

in which u_o = current abscissa (displacement), F_o = current ordinate (force), S = current stiffness just before reversal, s_{tp} = model coefficient related to the transition curves, S_1^+ = initial envelope loading curve stiffness (elastic) and α^+, F_c^+, u_c^+ = model coefficients.

The point of reversal is identified as **A** in Fig. 3-6. Point **B** is the intersection of the line that passes through A with slope S_o^+ as given by Eq. (3-45). The difference in abscissa Δu is then amplified by a factor x_{ng} to locate point **C**. Point C can be located in branch 5, 7, 13, 9 or 2.

Transition Unloading Curve

When a reversal occurs from any loading curve, other than the envelope loading curve (branch 2), the transition unloading curve will connect the reversal point with

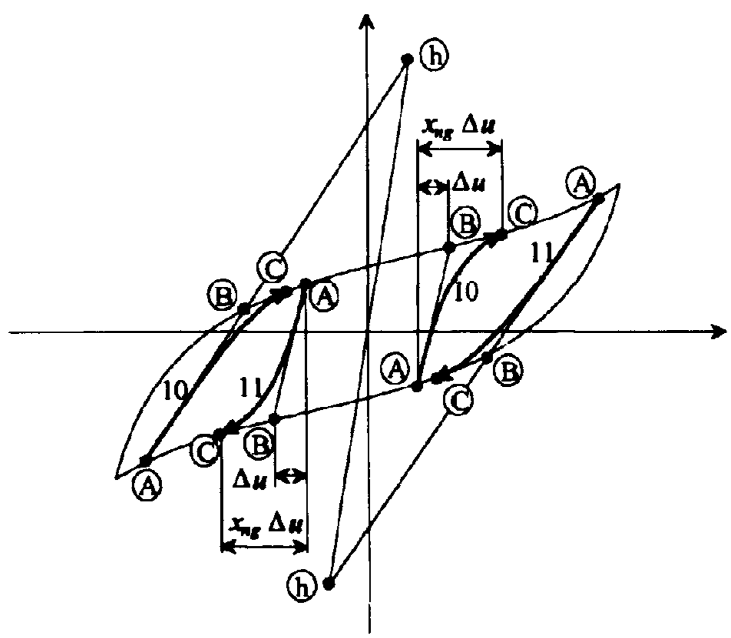

Fig. 3-6 Transition Curves

the reverse unloading curve or the envelope unloading curve. This curve is branch 7 in the model. The initial stiffness of the transition unloading curve is given by:

$$S_o^- = \frac{S + s_{lp} S_s^-}{1 + s_{lp}} \tag{3-47}$$

where

$$S_s^- = \begin{cases} S_1^- & ; u_o \le \dfrac{F_o}{S_1^-} \\ \dfrac{F_o - \alpha^- F_c^-}{u_o - \alpha^- u_c^-} & ; u_o > \dfrac{F_o}{S_1^-} \end{cases} \tag{3-48}$$

u_o, F_o, S, s_{lp} : same as in Eq. (3-37)

S_1^- : initial envelope unloading curve stiffness (elastic)

α^-, F_c^-, u_c^- : model parameters

Elastic Reversal

An elastic reversal occurs when $u_{max} < u_{o2}$ and $u_{min} > u_{o3}$. If the reversal is from the elastic unloading curve, the initial stiffness for the reversal branch is S_s^+ as given by Eq. (3-46). The ending stiffness is given by:

$$S_f^+ = \frac{F_y^+ - F_c^+}{u_y^+ - u_c^+} \tag{3-49}$$

So the starting point for the elastic reverse loading curve is the point of reversal (u_o, F_o), the ending point is (u_{o2}, F_{o2}) and the middle point is calculated by using the starting and ending slopes (S_s^+ and S_f^+) as:

$$u_m^+ = \frac{\left(S_f^+ u_{o2} - F_{o2}\right) - (S_s^+ u_o - F_o)}{S_f^+ - S_s^+} \tag{3-50}$$

$$F_m^+ = F_o + S_s^+ (u_m^+ - u_o) \tag{3-51}$$

If on the other hand, the reversal is from the elastic loading curve then the initial stiffness is S_s^- as given by Eq. (3-48). The ending stiffness is given by:

$$S_f^- = \frac{F_y^- - F_c^-}{u_y^- - u_c^-} \tag{3-52}$$

The starting point **A** for the elastic reverse unloading curve is (u_o, F_o), the ending point **B** is (u_{o2}, F_{o2}) and the middle point **C** as shown in Fig. 3-6 is given by:

$$u_m^- = \frac{\left(S_f^- u_{o3} - F_{o3}\right) - (S_s^- u_o - F_o)}{S_f^- - S_s^-} \tag{3-53}$$

$$F_m^- = F_o + S_s^-(u_m^- - u_o) \tag{3-54}$$

3.3.4 Model Summary

Curves and Branches: Three types of curves were described (1) Envelope Curves, (2) Reverse Curves and (3) Transition Curves. There are 13 branches in total. The relation between branches is summarized by the diagram shown in Fig. 3-7. Note that there are two types of arrows to distinguish between a reversal and a change in rule without reversing. Suppose that the model is in branch 8, if it reaches its ending point then branch 3 will follow, but if a reversal occurs then branch 10 will follow instead. Branch 3 moves in the reverse direction (it is at the left of branch 8), while branch 10 moves in the forward direction (it is at the right hand side of branch 8). Summarizing then:

(1) Monotonic Envelope Curves:

(a) Forward Direction: branches 1 and 2.

(b) Reverse Direction: branches 1 and 3.

(2) Reverse Curves:

(a) Elastic Loading: branch 1.

(b) Elastic Unloading: branch 1.

(c) Yielded Loading Elastic Positive: branches 5 and 7.

(d) Yielded Unloading Elastic Negative: branches 4 and 6.

(e) Fully Yielded Loading: branches 5, 13 and 9.

(f) Fully Yielded Unloading: branches 4, 12, 8.

(3) Transition Curves:

(a) Loading: branch 10.

(b) Unloading: branch 11.

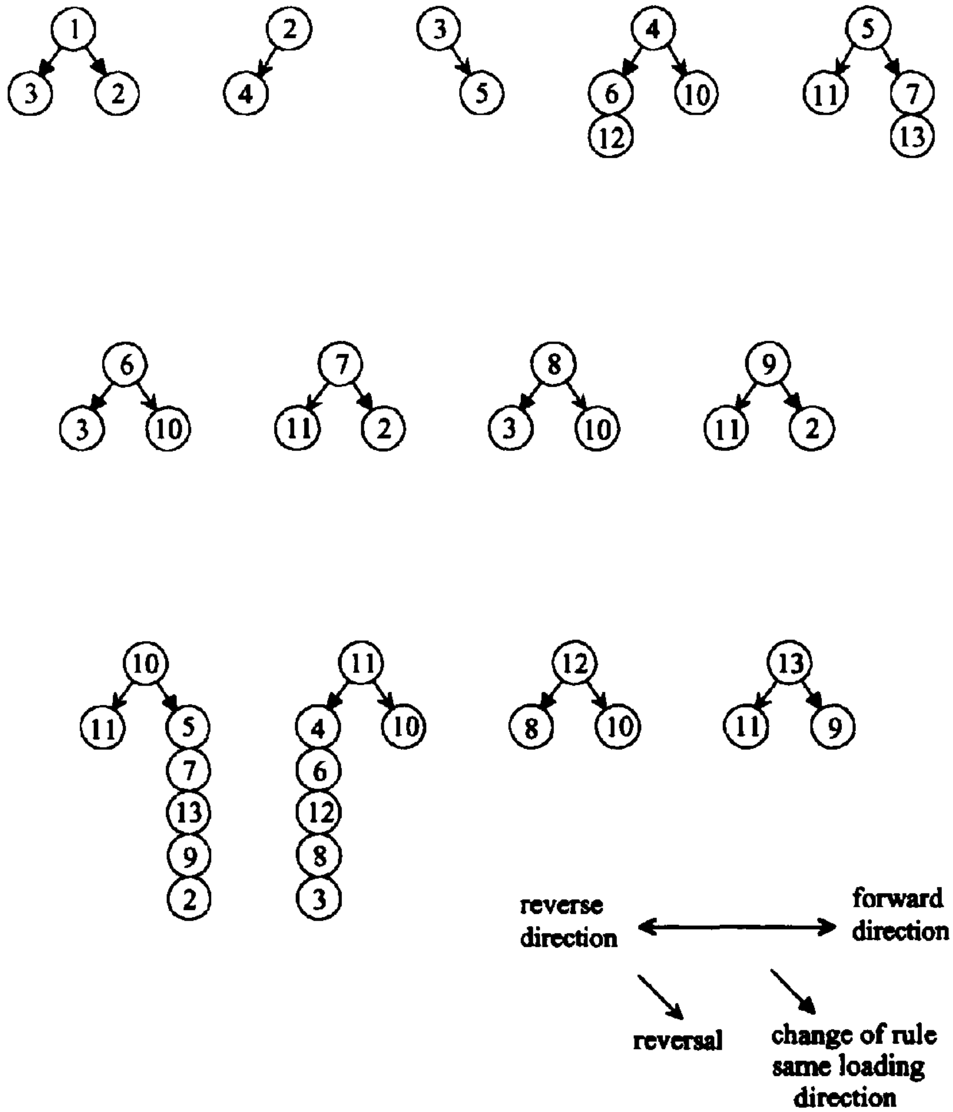

Fig. 3-7 Rule Flow Diagram

Parameters: There are 32 parameters in total. The numbering used in the program given in the appendix is summarized in Table 3-1.

(1) Related to Envelope Loading Curve: u_c^+, F_c^+, u_y^+, F_y^+, u_u^+, F_u^+ and k_1^+.

(2) Related to Envelope Unloading Curve: u_c^-, F_c^-, u_y^-, F_y^-, u_u^-, F_u^- and k_1^-.

(3) Related to Reverse Loading Curve: α^+, β^+, γ^+, k_2^+, k_3^+, k_4^+, k_5^+, r_{jn}.

(4) Related to Reverse Unloading Curve: α^-, β^-, γ, k_2^-, k_3^-, k_4^-, k_5^-.

(5) Related to Transition Curves: s_{lp}, x_{ng}.

(6) Related to Menegotto-Pinto Equation Curvature: R.

Table 3-1 Model Parameters

(1) u_c^+	(2) F_c^+	(3) u_y^+	(4) F_y^+	(5) u_u^+	(6) F_u^+
(7) u_c^-	(8) F_c^-	(9) u_y^-	(10) F_y^-	(11) u_u^-	(12) F_u^-
(13) α^+	(14) β^+	(15) γ^+			
(16) α^-	(17) β^-	(18) γ			
(19) k_1^+	(20) k_2^+	(21) k_3^+	(22) k_4^+	(23) k_5^+	
(24) k_1^-	(25) k_2^-	(26) k_3^-	(27) k_5.	(28) k_5^-	
(29) R	(30) x_{ng}	(31) r_{jn}	(32) s_{lp}		

3.4 Parameter Identification

One of the most discouraging tasks in the use of a macro model is the identification of the model's control parameters, if this has to be done manually. The trial and error process requires a good insight of the effect that every parameter has in the model and also of the interaction among them. Nevertheless, this process can be automated. Herein a method for the identification of model's control parameters is presented.

The identification of the parameters is a non-linear multidimensional constrained minimization problem. Given a discretized hysteretic behavior (u_i, F_i), it is necessary to find a set of parameters for which a certain function, representing the deviation from the actual behavior, is minimized. The function to minimized was chosen as a weighted variance:

$$Var = \sum_i \xi_i (F_i - \bar{F}_i)^2 \tag{3-55}$$

where: ξ_i is the weighting factor

F_i is the actual hysteretic force

$\bar{F}_i$ is the simulated force

The weighting factor was taken as:

$$\xi_i = \tfrac{1}{2}|u_{i+1} - u_i| + \tfrac{1}{2}|u_i - u_{i-1}| \tag{3-56}$$

3.4.1 Optimization Method

The derivatives of the function given in Eq. (3-55) respect to the parameters, $\left(\frac{\partial Var}{\partial u_c^+}, \frac{\partial Var}{\partial \alpha^+}, \frac{\partial Var}{\partial k_1^+}, \cdots\right)$ are not known explicitly. If these derivatives were needed they would have to be calculated numerically, which could be a very time consuming task. For this reason it was decided not to use an optimization method that would require functional derivatives. Brent's approach is a sure method for one-dimensional optimization with quadratic convergence that does not requires the first derivative, thus it was chosen as the line optimization method (Press et al., 1992). Brent's method uses a parabolic interpolation and a golden section search when the parabolic interpolation fails to provide a better estimate of the answer. The equation to find the abscissa x which is the minimum of a parabola through three points (x_a, y_a), (x_b, y_b), (x_c, y_c) is:

$$x = x_b - \frac{1}{2}\frac{(x_b - x_a)^2(y_b - y_c) - (x_b - x_c)^2(y_b - y_a)}{(x_b - x_a)(y_b - y_c) - (x_b - x_c)(y_b - y_a)} \tag{3-57}$$

The golden section search is related to the bisection method used to find roots of equations. The method needs to bracket a solution. A minimum is known to be bracketed if three points, (x_a, y_a), (x_b, y_b), (x_c, y_c) with $x_a < x_b < x_c$, are found such that $y_b < y_a$ and

$y_b < y_c$. After a solution is bracketed, the next step is to evaluate the function at a fraction 0.38197 into the larger of the two intervals (for a derivation of the origin of this number, refer to Press et al. (1992).

$$x = \begin{cases} x_b + 0.38197(x_a - x_b) & ;(x_b - x_a) > (x_c - x_b) \\ \\ x_b + 0.38197(x_c - x_b) & ;(x_c - x_b) > (x_b - x_a) \end{cases} \tag{3-58}$$

The interval is the reduced by including the new calculated point (x, y) and the next three point set is chosen to satisfy the bracketing conditions.

The procedure described above to minimize one dimension can be applied to a multidimensional problem. Starting at a point $\{\mathbf{X}_0\}$ in N-dimensional space, the minimum along a vector direction $\mathbf{n}_1$ can be found, given a new point $\{\mathbf{X}_1\}$. A set of N orthogonal directions is needed to minimize the function. Once the function has been minimized along all the directions, the procedure is repeated until convergence in two consecutive cycles is achieved. This procedure is known as Powell's method (Press et al., 1992). The set of directions in this application were chosen as the unit vectors $\mathbf{e}_1$, $\mathbf{e}_2$,.., $\mathbf{e}_N$. This means that every parameter is identified independently of each other. The procedure proved to be very effective in identifying the parameters.

3.4.2 Scaling

Scaling of force-displacement input history

Both the displacement u_i and the force F_i are scaled before they are passed to the optimization routine. Because a minimization problem needs the variables to be of the same magnitude, it is necessary to scale the variables. It is desirable to have all the variables in the order of magnitude from one to ten. This minimizes round-off problems, avoids having to provide scaling factors for every variable and equally weights all parameters. Thus the scaling is done by using:

$$\tilde{u}_i = u_i \frac{20}{u_{\max} - u_{\min}} \tag{3-59}$$

$$\tilde{F}_i = F_i \frac{20}{F_{\max} - F_{\min}} \tag{3-60}$$

Scaling of Parameters

Model parameters are also scaled to have them in an appropriate range of values. The monotonic parameters u_c , F_c , u_y , F_y , u_u , F_u need not be scaled as the force-displacement history is scaled. The hysteretic control parameters α, R, x_{ng} , r_{jn} and s_{lp} do not need to be scaled. However γ, k_1, k_2 , k_3 , k_4 are multiplied by 10, and β and k_5 are multiplied by 100.

3.4.3 Constraining the Parameters

Parameters have to be constrained not only within certain bounds but also in their relation to other parameters. If this constraint is not provided, the model may behave in a chaotic fashion. Such constraints apply to the unscaled parameters. Table 3-2 below summarizes all the constraints used in the model.

Table 3-2 Parameter Constraints

$0.08 \le u_c^+$	$1.0 \le F_c^+$	$0.9F_c^+ \le F_y^+$	$1.10u_c^+ \le 1.05u_y^+ \le u_u^+$	
$u_c^- \le -0.08$	$F_c^- \le -1.0$	$F_y^- \le 0.9F_c^-$	$u_u^- \le 1.05u_y^- \le 1.10u_c^-$	
$0.10 \le \alpha^+ < 9999$	$0.0 \le \beta^+ \le 0.5$	$0.001 \le \gamma^+$		
$0.10 \le \alpha^- < 9999$	$0.0 \le \beta^- \le 0.5$	$0.001 \le \gamma^-$		
$0.15 \le k_1^+ \le 0.85$	$0.15 \le k_2^+ \le 0.85$	$-4.0 \le k_3^+ \le 2.0$	$0.15 \le k_4^+ \le 0.85$	$0.002 \le k_5^+ \le 5$
$0.15 \le k_1^- \le 0.85$	$0.15 \le k_2^- \le 0.85$	$-4.0 \le k_3^- \le 2.0$	$0.15 \le k_4^- \le 0.85$	$0.002 \le k_5^- \le 5$
$1.0 \le R \le 10.0$	$1.05 \le x_{ng} \le 5.0$	$1.05 \le r_{jn} \le 5.0$	$0.05 \le s_{lp} \le 9999$	

3.4.4 Initial Estimate

The initial estimate may have some influence on the final result obtained. If an initial guess is far from the solution, the minimization algorithm may fall into a local minima that does not accurately represent the true optimal solution. An initial estimate is found by isolating the points that define the positive and negative envelope curves. The optimization routine is then used to identify the parameters that define these two curves. It was found that if these parameters are accurately identified the optimization of the hysteretic control parameters will converge to a good solution.

3.4.5 Order of Parameter Identification

It was found that the order in which the parameters are identified also has an effect on the convergence of the minimization algorithm. After the parameters related to the envelope have been identified it is better to identify the parameters in order of importance, that is, those that have more influence on the overall behavior are identified first. The optimization routine can be called with four different purposes: (1) Identify the Positive Envelope parameters, (2) Identify the Negative Envelope parameters, (3) Identify all the parameters, (4) Identify the parameters for symmetric case. The order in which the parameters are identified for each case is:

(a) Positive Envelope: F_c^+, u_c^+, F_y^+, F_u^+, u_y^+, F_y^+, k_1^+

(b) Negative Envelope: F_c^+, u_c^-, F_y^-, F_u^-, u_y^-, F_y^-, k_1^-

(c) Full Identification after envelope has been defined: γ^+, k_3^+, γ, k_3^-, k_2^+, k_2^-, k_5^+, k_5^-, β^+, β^-, k_4^+, k_4^-, R, x_{ng}, r_{jn}, s_{lp}, α^-, α^+, u_c^+, F_c^+, u_y^+, F_y^+, u_u^+, F_u^+, u_c^-, F_c^-, u_y^-, F_y^-, u_u^-, F_u^-, k_1^+, k_1^-

(d) Symmetric Identification: γ^+, k_3^+, k_2^+, k_5^+, β^+, k_4^+, R, x_{ng}, r_{jn}, s_{lp}, α^+, u_c^+, F_c^+, u_y^+, F_y^+, u_u^+, F_u^+, k_1^+

3.5 Verification of Smooth Model and System Identification Method

The model was tested on three different columns with low to moderate levels of axial load. Of great importance in this simulation are the result for a full size bridge pier tested by Mander et al. (1993). The macro model was calibrated against experimental data and also against a Fiber Element Simulated Experiment. This is to show that actual bridge pier behavior can be indirectly simulated by using an indirect fiber model simulation. The comparison of the macro model behavior, when calibrating a simulated experiment, and the actual experimental behavior of the full size bridge pier is shown in Fig. 3-8c. It can be observed that this procedure can produce excellent agreement. The calibrated parameters are given in Tables 3-3 through 3-5. No attempt was made to define any trend, as the purpose of the procedure is to eliminate the empiricism from the modeling of bridge piers. Typical parameter values are, nevertheless, useful as seed values for the optimization algorithm to minimize the possibility of a local minima.

Macro simulations were carried out on the experimental and analytical results of a column test on a 1/3 scaled reinforced concrete column conducted by Aycardi et al. (1991) and a hollow column tested by Mander et al. (1984). The results of the parameter identification are given in Tables 3-4 and 3-5, and the results are shown graphically in Figs. 3-11 to 3-13.

It is important to note that in the context of a structural analysis program the assessment of the approximate level of axial load, $P-\Delta$ effect, etc., are important factors, as these variables have a strong influence on the shape of the hysteretic behavior. If a high degree of refinement is needed, a preliminary analysis becomes necessary, and then through a backfeed approach a more precise analysis may be achieved. In this preliminary analysis, it may be possible to use typical or average parameters, that may to a certain extent approximately simulate the hysteretic behavior.

In general, the degree of detail simulated by the proposed macro model when compared with the experimental and analytical results, was very good.

3.6 Conclusions

In this section a generalized smooth degrading model with strength and stiffness degradation has been presented. The model has a total of 32 envelope and hysteretic control parameters. This makes the manual process of choosing of an appropriate set of control parameters for a given set of hysteretic loops a cumbersome task. However, it should noted that the envelope parameters as well as the α, β and γ parameters may be initially estimated from geometrical considerations.

A system identification routine was implemented for an automatic selection of a suitable set of parameters to a specific structural element. Excellent agreement was achieved between the output simulation and the experimental or analytical supplied hysteretic behavior. Of particular importance is the high degree of agreement between the macro modeling and the experimental behavior of a full size bridge pier, as this would be the basis of an inelastic spectral energy assessment presented in the next section.

The system identification procedure, where the backbone curve is identified first, and then the rest of the parameters are identified in the order of influence over the hysteretic shape, proved to be a robust approach to achieve good agreement with the input hysteretic history.

Table 3-3a Parameters for a Full Size Bridge Pier (Experimental)

0.5722	0.5722	1.4928	1.0148	8.8749	1.2360
-0.5722	-0.5722	-1.4928	-1.0148	-8.8749	-1.2360
56.59	0.01989	0.3802			
56.59	0.01989	0.3802			
0.85	0.85	-0.07061	0.85	0.01	
0.85	0.85	-0.07061	0.85	0.01	
1.715	4.00	1.3026	9606		

Table 3-3b Parameters for a Full Size Bridge Pier (Fiber Element)

0.5263	0.5263	1.3468	1.0075	7.1821	1.1343
-0.5263	-0.5263	-1.3468	-1.0075	-7.1821	-1.1343
39.89	0.200	0.900			
39.89	0.200	0.900			
0.85	0.7181	0.1395	0.85	0.03842	
0.85	0.7181	0.1395	0.85	0.03842	
1.000	4.00	2.8412	9999		

Table 3-4a Parameters for a 1/3 Scale Column (Experimental)

0.5997	0.5997	1.4498	0.9737	11.067	0.4121
-0.5997	-0.5997	-1.4498	-0.9737	-11.067	-0.4121
1.257	0.200	0.900			
1.257	0.200	0.900			
0.4402	0.85	0.5344	0.15	0.0331	
0.4402	0.85	0.5344	0.15	0.0331	
1.000	5.00	1.05	1577.9		

Table 3-4b Parameters for a 1/3 Scale Column (Fiber Element)

0.2434	0.2434	1.1612	0.9883	7.7777	0.5085
-0.2434	-0.2434	-1.1612	-0.9883	-7.7777	-0.5085
2.052	0.200	0.90			
2.052	0.200	0.90			
0.5211	0.85	-0.2447	0.85	0.01	
0.5211	0.85	-0.2447	0.85	0.01	
1.292	3.100	2.8296	2120.1		

Table 3-5 Parameters for a Hollow Column (Fiber Element)

0.4300	0.4300	1.3525	0.9999	7.8080	0.9985
-0.4300	-0.4300	-1.3525	-0.9999	-7.8080	-0.9985
18.44	0.02567	0.90			
18.44	0.02567	0.90			
0.15	0.85	0.03945	0.5017	0.02	
0.15	0.85	0.03945	0.5017	0.02	
3.877	4.430	1.854	214.5		

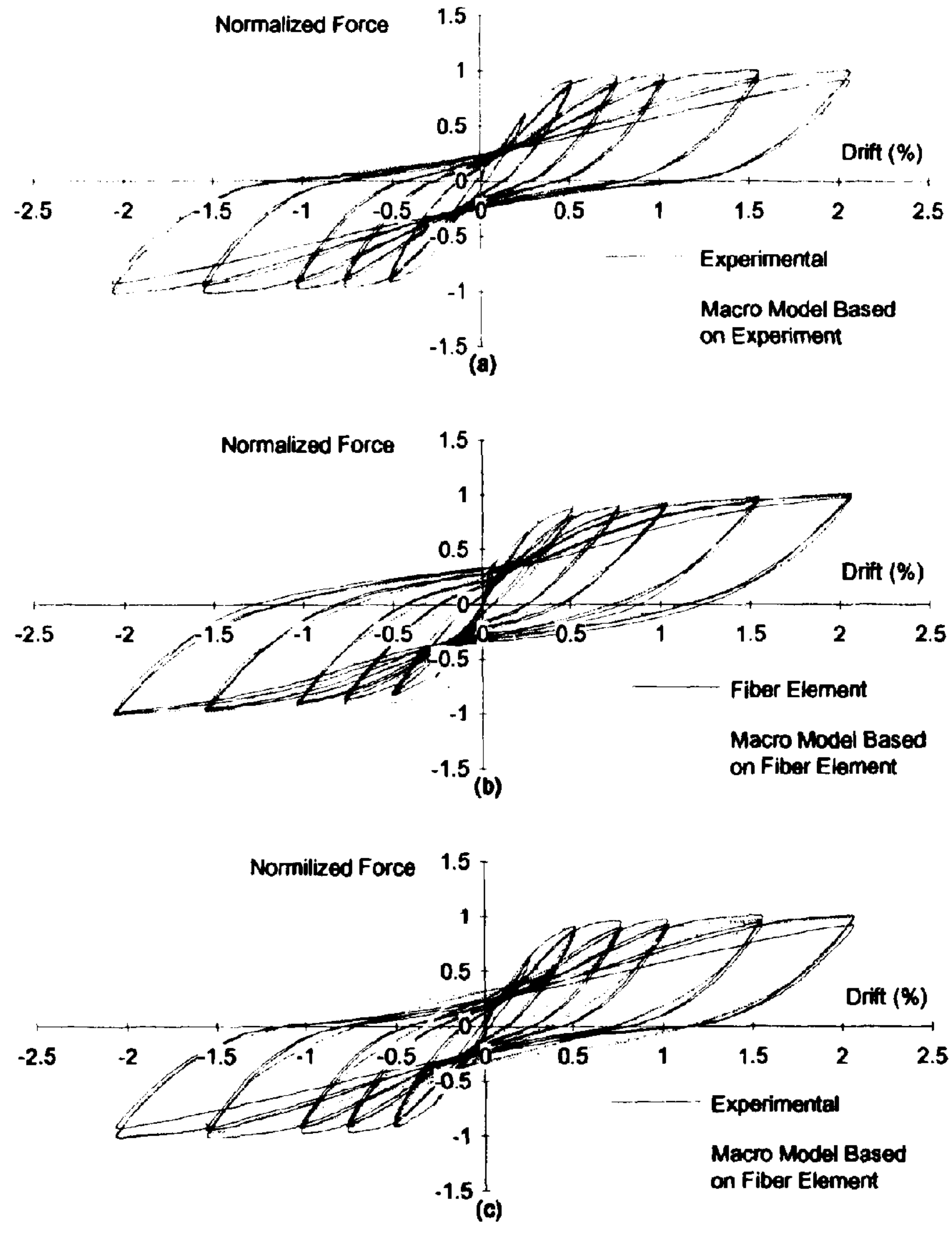

Fig. 3-8 Comparison of Macro Model Simulations Genarated through (a) Experimental Data, and (c) Fiber Element Experiment Simulation

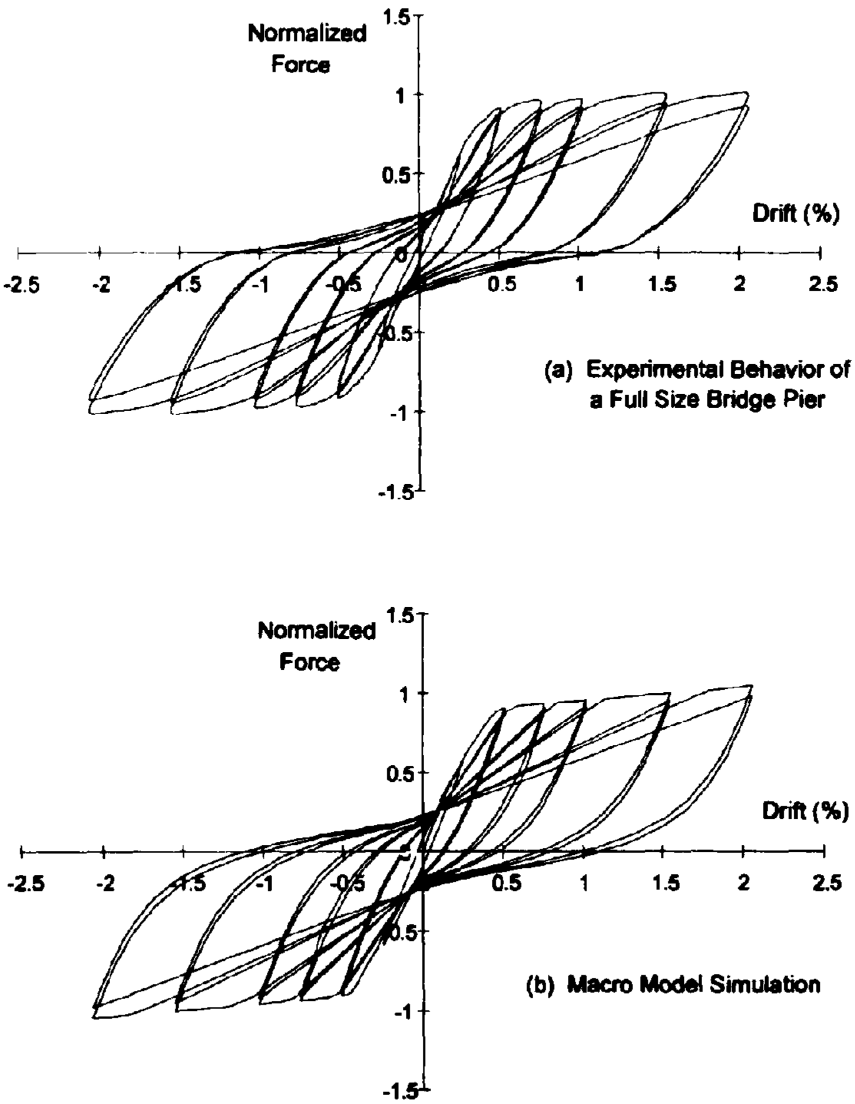

Fig. 3-9 Macro Model Simulation of a Full Size Bridge Pier Based on Actual Experimental Data

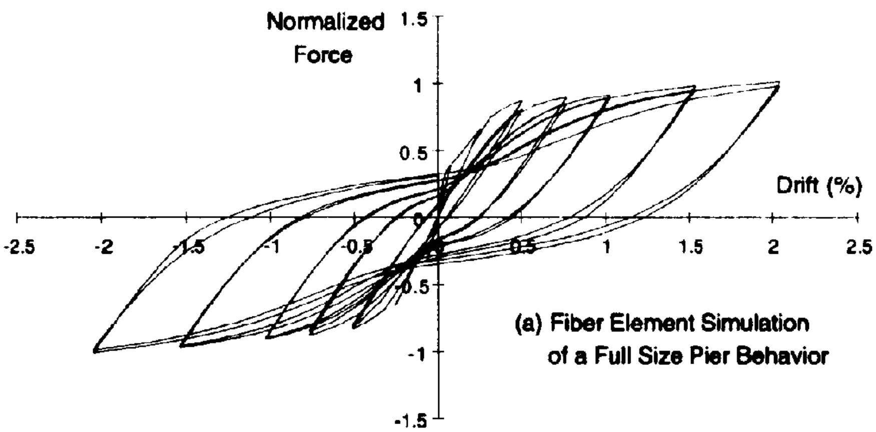

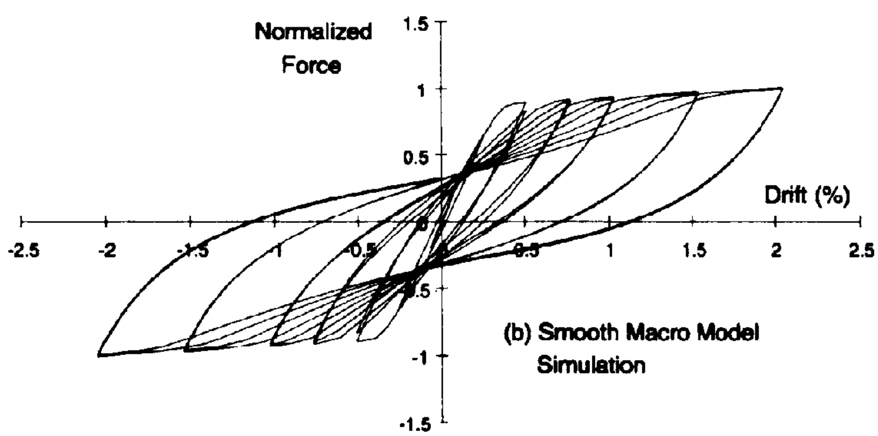

Fig. 3-10 Simulation of the Cyclic Behavior of a Full Size Bridge Pier Based on a Fiber Element Simulated Experiment

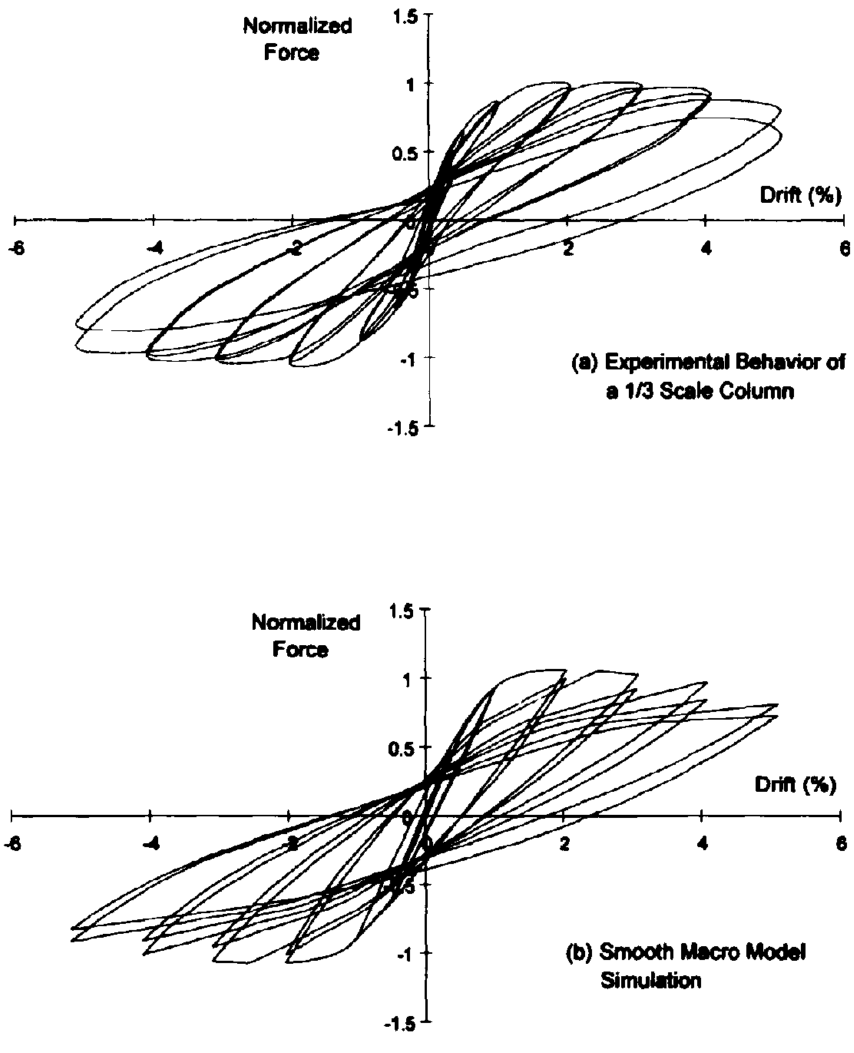

Fig. 3-11 Macro Model Simulation of a 1/3 Scale Column Based on Experimental Data

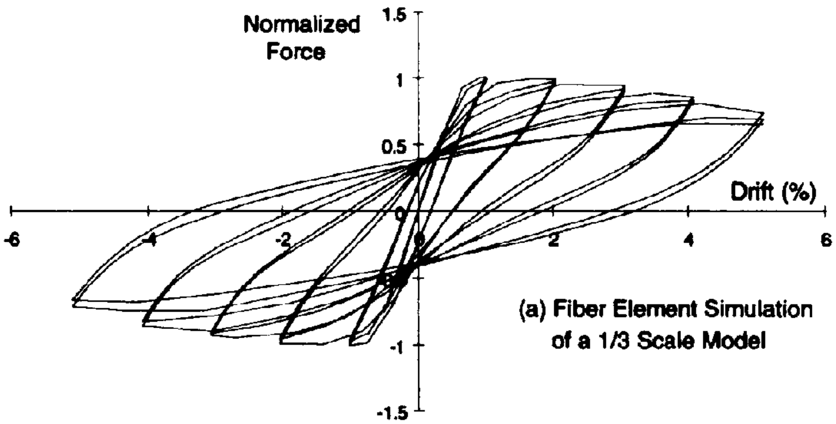

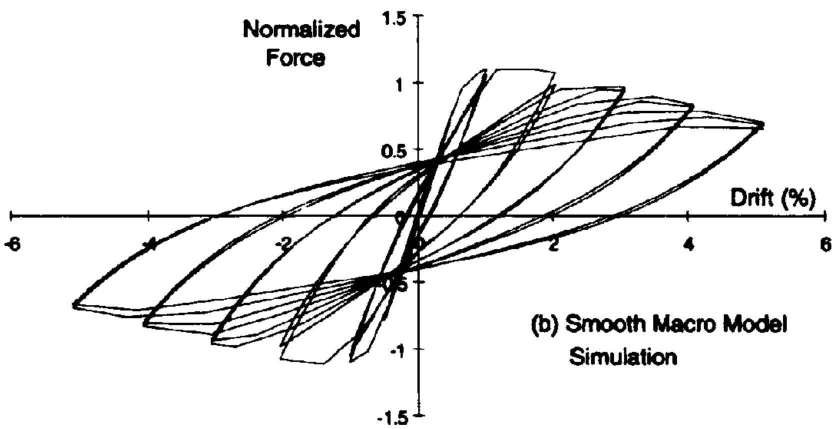

Fig. 3-12 Macro Model Simulation of a 1/3 Scale Column Based on Fiber Model Simulated Experiment

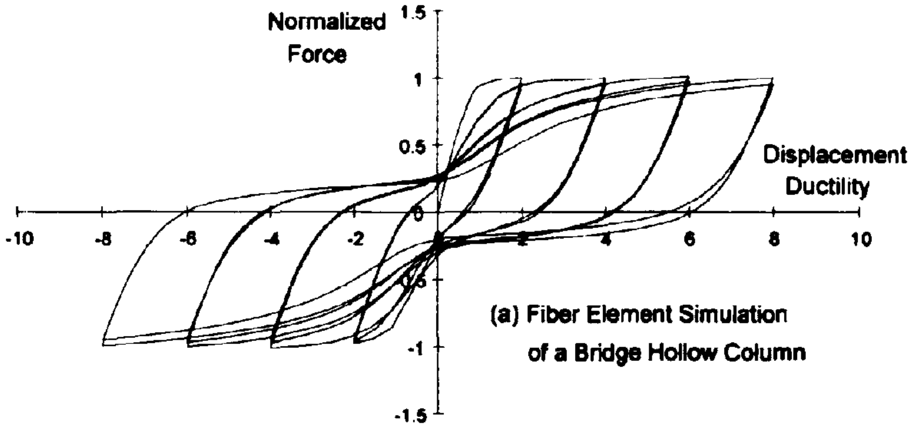

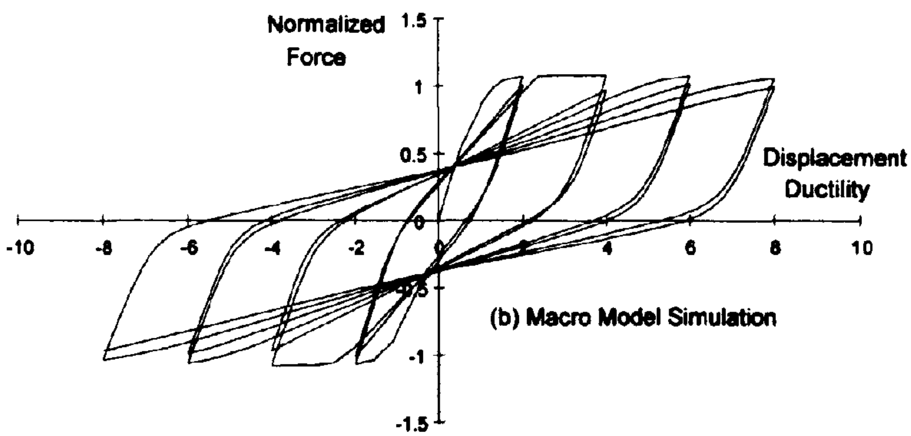

Fig. 3-13 Macro Model Simulation of a Bridge Hollow Column Based on a Fiber Element Simulated Experiment.

Section 4

Assessment of Hysteretic Energy DEMAND

4.1 Introduction

Deterministic methods of analysis are necessary to assess the energy and ductility demand on reinforced concrete structures. The ductility demand is dependent only on the maximum inelastic seismic displacement response, whereas energy demand depends on the duration and magnitude of the response. A methodology to simulate the behavior of reinforced concrete column CAPACITY starting from the hysteretic characteristics of concrete and steel has been developed, which can be applied to calibrate the macro model hysteretic parameters for the determination of hysteretic DEMAND on bridge columns. The macro model parameters can then be used to represent more realistically the behavior of a structural concrete member, or a SDOF idealization of a structural system. In this section a nonlinear single-degree-of-freedom dynamic analysis is used to determine the response DEMAND on a reinforced concrete structure when using the more realistic macro modeling technique, and it is compared with more traditional models. Particular emphasis is given to assessing energy-based low cycle fatigue spectral demands, which can in turn be related to CAPACITY via the fiber-element analysis which in the overall context of seismic evaluation is shown in Fig. 4-1.

4.2 Elastic Response of a SDOF System

Consider the single-degree-of-freedom system shown in Fig. 4-2a. The equation of motion is given by:

$$m(\ddot{x}-\ddot{x}_g)+c(\dot{x}-\dot{x}_g)+k(x-x_g)=p(t)=-m\ddot{x}_g \tag{4-1}$$

where k = stiffness, c = damping coefficient, m = total mass; $x_g, \dot{x}_g, \ddot{x}_g$ are the ground displacement, velocity and acceleration respectively; and $x, \dot{x}, \ddot{x}$ are the system displacement, velocity and acceleration respectively.

Eq. (4-1) can also be written as:

$$\ddot{u} + 2\xi\omega_n\dot{u} + \omega_n^2 u = \frac{p(t)}{m} = -\ddot{x}_g \qquad \textbf{(4-2)}$$

in which u = displacement of the system respect to the ground (deformation), ξ = damping ratio and ω_n = natural angular frequency given by

$$\omega_n = \sqrt{\frac{k}{m}} \qquad \textbf{(4-3)}$$

and the damping coefficient by:

$$\xi = \frac{c}{2m\omega_n} \qquad \textbf{(4-4)}$$

The solution to the equation of motion of a linear SDOF system can be found by using the Duhamel's Integral given by:

$$u(t) = \frac{1}{m\omega_d} e^{-\xi\omega_n t} \int_0^t [p(t) e^{\xi\omega_n\tau} \sin\omega_d(t-\tau)] d\tau \qquad \textbf{(4-5)}$$

This equation can be solved numerically by using standard procedures. An alternative procedure given by Craig (1981), which appears to be more efficient, is given in theP following recursive equations:

$$u_{i+1} = Ap_i + Bp_{i+1} + Cu_i + D\dot{u}_i \qquad \textbf{(4-6)}$$

$$\dot{u}_{i+1} = \tilde{A}p_i + \tilde{B}p_{i+1} + \tilde{C}u_i + \tilde{D}\dot{u}_i \qquad \textbf{(4-7)}$$

where the constants A through $\tilde{D}$ are defined in Eqs. (4-8) through (4-19) in which h is the integration time step.

$$A = \frac{1}{k\omega_n h}\{e^{-\beta h}[(v_1 - \beta h)\sin(\omega_d h) - (v_2 + \omega_d h)\cos(\omega_d h)] + v_2\} \qquad \textbf{(4-8)}$$

$$B = \frac{1}{k\omega_n h}\{e^{-\beta h}[-v_1\sin(\omega_d h) + v_2\cos(\omega_d h)] + \omega_d h - v_2\} \qquad \textbf{(4-9)}$$

$$C = e^{-\beta h}\left[\cos(\omega_d h) + \frac{\beta}{\omega_d}\sin(\omega_d h)\right] \qquad \textbf{(4-10)}$$

$$D = \frac{1}{\omega_d} e^{-\beta h}\sin(\omega_d h) \qquad \textbf{(4-11)}$$

$$\widetilde{A}=\frac{1}{k\omega_d h}\{e^{-\beta h}[(\beta+\omega_n^2 h)\sin(\omega_d h)+\omega_d\cos(\omega_d h)]-\omega_d\} \qquad \textbf{(4-12)}$$

$$\widetilde{B}=\frac{1}{k\omega_d h}\{-e^{-\beta h}[\beta\sin(\omega_d h)+\omega_d\cos(\omega_d h)]+\omega_d\} \qquad \textbf{(4-13)}$$

$$\widetilde{C}=\frac{\omega_n^2}{\omega_d}e^{-\beta h}\sin(\omega_d h) \qquad \textbf{(4-14)}$$

$$\widetilde{D}=e^{-\beta h}\left[\cos(\omega_d h)-\frac{\beta}{\omega_d}\sin(\omega_d h)\right] \qquad \textbf{(4-15)}$$

$$\nu_1 = 1-2\xi^2 \qquad \textbf{(4-16)}$$

$$\nu_2 = 2\xi\sqrt{1-\xi^2} \qquad \textbf{(4-17)}$$

$$\omega_d = \omega_n\sqrt{1-\xi^2} \qquad \textbf{(4-18)}$$

$$\beta = \xi\omega_n \qquad \textbf{(4-19)}$$

This approach was used to compute the elastic response of a SDOF to a given earthquake ground motion, as the inelastic response is to be compared to the elastic one.

4.3 Inelastic Response of a SDOF System

Consider now the case where the stiffness of the system k is not a constant during the analysis. In this case the integration procedure given previously does not represent the solution for this equation, as it is based on the superposition principle which is not valid for nonlinear systems. A step by step integration procedure is needed during which the stiffness of the system is being kept track of. The macro-model presented in the previous section is ideal for this kind of analysis, because it can represent very accurately the hysteretic behavior of the system. Consider a viscous damped SDOF system subjected to a horizontal ground motion. The equation of motion is given by:

$$m\ddot{x}+c\dot{x}+f_S=p(t)=-m\ddot{x}_g \qquad \textbf{(4-20)}$$

A procedure given by Clough and Penzien (1993) was modified to improve convergence and is outlined below:

(1) Knowing the displacement and velocity of the system at any given time t, calculate the damping force as:

$$f_D=c(t)\,\dot{x}(t) \qquad \textbf{(4-21)}$$

(2) The inertia force in the mass and the acceleration can be computed by:

$$f_I(t) = p(t) - f_S(t) - f_D(t) \tag{4-22}$$

$$\ddot{x}(t) = \frac{f_I(t)}{m} \tag{4-23}$$

where $f_s(t)$ is the force in the spring. This force and the instantaneous stiffness $k(t)$ are computed by using a suitable hysteresis macro model.

(3) An equivalent instantaneous stiffness is calculated by:

$$\tilde{k}(t) = k(t) + \frac{6}{h^2}m + \frac{3}{h}c(t) \tag{4-24}$$

(4) And an equivalent force is given by:

$$\Delta\tilde{p}(t) = \Delta p(t) + m\left[\frac{6}{h}\dot{x}(t) + 3\ddot{x}(t)\right] + c(t)\left[3\dot{x}(t) + \frac{h}{2}\ddot{x}(t)\right] + f_{err} \tag{4-25}$$

where

$$\Delta p(t) = p(t+h) - p(t) \tag{4-26}$$

and

$$f_{err} = f_s(t-h) + k(t-h)[x(t) - x(t-h)] - f_s(t) \tag{4-27}$$

in the original procedure presented by Clough and Penzien this last factor of Eq. (4-25) does not appear, but the introduction of this force correction factor, Fig. 4-2b, greatly improves convergence, as shown in Fig. 4-2c. This force correction factor has been used before in programs as IDARC (Kunnath et al., 1992) and DRAIN-2DX (Allahabadi et al., 1988).

(4) The change in displacement and velocity can then be computed by:

$$\Delta x(t) = \frac{\Delta\tilde{p}(t)}{\tilde{k}(t)} \tag{4-26}$$

$$\Delta\dot{x}(t) = \frac{3}{h}\Delta x(t) - 3\dot{x}(t) - \frac{h}{2}\ddot{x}(t) \tag{4-27}$$

(5) The displacement and velocity are updated by:

$$x(t+h) = x(t) + \Delta x(t) \tag{4-28}$$

$$\dot{x}(t+h) = \dot{x}(t) + \Delta\dot{x}(t) \tag{4-29}$$

the procedure is thus repeated until the ending of analysis time is reached.

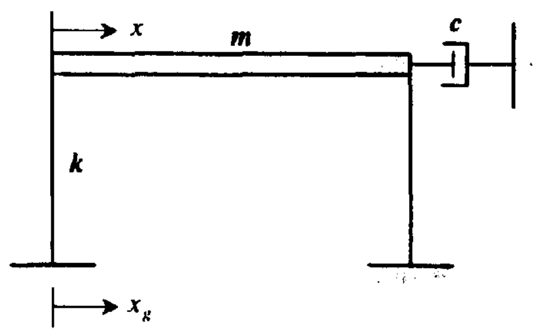

Fig. 4-2a Equivalent Single-Degree-Of-Freedom System

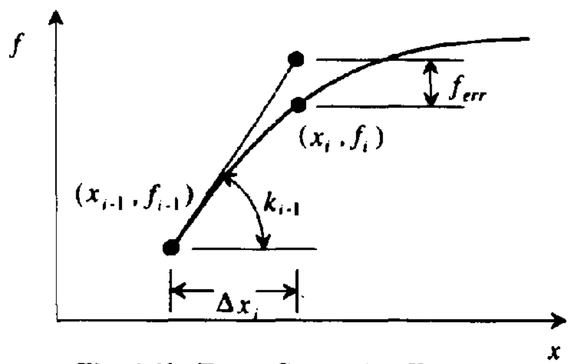

Fig. 4-2b Force Correction Factor

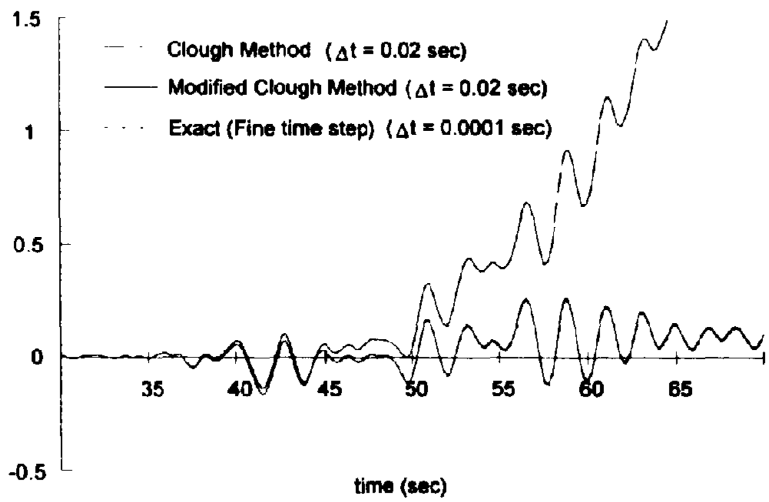

Fig. 4-2c Step-By-Step Integration

4.4 Elastic and Inelastic Response Spectra

The description of the maximum dynamic response quantities for a structure subjected to earthquake excitation as a function of its basic characteristics (natural period, damping ratio and hysteretic rule) is commonly referred to as response spectra. Both displacement ductility and energy based spectra are considered herein and are described in what follows:

4.4.1 Displacement Ductility Spectra

The Spectral Displacement S_d of an <u>elastic</u> system is the maximum displacement that the structure undergoes during the entire time history for a given earthquake. It is a function of the period of the structure T, the damping ratio ξ (normally assumed to be 5% for design).

Elastic Displacement Spectrum

$$S_d = \max[x(t)] \text{ for a linear elastic structure} \tag{4-30}$$

Elastic Pseudo Velocity Spectrum

$$S_v = \omega_n S_d = \frac{2\pi}{T} S_d \tag{4-31}$$

Elastic Pseudo Acceleration Spectrum

$$S_a = \omega_n S_v = \frac{2\pi}{T} S_v \tag{4-32}$$

This three quantities can be plotted in a single graph known as the elastic log tripartite plot, as shown in Fig. 4-6a.

Displacement Spectrum of Inelastic Response

$$X_u = f\,[R_\mu, \text{hysteretic rule}, \ddot{x}_g(t)] = \max\,[x(t)] \tag{4-33}$$

Displacement Ductility Spectrum

$$\mu = \frac{X_u}{X_y} \tag{4-34}$$

in which X_y is the yield displacement.

Inelastic Displacement Magnification Spectrum

$$D_m = D_{inelast} / D_{elast} = \frac{X_u}{S_d} = \frac{\mu}{R_\mu} \tag{4-35}$$

Note that for "long" periods this ratio is approximately equal to 1 and is commonly referred to as Newmark's "equal displacement " principle. As the period tends toward zero, the ratio increases to infinity.

4.4.2 Energy Based Spectrum

According to the procedures described by Uang and Bertero (1990) the total absolute energy at any given instant is given by:

$$E_t = E_k + E_s + E_\xi + E_h \tag{4-36}$$

where E_k = absolute kinetic energy, E_s = strain energy, E_ξ = absorbed viscous damping energy, and E_h = hysteretic energy absorbed by the structure. When the ground motion stops, both the kinetic and the strain energy vanish after a few seconds, as the structures vibrates in damped free motion. On the other hand, the damping and hysteretic energy are indications of the energy dissipated (absorbed) by the structure. The absolute kinetic energy is given by:

$$E_k = \frac{1}{2} m (\dot{x} + \dot{x}_g)^2 \tag{4-37}$$

where $\dot{x}$ = relative structural velocity with respect to the ground, and $\dot{x}_g$ = velocity of the moving ground.

The hysteretic energy is computed as:

$$E_h = E_a - E_s \tag{4-38}$$

where E_a is the total energy absorbed by the structure, computed as,

$$E_a = \int_0^t f\,dx = \sum_{i=1}^{n} \frac{1}{2}(f_i + f_{i-1})(x_i - x_{i-1}) \tag{4-39}$$

and E_s is the strain energy computed as,

$$E_s = \frac{1}{2}\frac{f_n^2}{k(t=0)} \tag{4-40}$$

Note that the recoverable strain energy is a function of the original initial stiffness of the system. The damping energy is always a positive increasing quantity, as it is a non-recoverable energy, and is given by:

$$E_\xi = \int c\,\dot{x}\,dx = c\sum_{i=1} \frac{1}{2}(\dot{x}_i + \dot{x}_{i-1})(x_i - x_{i-1}) \tag{4-41}$$

In the case of an elastic structure the hysteretic energy vanishes, thus the total energy is composed of damping energy, kinetic energy and strain energy. In Fig. 4-6b the kinetic energy spectra for an elastic structure is shown.

Elastic Equivalent Number of Cycles

For an elastic structure an equivalent number of cycles at the spectral displacement can be defined in terms of fatigue damage analysis. Numerous investigations on fatigue have confirmed the Manson-Coffin relation:

$$\varepsilon_a = c(2N_f)^b \tag{4-42}$$

in which ε_a = strain amplitude, N_f = number of cycles to failure, b and c = fatigue coefficients obtained from constant strain amplitude tests. In the case of variable amplitude tests, two questions arise: (1) how the damage is accumulated and (2) how to count the cycles. In answer to the first question, the most simple and common assumption is that the accumulation of damage is linear. This assumption is known as Miner's rule and is expressed as:

$$D = \sum_i \frac{1}{N_{fi}} \tag{4-43}$$

in which D = fatigue damage and N_{fi} = number of cycles at a given strain amplitude. In this equation it is assumed that there are individual cycles of amplitude ε_{ai}, each causing a cummulative damage.

A variable amplitude test can bc converted to an equivalent contant amplitude test by equating the amount of damage, so that,

$$D = \sum_i \frac{1}{N_{fi}} = \frac{N_c}{N_{feff}} \tag{4-44}$$

where N_c = equivalent number of a predifined amplitude ε_{aeff} for the whole strain history, and N_{feff} = number of cycles to failure at that same amplitude. In terms of amplitude this can be expressed as:

$$N_c = N_{feff} \sum_i \frac{1}{N_{fi}} = c(\varepsilon_{aeff})^{1/b} \sum_i \frac{1}{c(\varepsilon_{ai})^{1/b}} = \frac{1}{(\varepsilon_{aeff})^{-1/b}} \sum_i (\varepsilon_{ai})^{-1/b} \tag{4-45}$$

The previous equation can be also expressed in terms of displacement, as:

$$N_c = \sum_i \left(\frac{x_{ai}}{S_d}\right)^{-1/b} \tag{4-46}$$

where x_{ai} = amplitude of the *ith* cycle on a variable amplitude displacement history. In this equation N_c = number of cycles at a constant amplitude S_d. The amplitudes in a variable amplitude displacement history may be computed by using the standard cycle counting technique known as rainflow counting method. This procedure was used herein to assess the equivalent number of elastic cycles.

Equivalent Elasto-Plastic Cycles

The energy absorbed in an equivalent elastic-perfectly plastic loop of amplitude X_{eff} is given by:

$$E_{ep} = 4\, f_y X_{eff} \tag{4-47}$$

Equivalent or Effective Equi-Amplitude Cycles

The standard deviation of a constant amplitude sinusoidal displacement history may be shown to be:

$$x_{STD}(t) = STD[A \sin(wt)] = \frac{A}{\sqrt{3}} \tag{4-48}$$

where A is the amplitude of the sine wave and the values of x are taken at arbitrary steps. For a general displacement response, the standard deviation of the inelastic displacements can be readily computed and thus an equivalent effective amplitude may be defined as:

$$X_{eff} = \sqrt{3}\, x_{STD} + X_y \tag{4-49}$$

An effective ductility may also be defined as the ratio between the effective amplitude X_{eff} and the yield deformation,

$$\mu_{eff} = \frac{X_{eff}}{X_y} \tag{4-45}$$

Effective Number of Inelastic Cycles

An effective number of cycles may be defined as the number of cycles at the effective ductility, given by Eq. (4-45), that would give the same hysteretic energy computed for the whole deformation history. To compute this value, after the analysis ended, the hysteretic macro model was used to simulate 4 cycles with a ductility amplitude equal to the effective equi-amplitude ductility. The average of the loop area was then taken as the loop energy,

$$E_{h\,loop} = E_h(\pm\mu_{eff}) \tag{4-46}$$

The effective number of inelastic cycles are thus defined as:

$$N_c = \frac{E_h}{E_{h\,loop}} \tag{4-47}$$

Factor of Symmetry Spectra

A symmetry factor is commonly used in fatigue studies when describing the relative magnitude of positive and negative displacement peaks. The parameter R is normally used to express the degree of asymmetry of the deformation history. This factor is formally expressed as:

$$R = \frac{\mu_{min}}{\mu_{max}} \tag{4-48}$$

in which μ_{max} = the maximum ductility, and μ_{min} = the minimum ductility. The maximum ductility is taken so that, μ_{max} is positive and μ_{min} is negative giving a normal range of from -1 (equi-amplitude) to about 0.4 as shown in Fig. 4-4.

An effective ductility may also be defined as the ratio between the effective amplitude X_{eff} and the yield deformation,

$$\mu_{eff} = \frac{X_{eff}}{X_y} \tag{4-45}$$

Effective Number of Inelastic Cycles

An effective number of cycles may be defined as the number of cycles at the effective ductility, given by Eq. (4-45), that would give the same hysteretic energy computed for the whole deformation history. To compute this value, after the analysis ended, the hysteretic macro model was used to simulate 4 cycles with a ductility amplitude equal to the effective equi-amplitude ductility. The average of the loop area was then taken as the loop energy,

$$E_{h\ loop} = E_h(\pm\mu_{eff}) \tag{4-46}$$

The effective number of inelastic cycles are thus defined as:

$$N_c = \frac{E_h}{E_{h\ loop}} \tag{4-47}$$

Factor of Symmetry Spectra

A symmetry factor is commonly used in fatigue studies when describing the relative magnitude of positive and negative displacement peaks. The parameter R is normally used to express the degree of asymmetry of the deformation history. This factor is formally expressed as:

$$R = \frac{\mu_{min}}{\mu_{max}} \tag{4-48}$$

in which μ_{max} = the maximum ductility, and μ_{min} = the minimum ductility. The maximum ductility is taken so that, μ_{max} is positive and μ_{min} is negative giving a normal range of from -1 (equi-amplitude) to about 0.4 as shown in Fig. 4-4.

(vi) An artificial sinusoidal ground input with PGA = 1g and a frequency of 1Hz.

These ground input motions are plotted in Fig. 4-5.

The macro model used the calibrated parameters that very accurately represented the behavior of an actual full size bridge pier, thus the inelastic spectral quantities shown in Figs. 4-6 through 4-11 are considered to be a reliable representation of actual bridge pier inelastic response.

In Figs. 4-12 through 4-17, inelastic spectra generated by using an elastic-perfectly plastic model are shown. This second type of hysteretic model and resulting spectra may be considered typical of bridge structures seated on steel or PTFE bearings. Such curves are necessary in a seismic limit analysis for establishing the hierarchy of failure mechanisms (i.e. bearing vs. pier failure).

In order to study the sensitivity of the spectral quantities to the model used, a third set of spectra, shown in Figs. 4-18 through 4-23, was generated using the modified Takeda model described in Section 2.

4.6 Conclusions

The piecewise linear and smooth macro models described respectively in Sections 2 and 3 proved to be useful in describing the hysteretic behavior of a bridge pier structure. The inelastic spectra produced through a well calibrated model is believed to be a realistically representation of bridge pier structures, as they were generated by the calibration of a full size actual bridge pier. The procedure can be use to generate inelastic spectra for other kind of structures by following the procedure outlined throughout this investigation: (1) realistic hysteretic behavior can be known directly (experiment) or indirectly (Fiber Element modeling); (2) the macro model can be calibrated to simulate the structure behavior; (3) a non-linear time history dynamic analysis program is used to evaluate the inelastic response.

A spectral study of the inelastic behavior of typical bridge structures may lead to identify design envelopes for the hysteretic parameters. This, may in turn lead to rational ways of assessing inelastic design demand.

It should be emphasized that the low cycle fatigue demand is both earthquake and hysteretic model dependent. This is evident by comparing the different responses amongst earthquakes, and different responses for a given earthquake comparing the bridge and EPP models. Therefore, further sensitivity studies are necessary for the determination of spectral fatigue demands for different structural types, where the hysteretic model should be varied to properly reflect global response. In this manner a rational assessment can be made of energy based fatigue demands on structural elements.

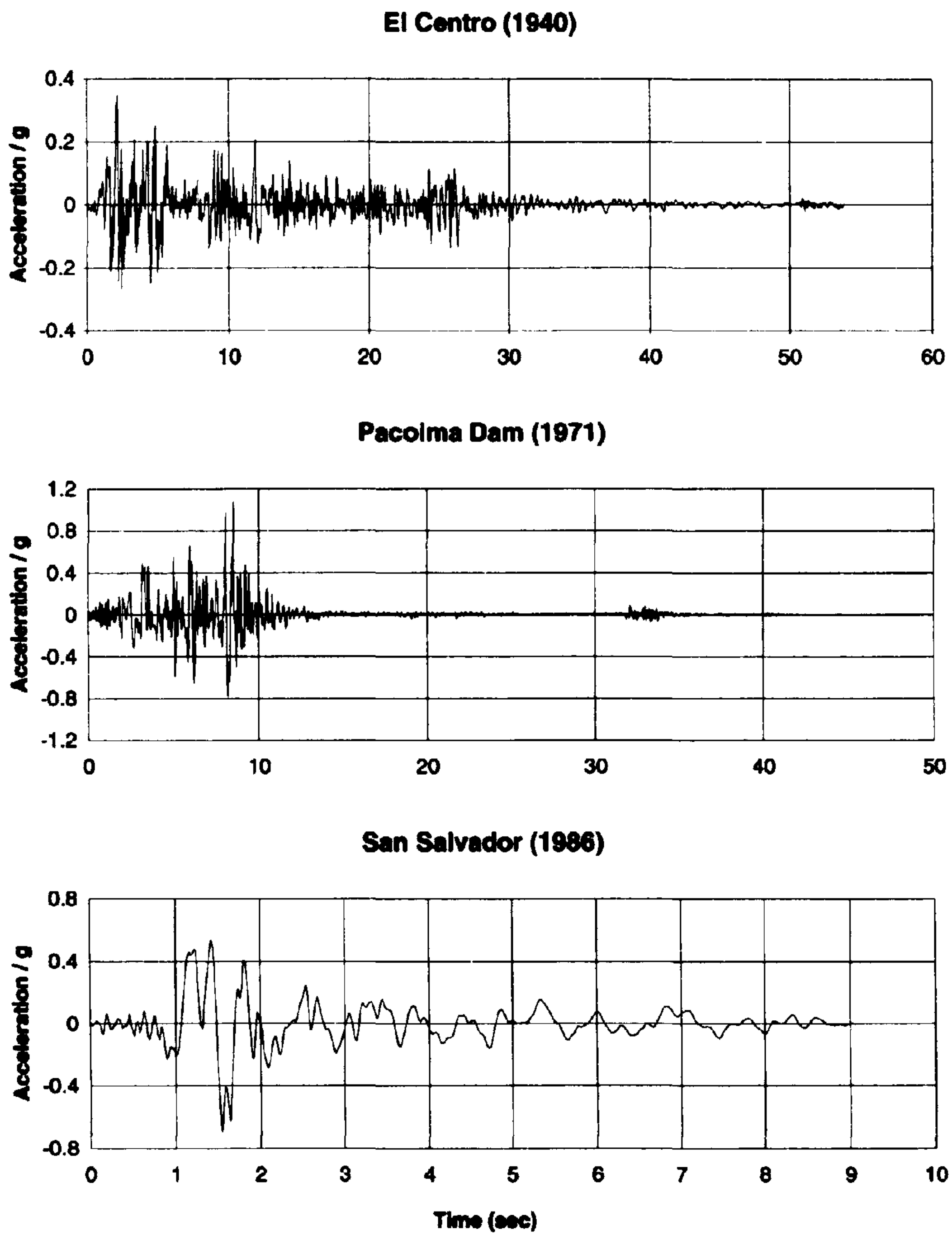

Fig. 4-4 Input Ground Motions Used for Spectral Analysis

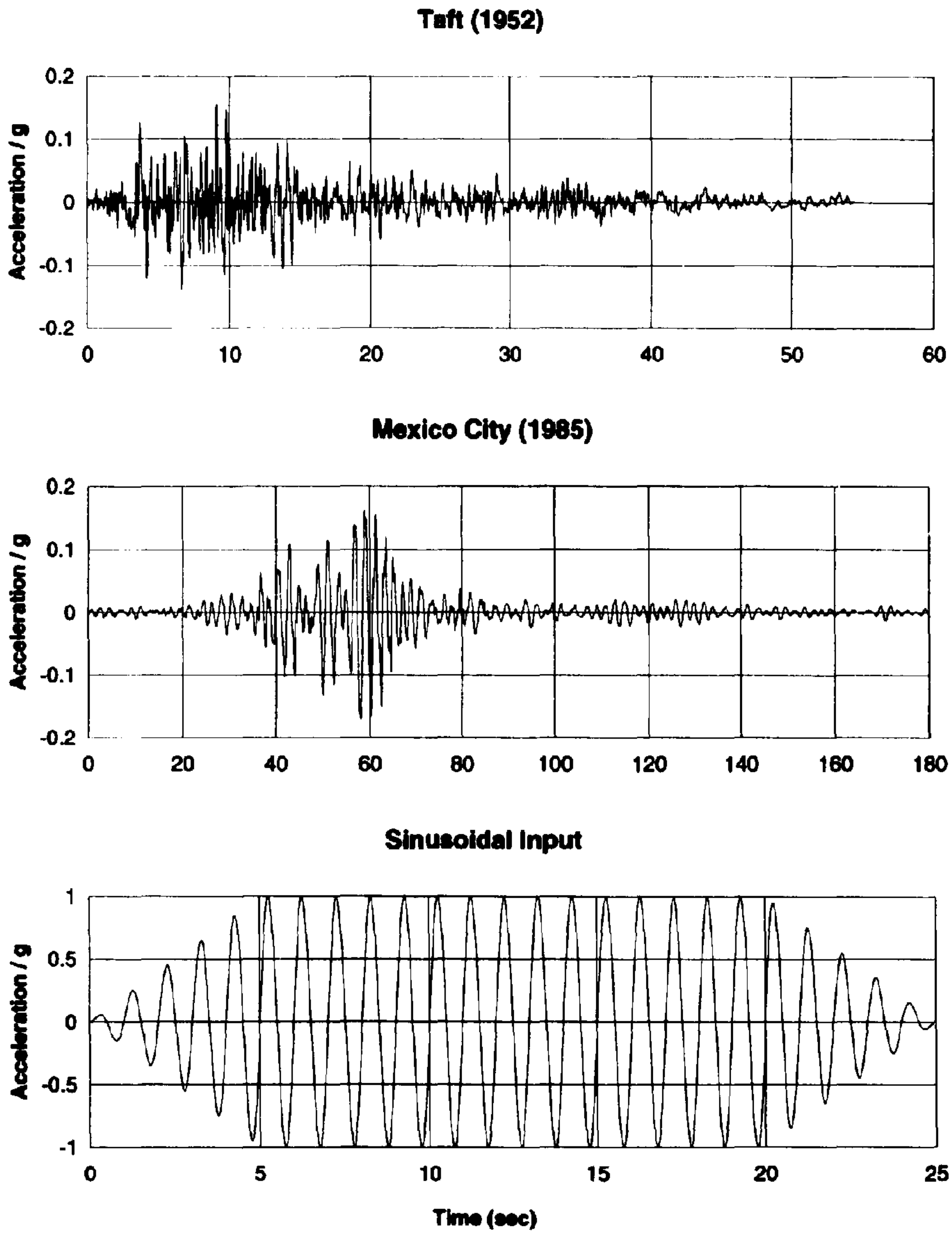

Fig. 4-4 Continuation

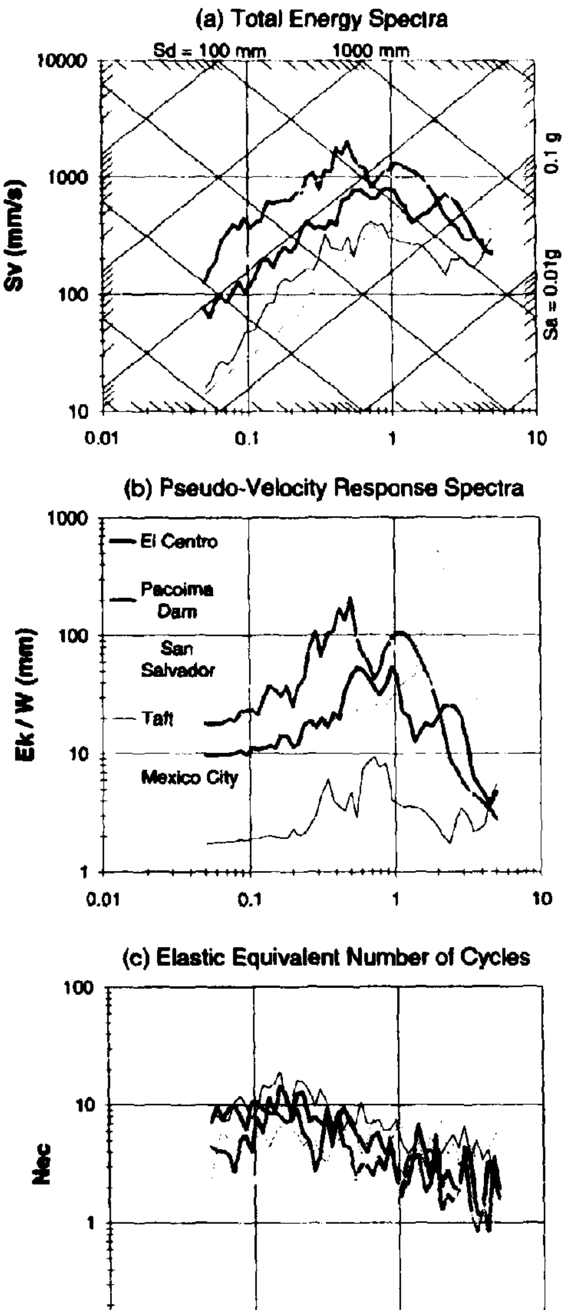

Fig. 4-5 Total Energy, Pseudo-Velocity and Equivalent Number of Cycles of Elastic Structures for Different Types of Input Motion and 5% Viscous Damping Ratio

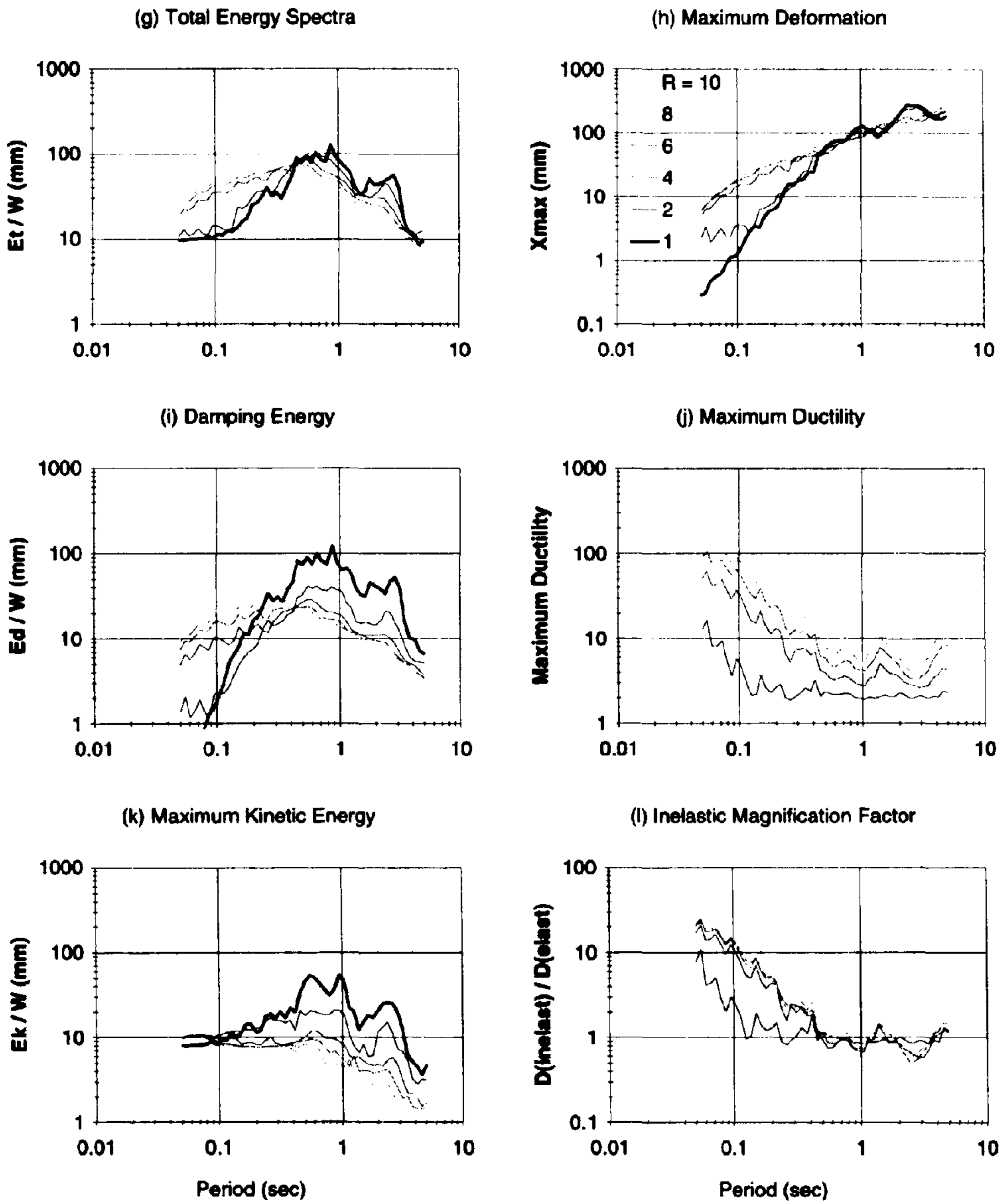

Fig. 4-6 Continued.

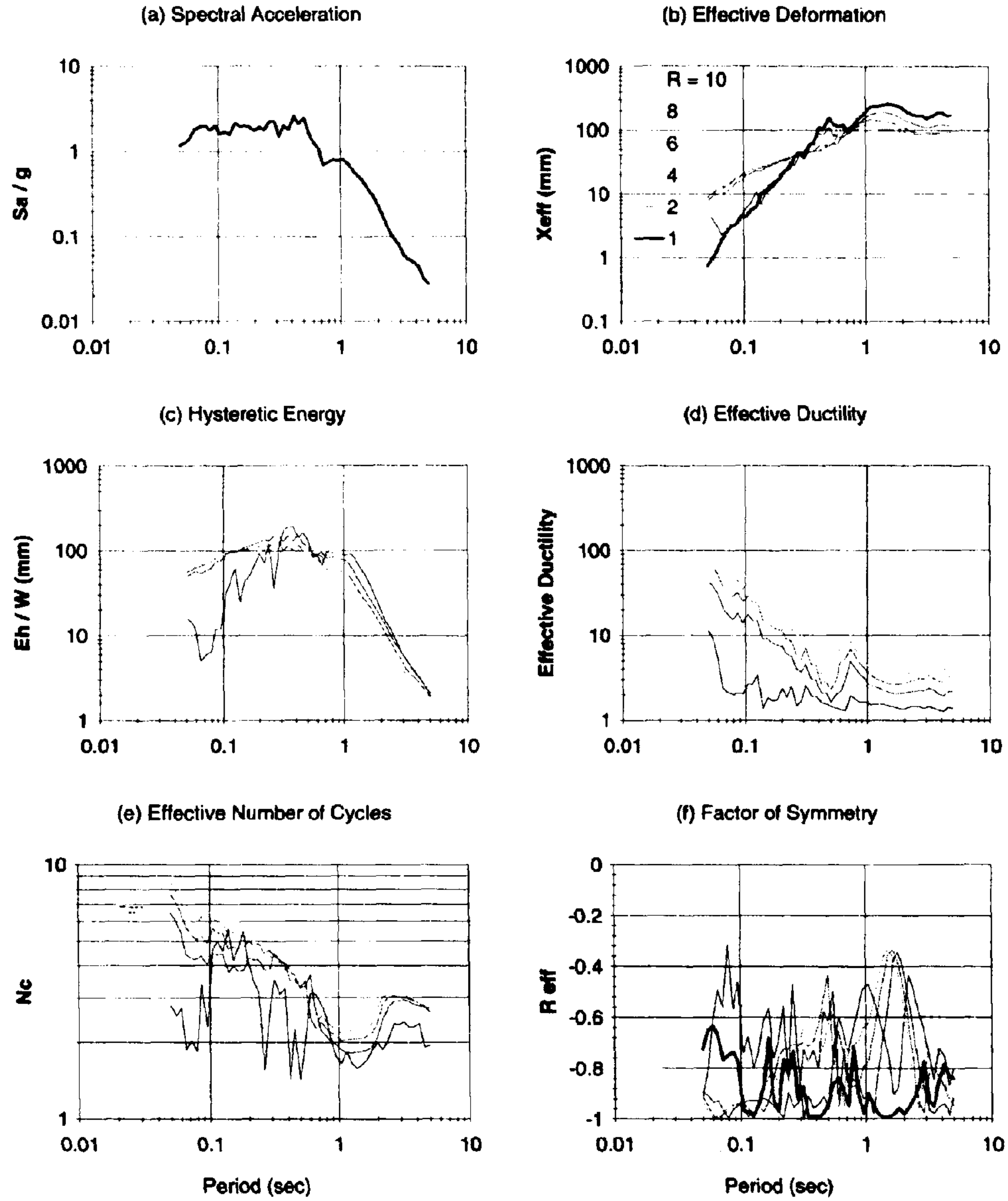

Fig. 4-7 Energy, Ductility and Low-Cycle Fatigue Demand Spectra for Pacoima Dam (1971), with 5% Viscous Damping Ratio and PGA = 1.17 g. (Smooth Model)

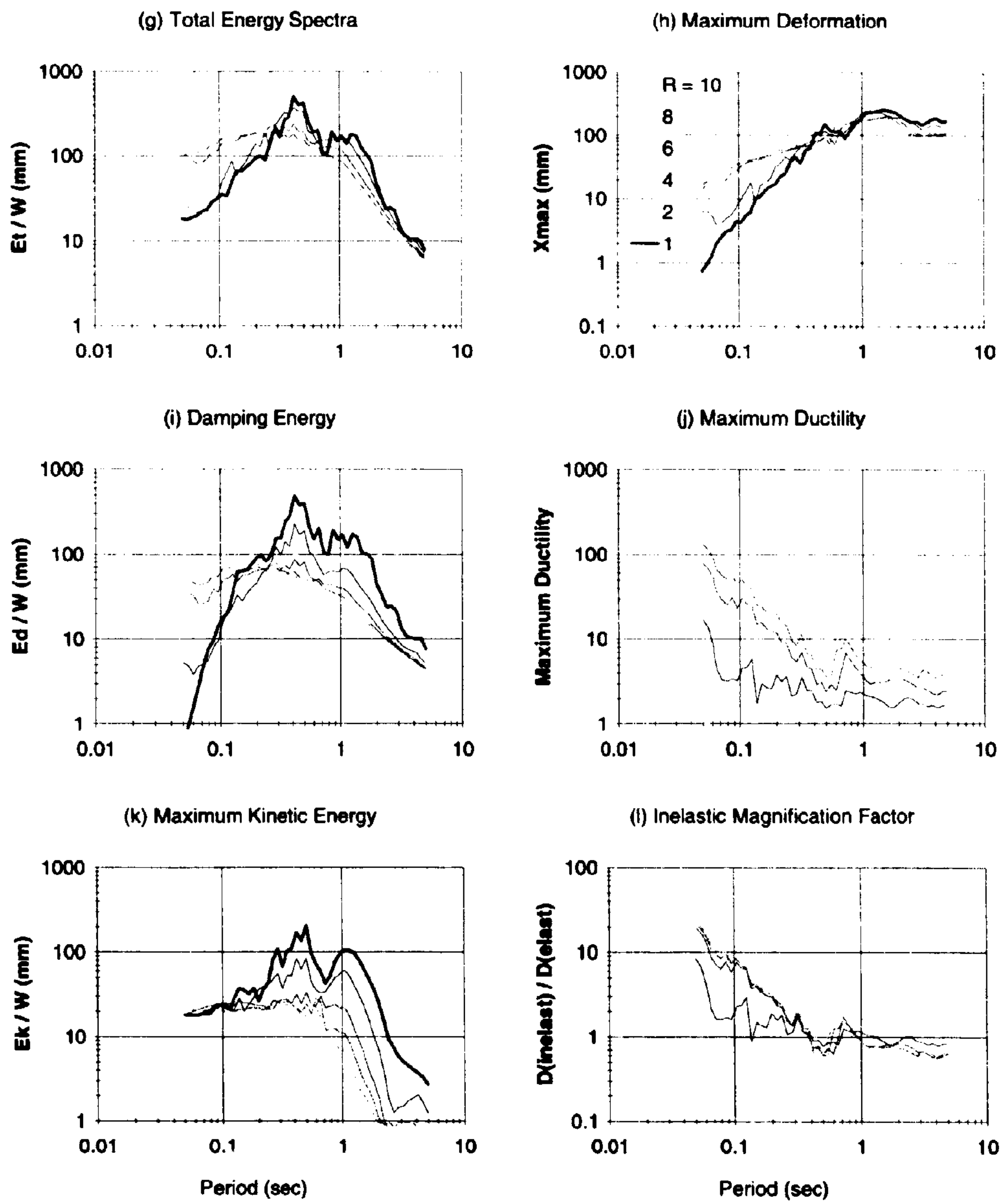

Fig. 4-7 Continued.

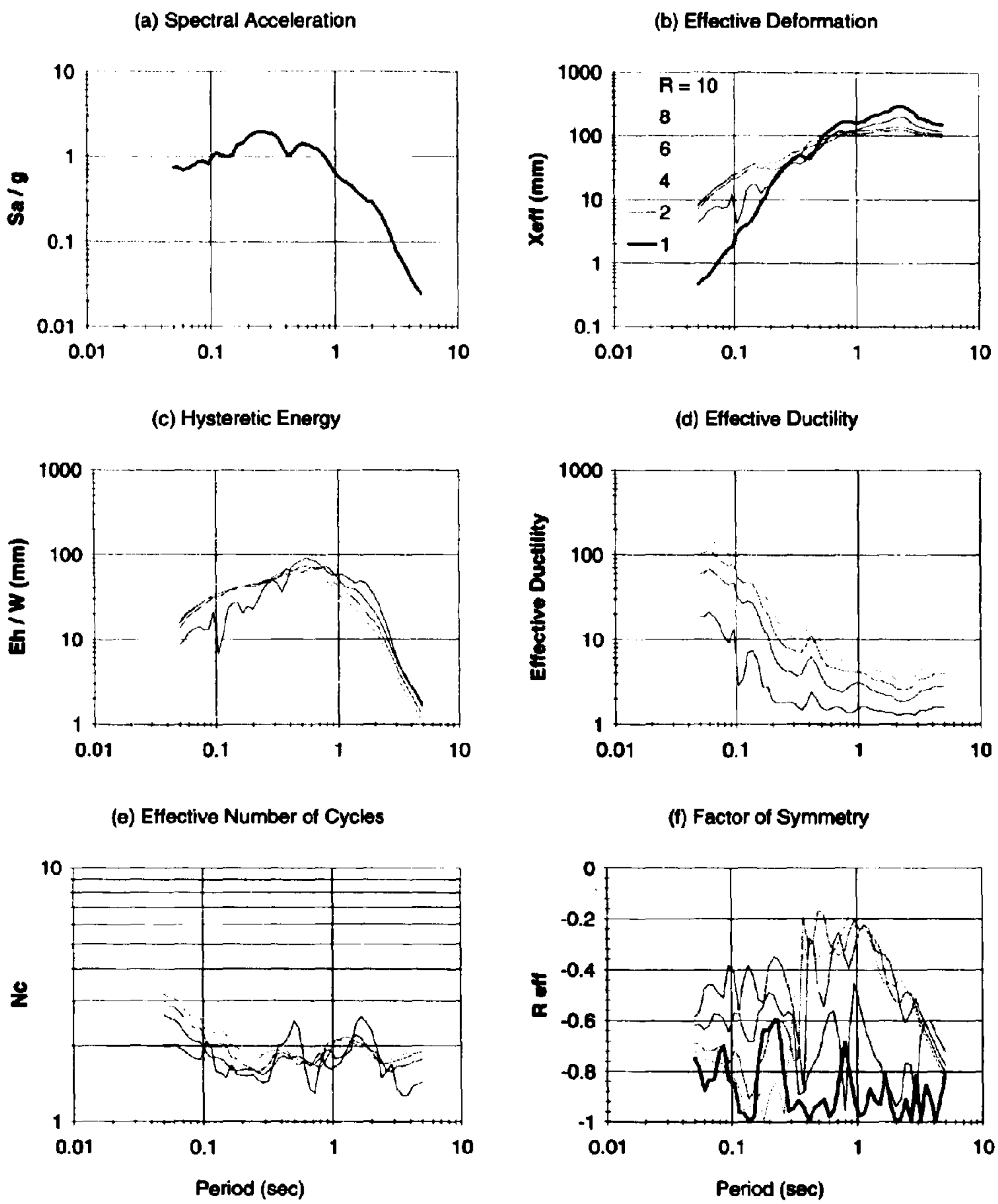

Fig. 4-8 Energy, Ductility and Low-Cycle Fatigue Demand Spectra for San Salvador (1986), with 5% Viscous Damping Ratio and PGA = 0.695 g. (Smooth Model)

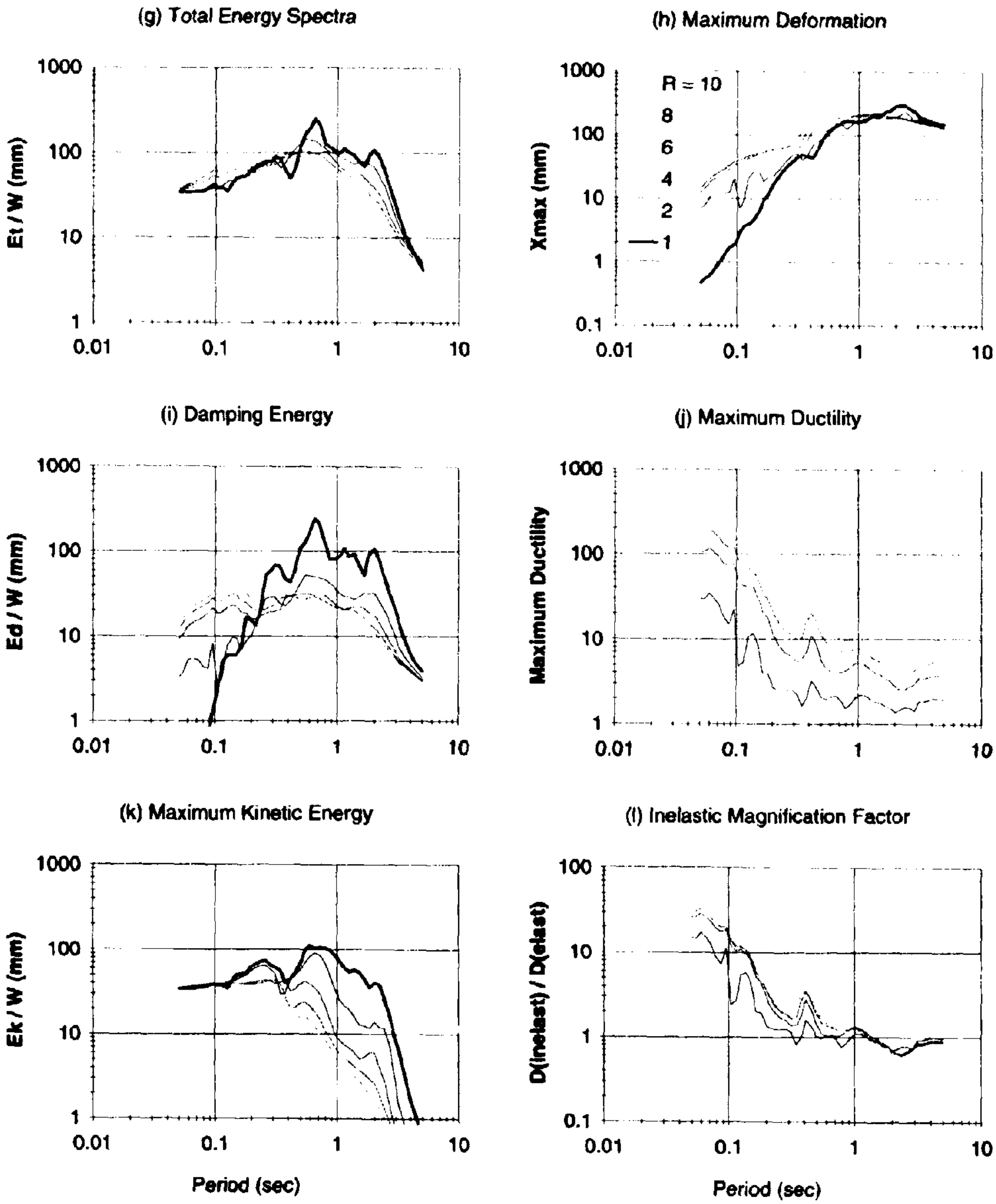

Fig. 4-8 Continued.

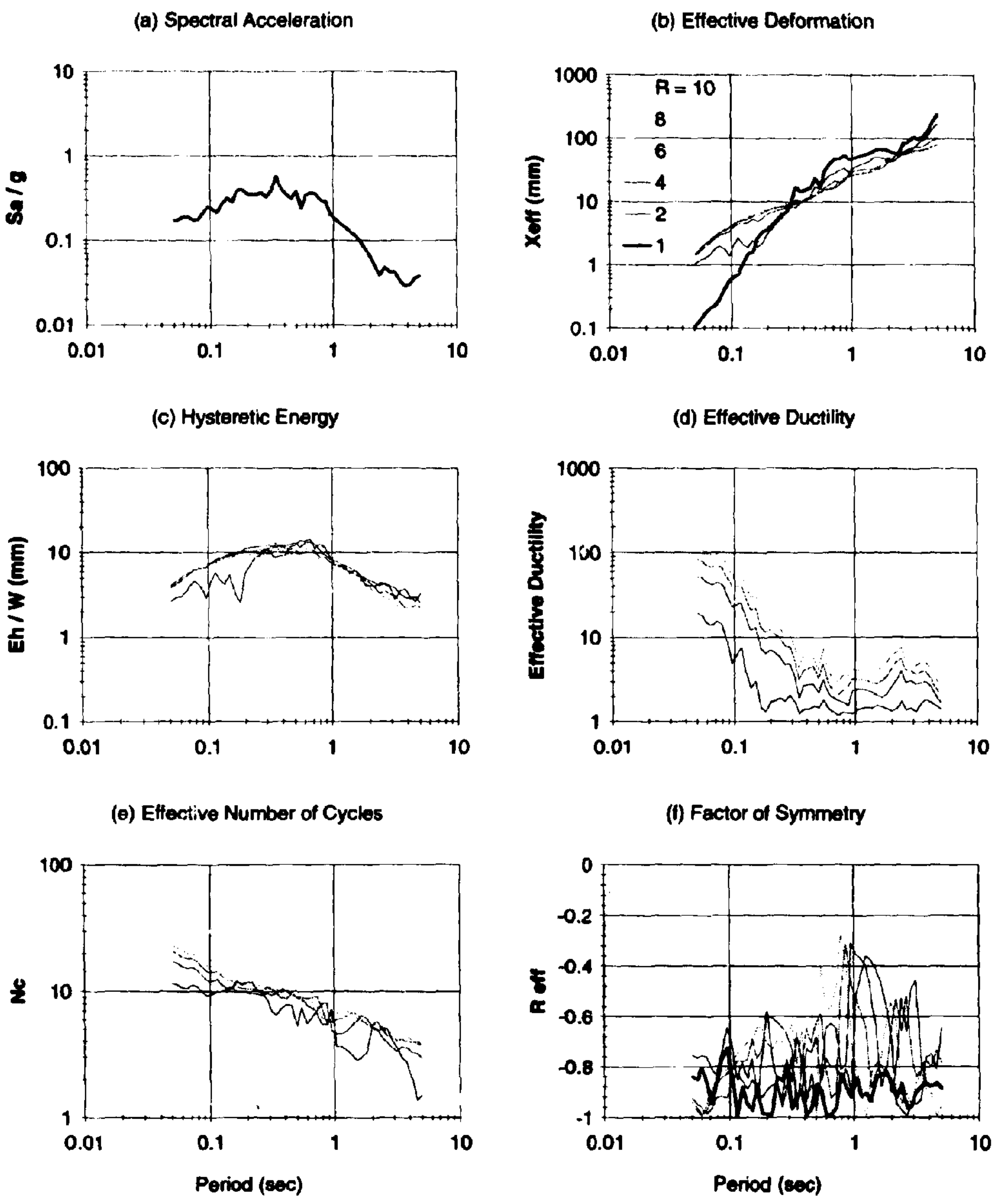

Fig. 4-9 Energy, Ductility and Low-Cycle Fatigue Demand Spectra for Taft (1952) N21E, with 5% Viscous Damping Ratio and PGA = 0.156 g. (Smooth Model)

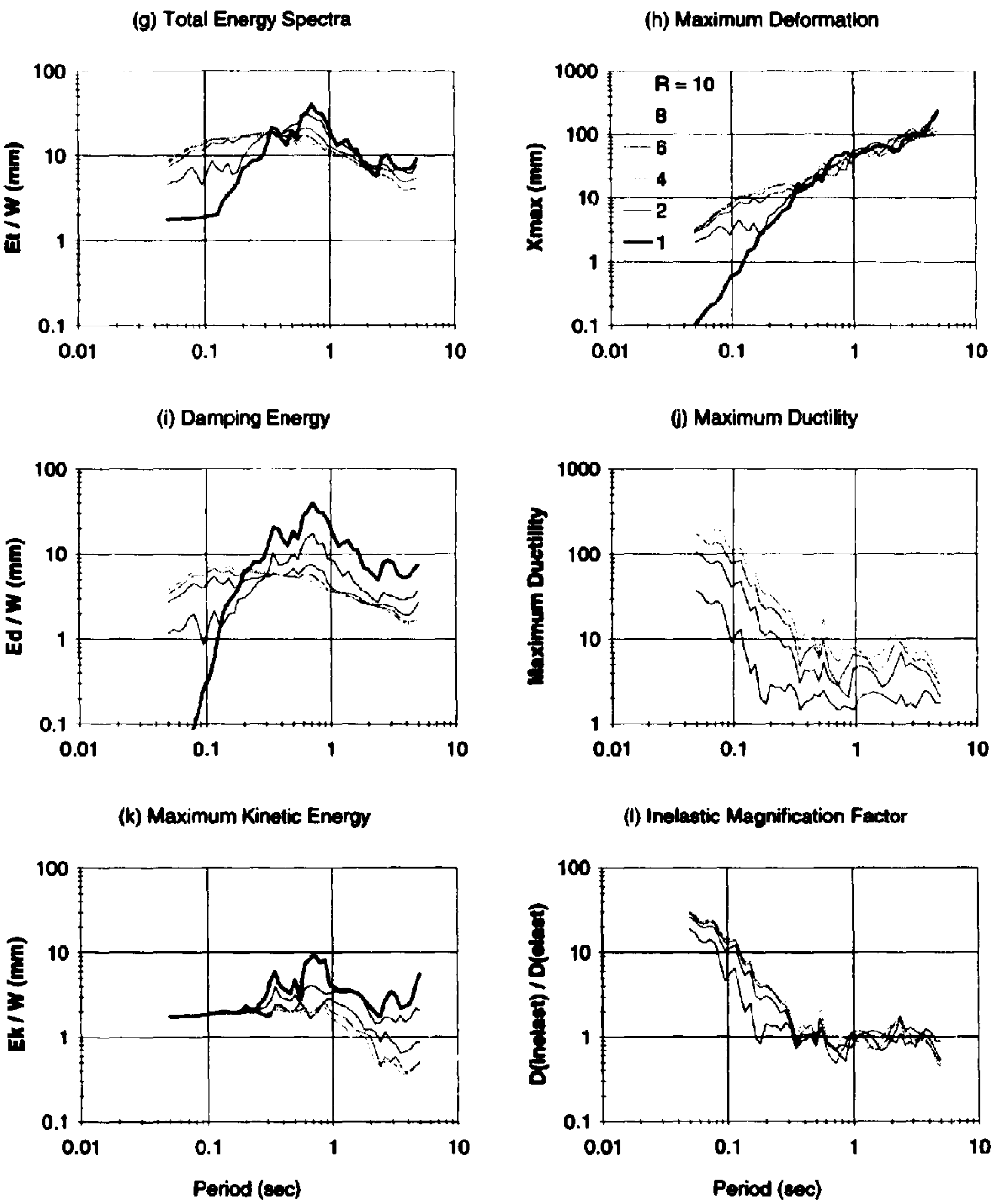

Fig. 4-9 Continued.

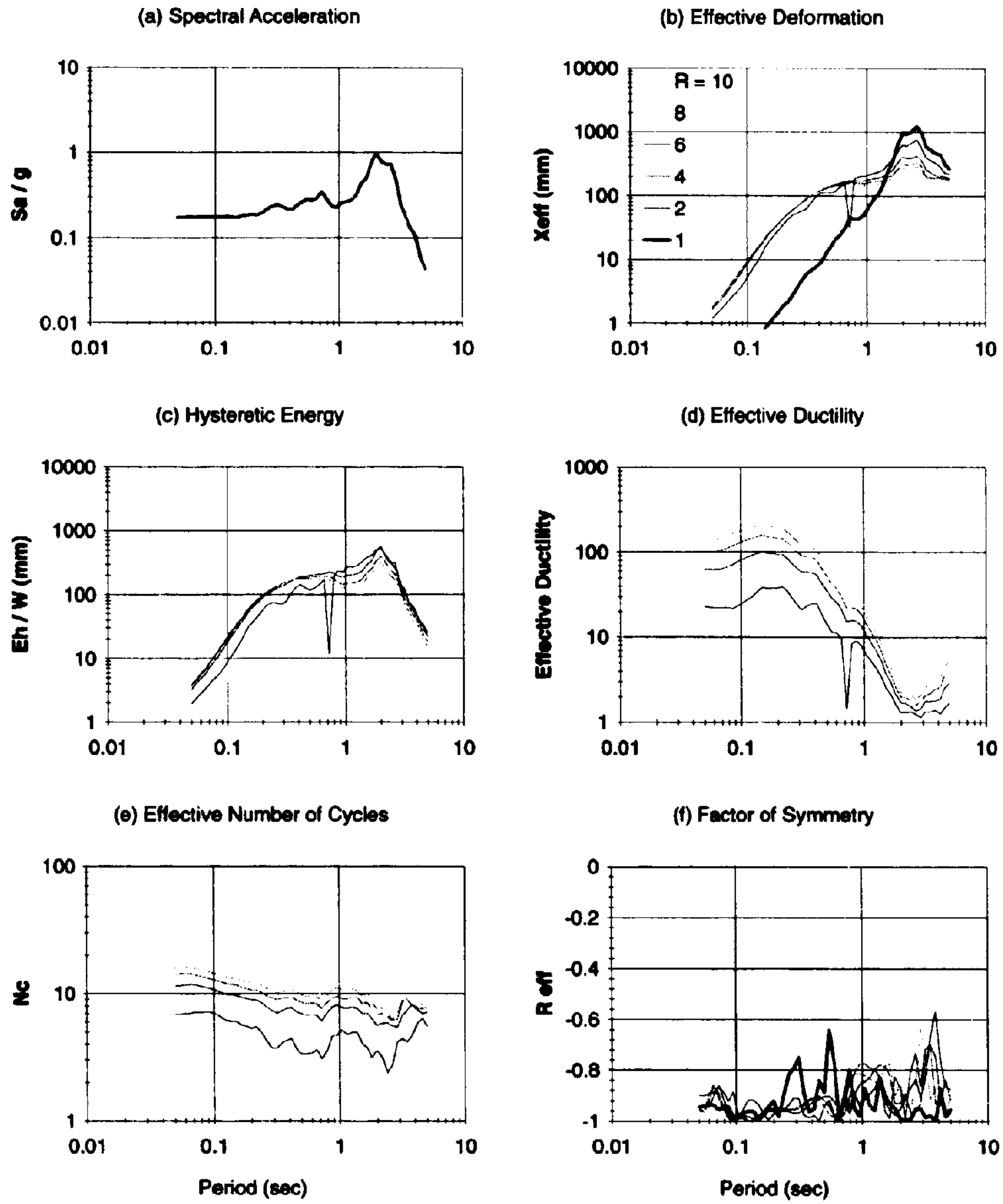

Fig. 4-10 Energy, Ductility and Low-Cycle Fatigue Demand Spectra for Mexico City (1985), with 5% Viscous Damping Ratio and PGA = 0.171 g. (Smooth Model)

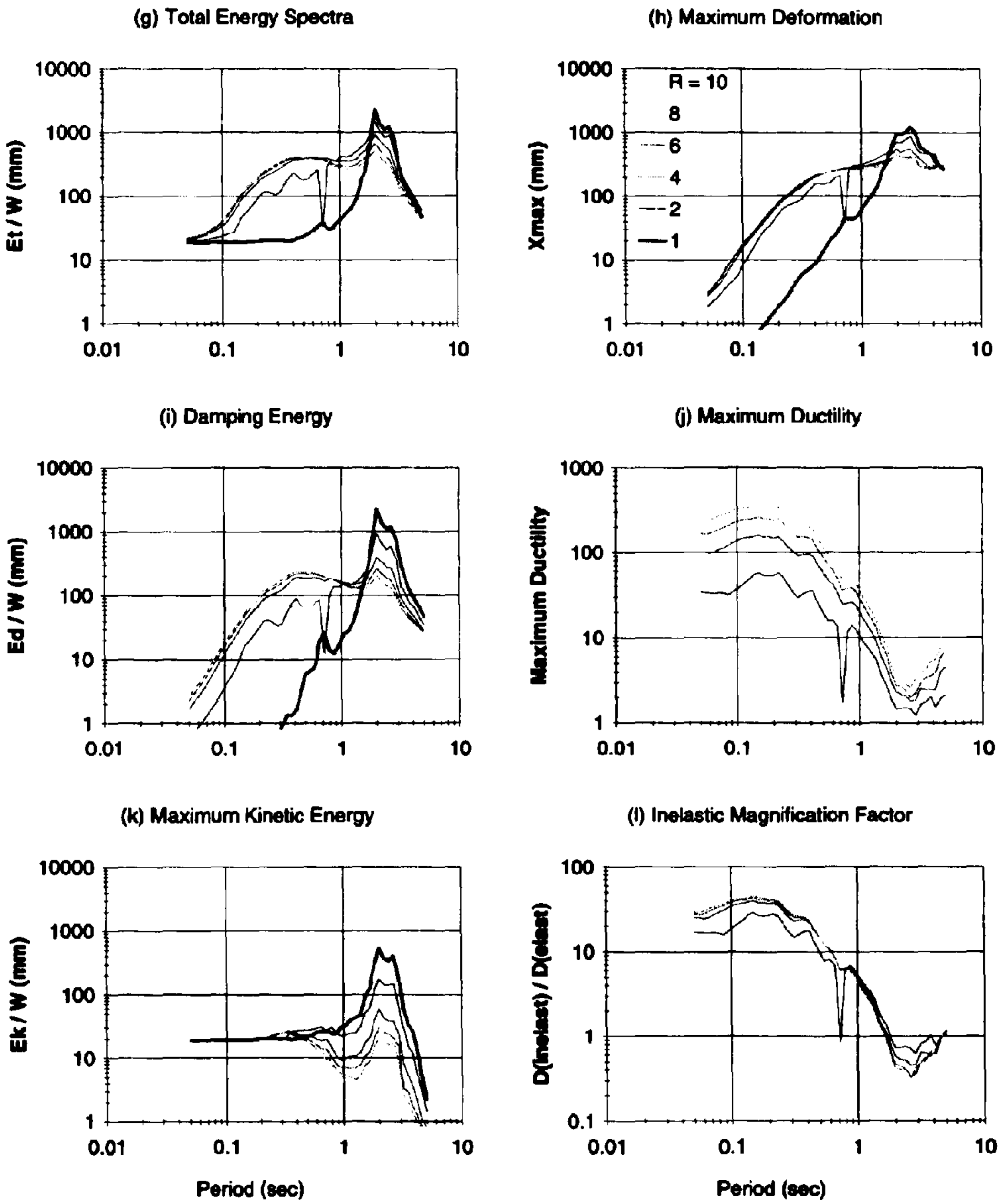

Fig. 4-10 Continued.

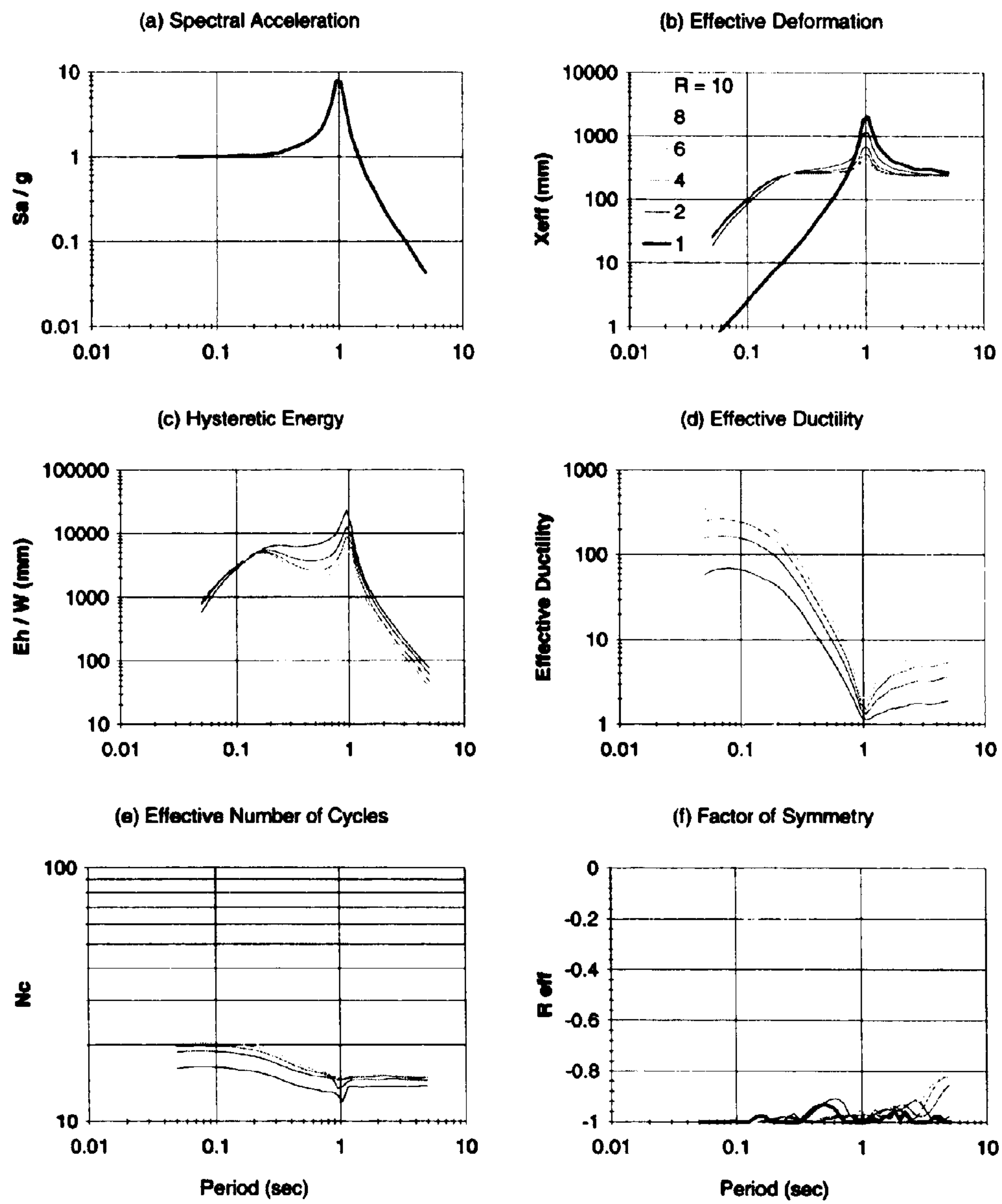

Fig. 4-11 Energy, Ductility and Low-Cycle Fatigue Demand Spectra for Sinusoidal Input, with 5% Viscous Damping Ratio and PGA = 1.0 g. (Smooth Model)

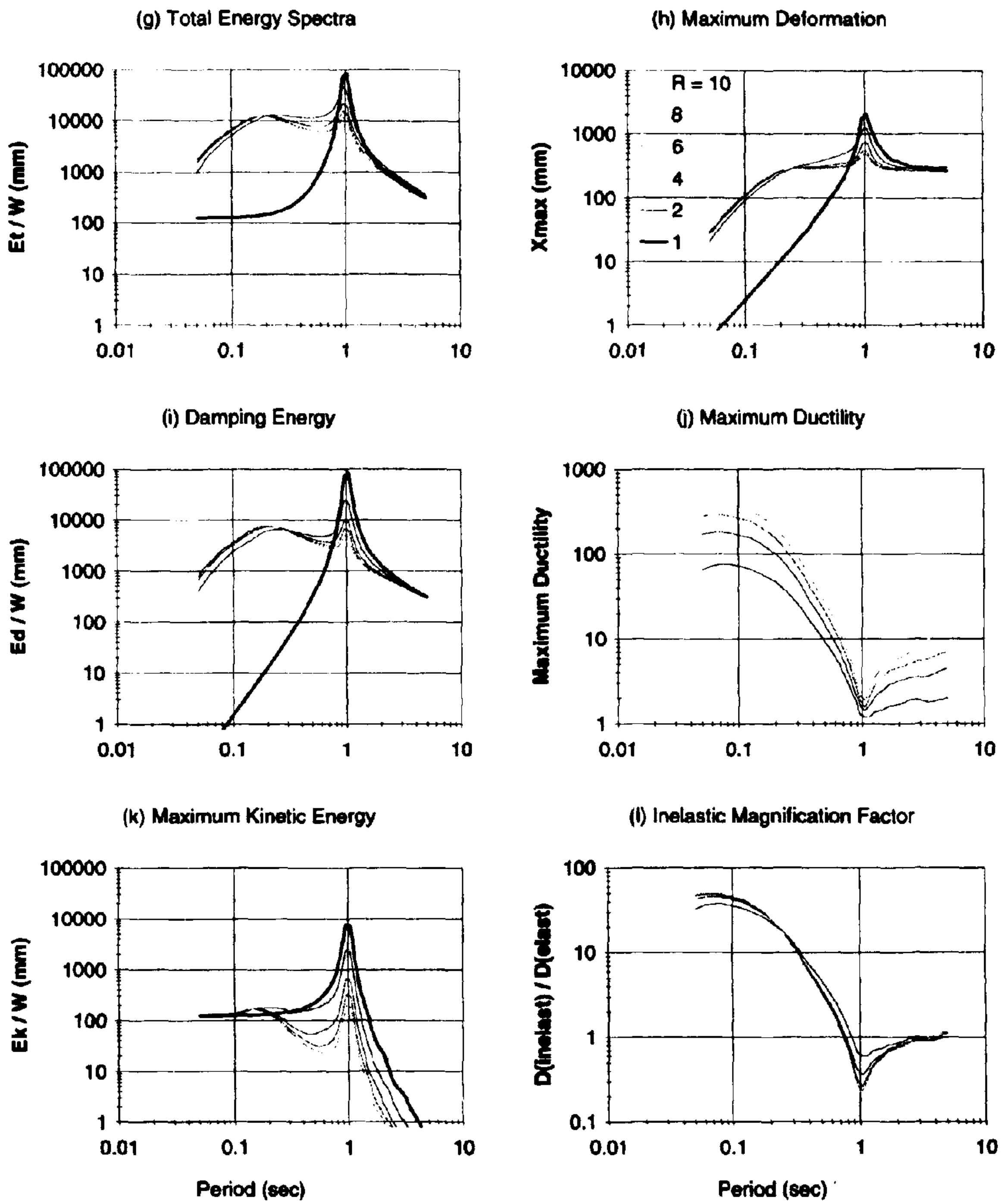

Fig. 4-11 Continued.

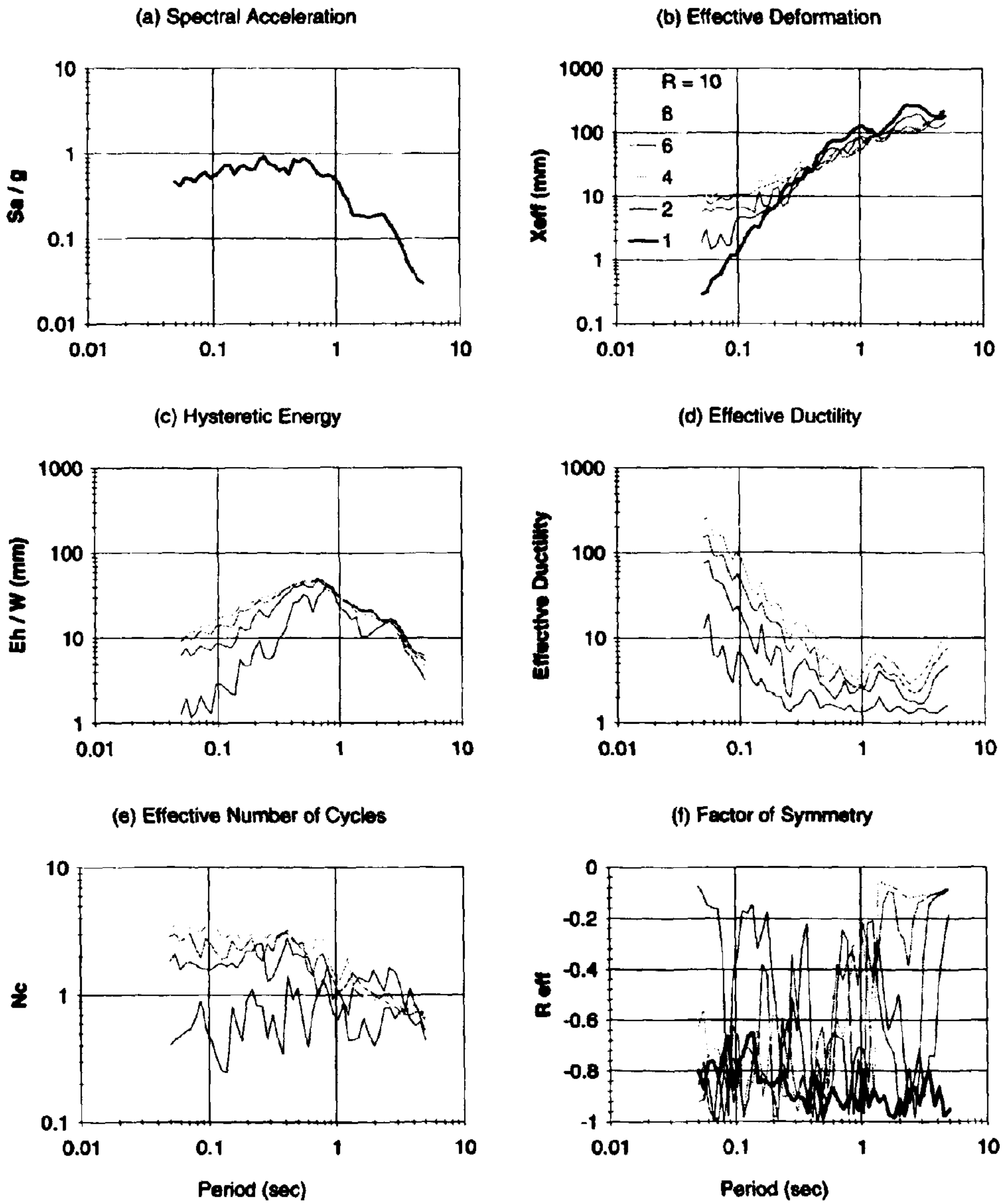

Fig. 4-12 Energy, Ductility and Low-Cycle Fatigue Demand Spectra for El Centro (1940) N-S, with 5% Viscous Damping Ratio and PGA = 0.348 g. (Elasto-Perfectly Plastic Model)

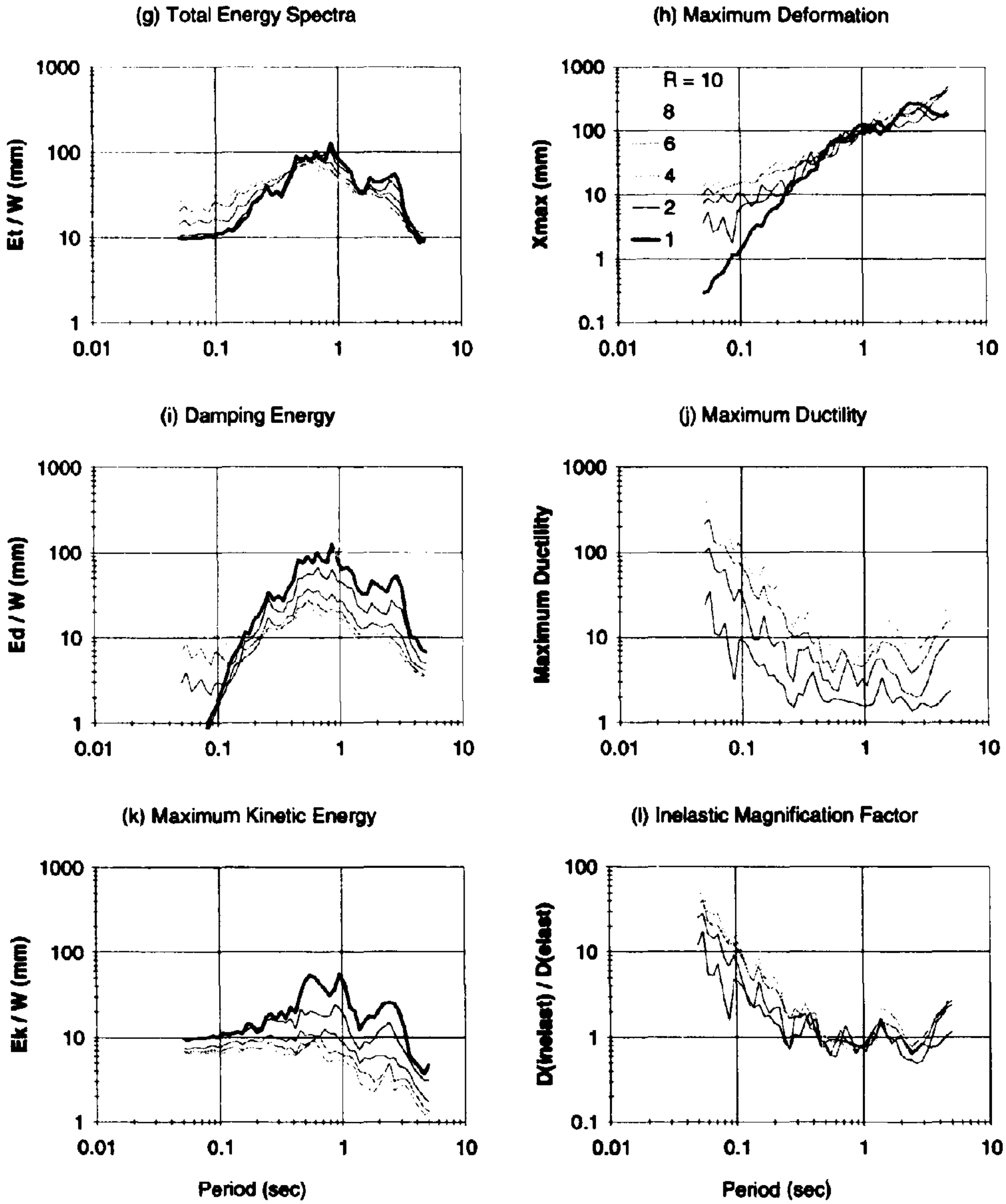

Fig. 4-12 Continued.

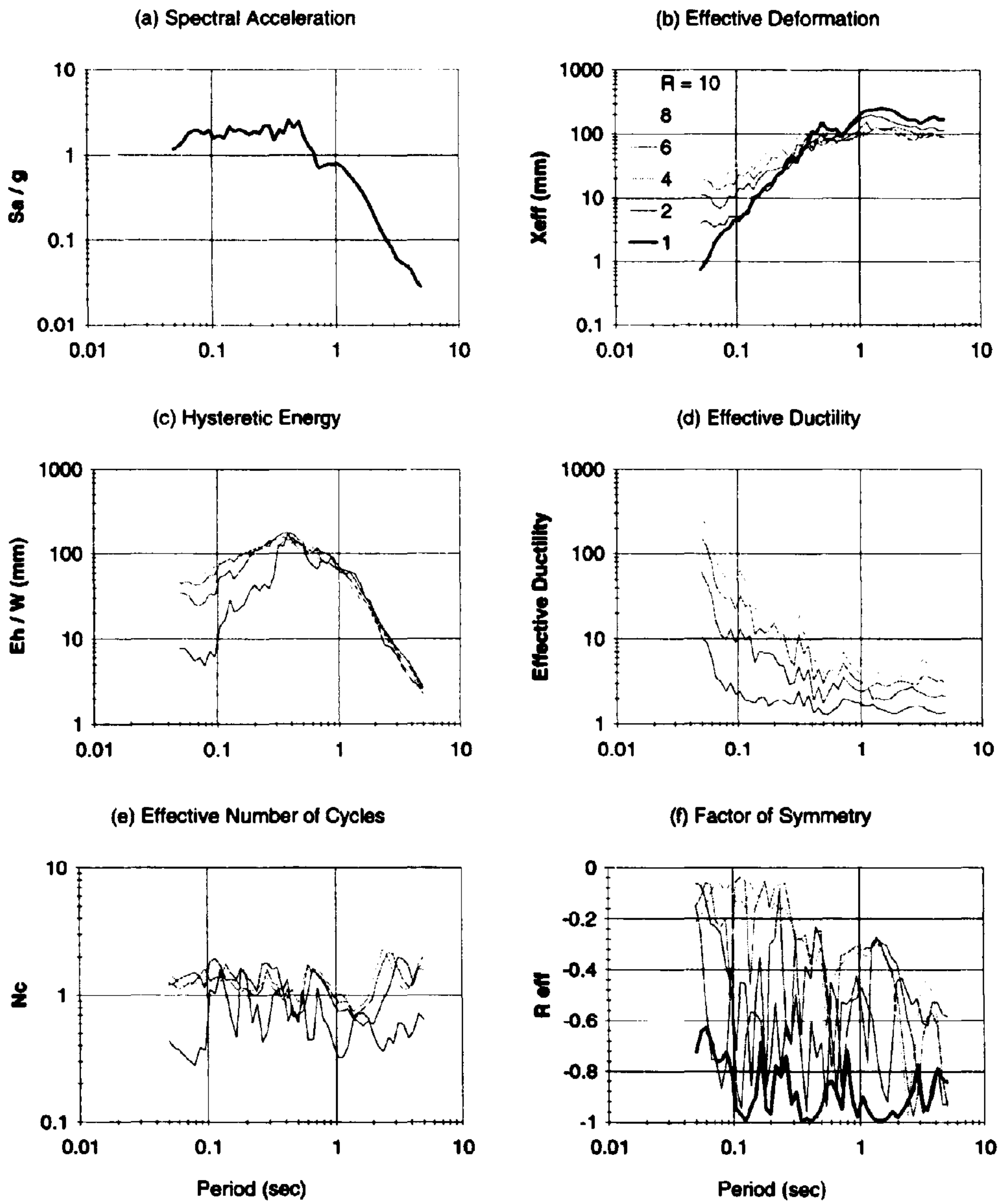

Fig. 4-13 Energy, Ductility and Low-Cycle Fatigue Demand Spectra for Pacoima Dam (1971), with 5% Viscous Damping Ratio and PGA = 1.17 g. (Elasto-Perfectly Plastic Model)

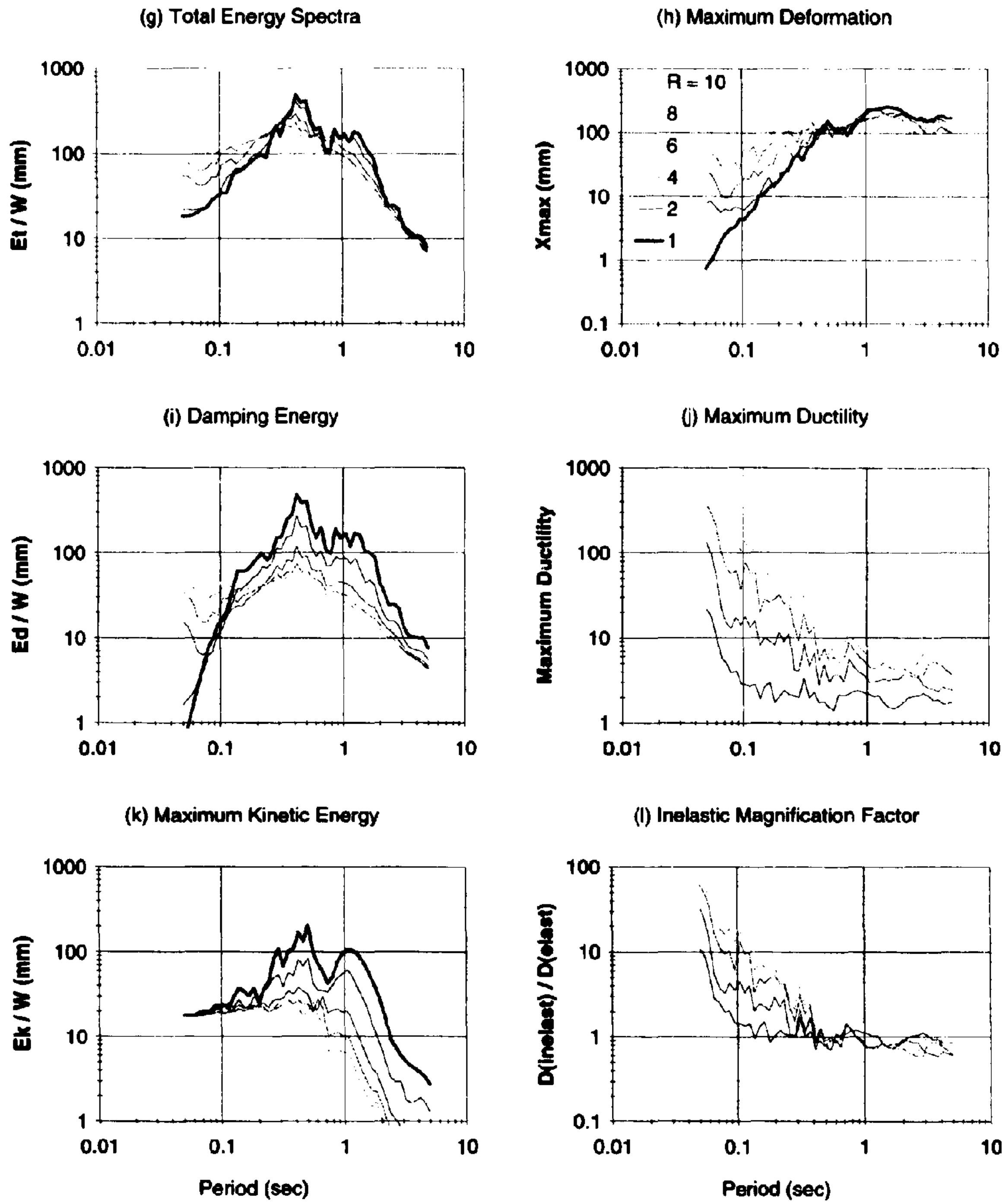

Fig. 4-13 Continued.

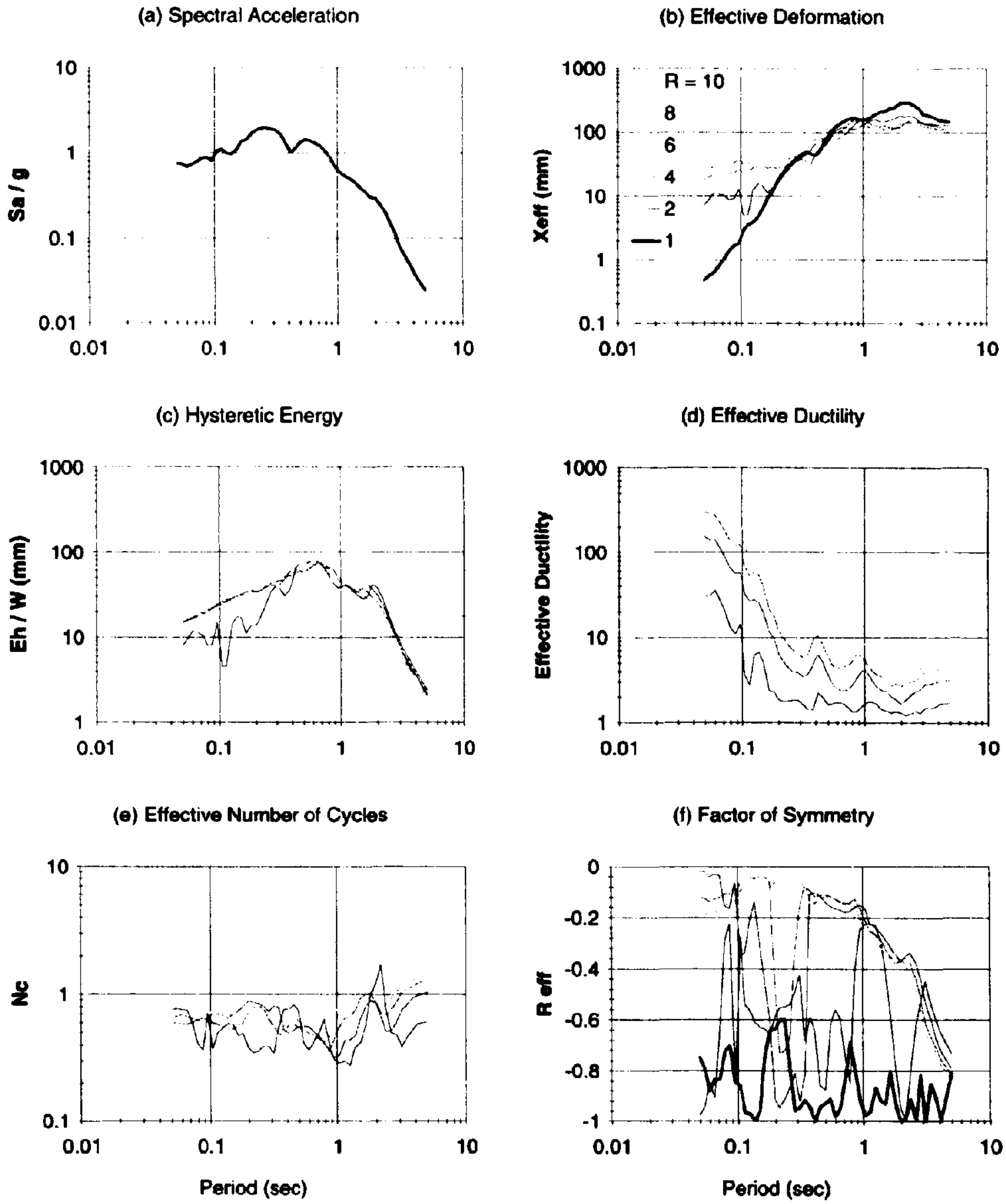

Fig. 4-14 Energy, Ductility and Low-Cycle Fatigue Demand Spectra for San Salvador (1986), with 5% Viscous Damping Ratio and PGA = 0.695 g. (Elasto-Perfectly Plastic Model)

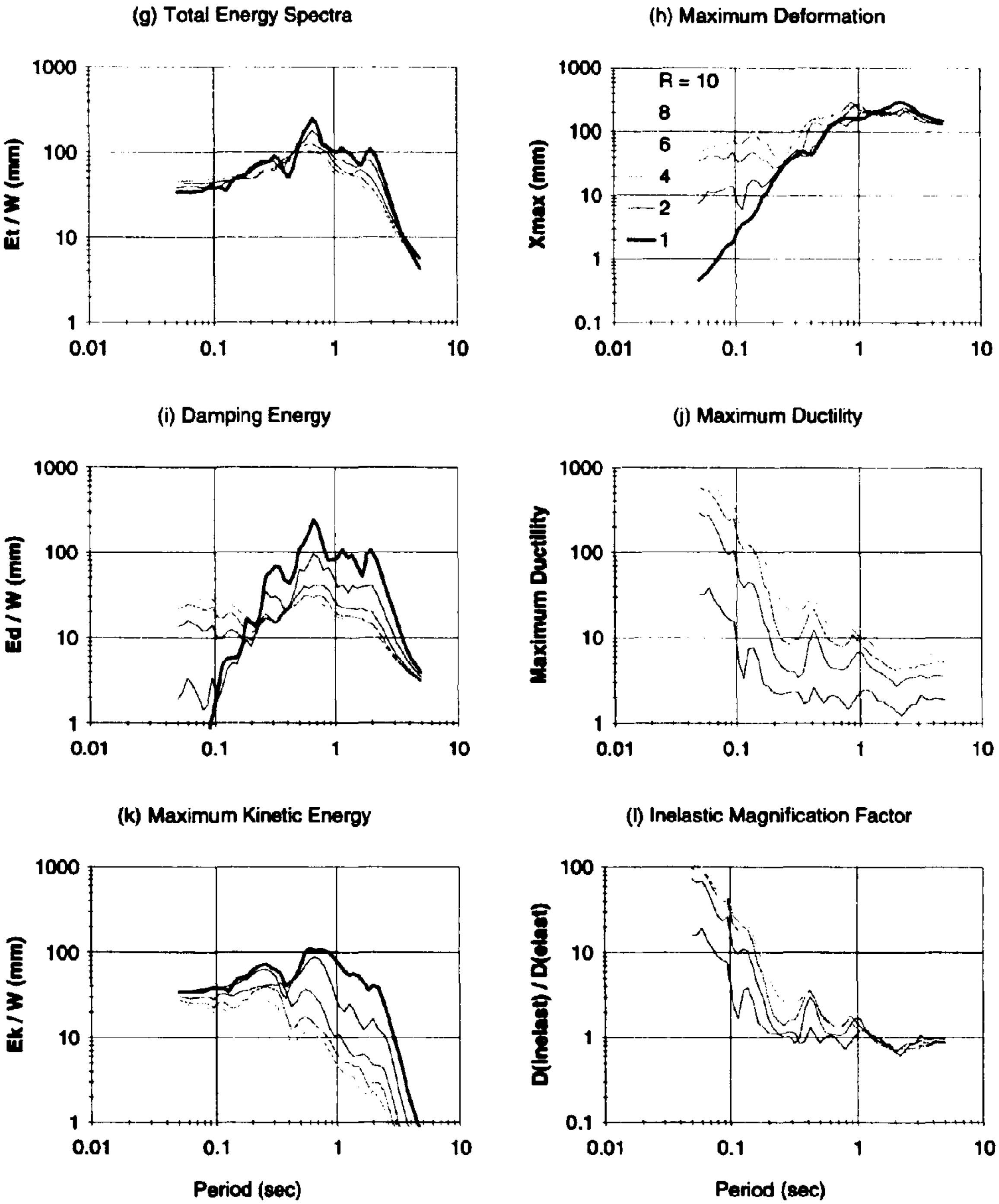

Fig. 4-14 Continued.

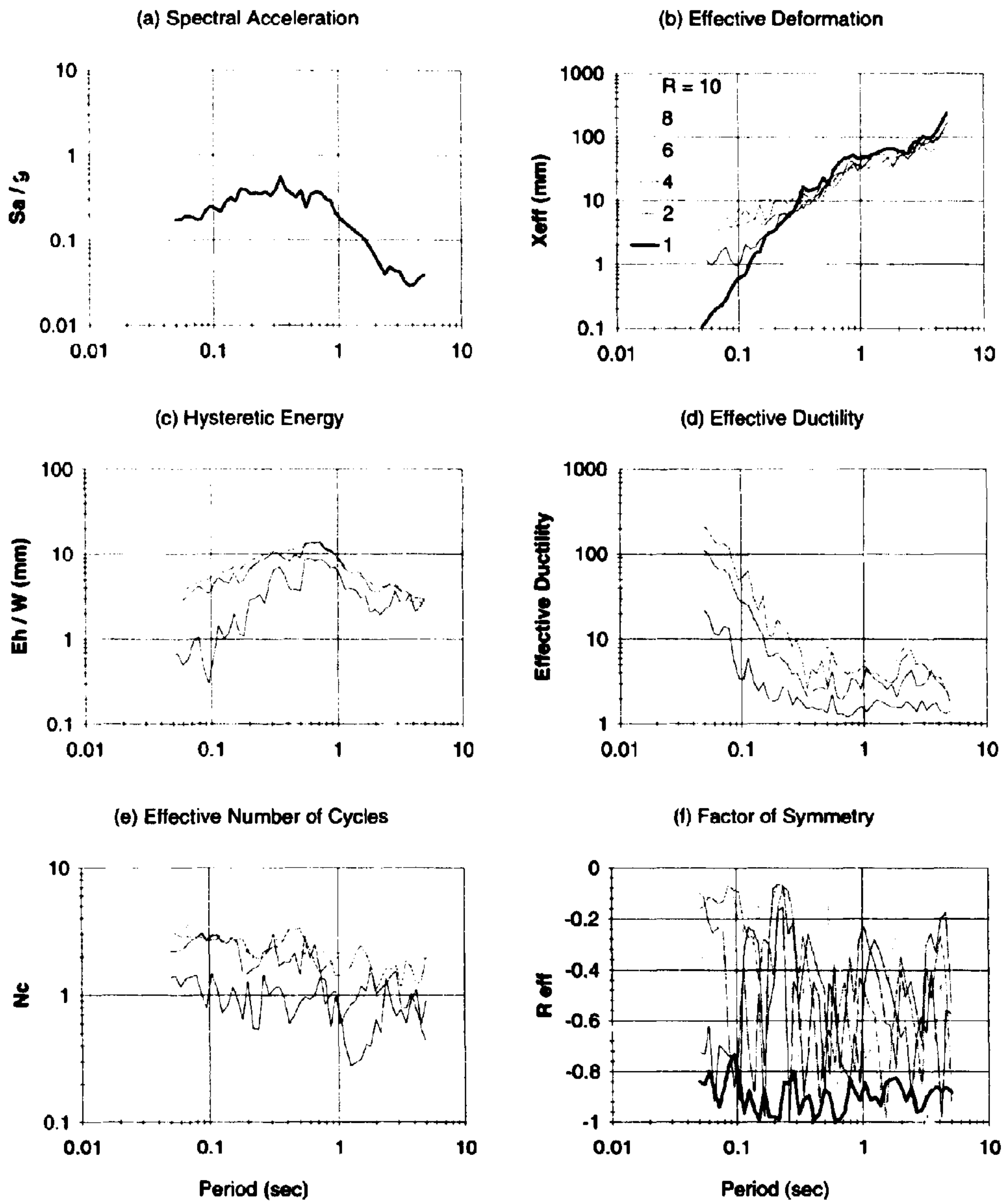

Fig. 4-15 Energy, Ductility and Low-Cycle Fatigue Demand Spectra for Taft (1952) N21E, with 5% Viscous Damping Ratio and PGA = 0.156 g. (Elasto-Perfectly Plastic Model)

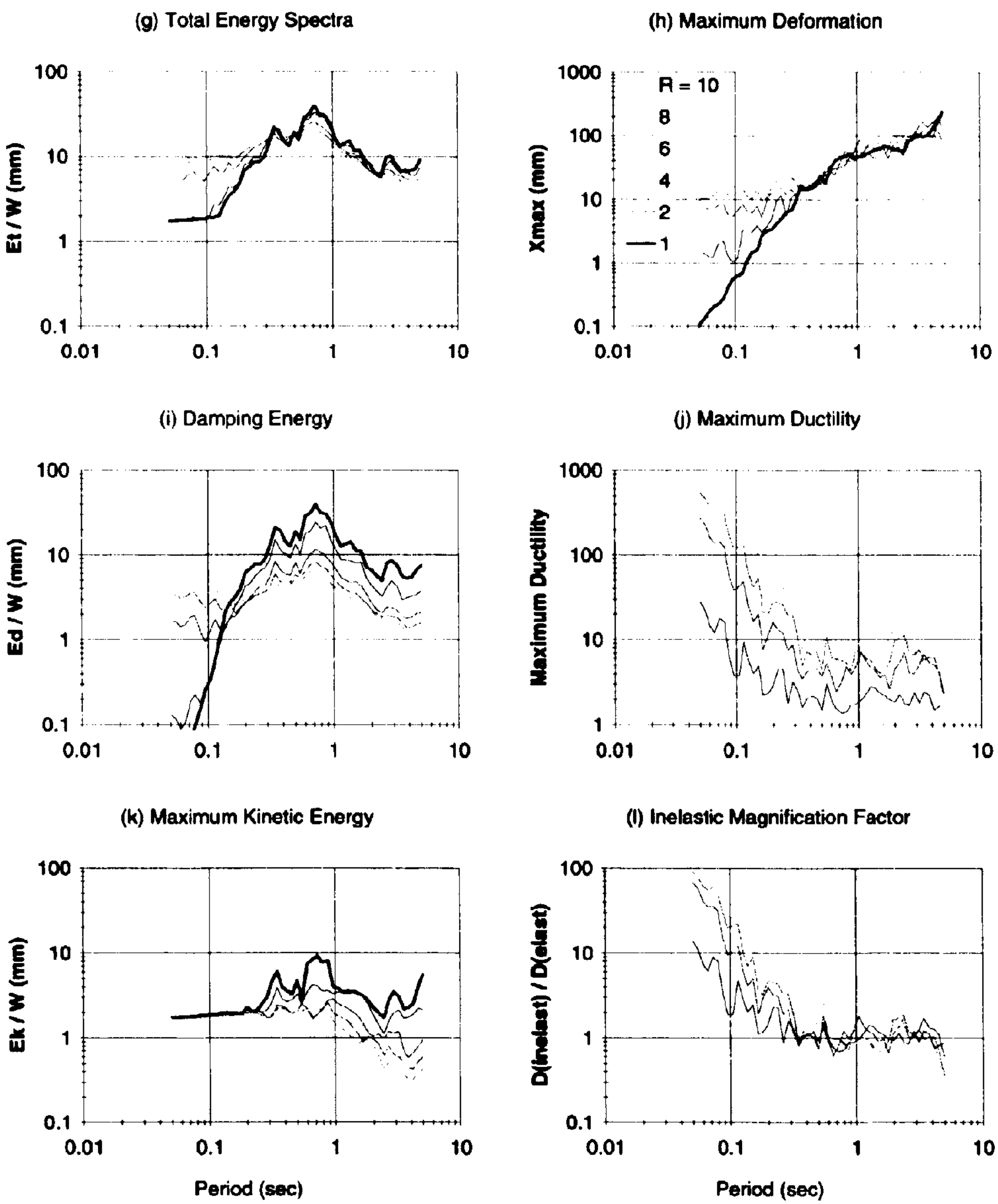

Fig. 4-15 Continued.

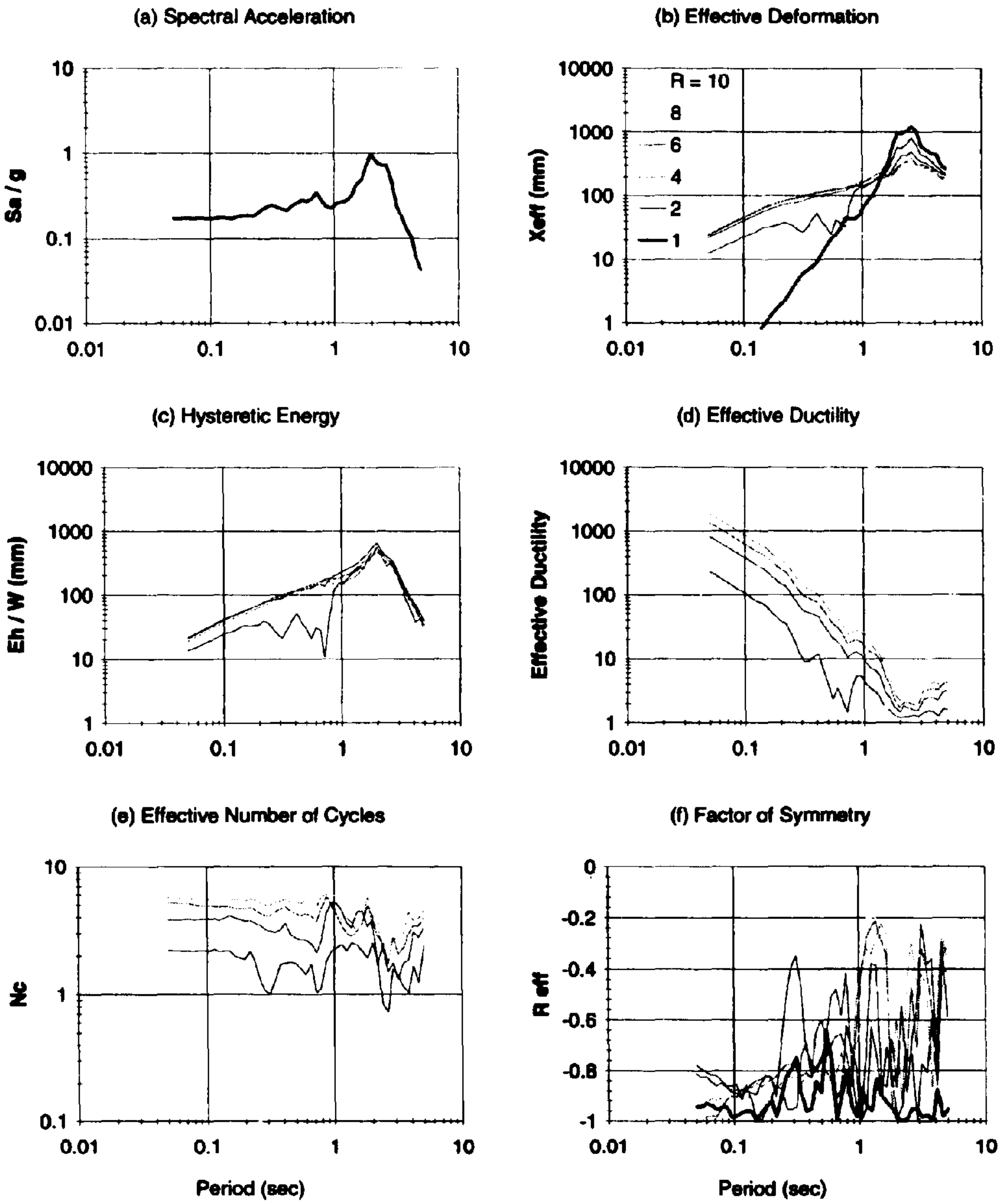

Fig. 4-16 Energy, Ductility and Low-Cycle Fatigue Demand Spectra for Mexico City (1985), with 5% Viscous Damping Ratio and PGA = 0.171 g. (Elasto-Perfectly Plastic Model)

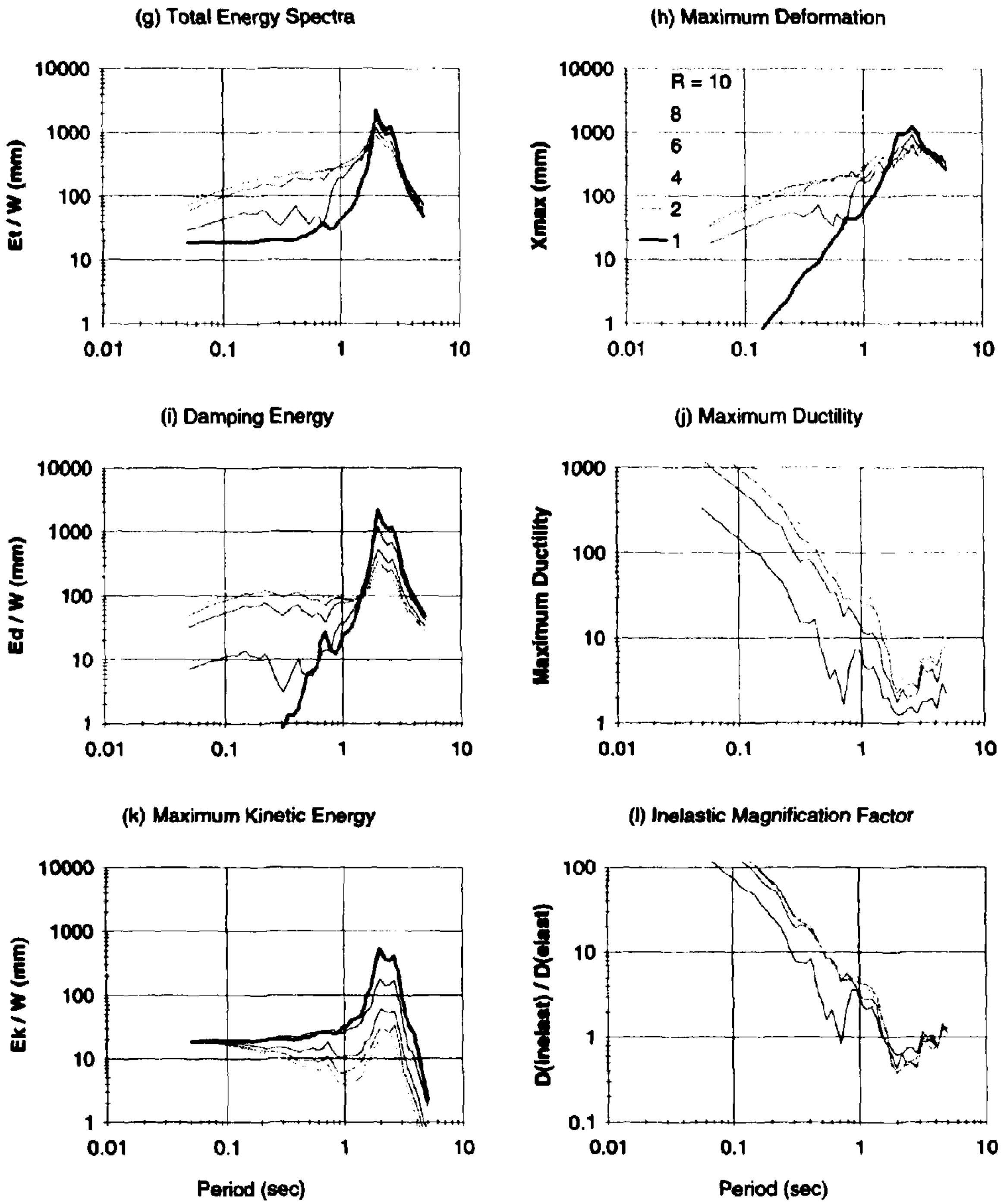

Fig. 4-16 Continued.

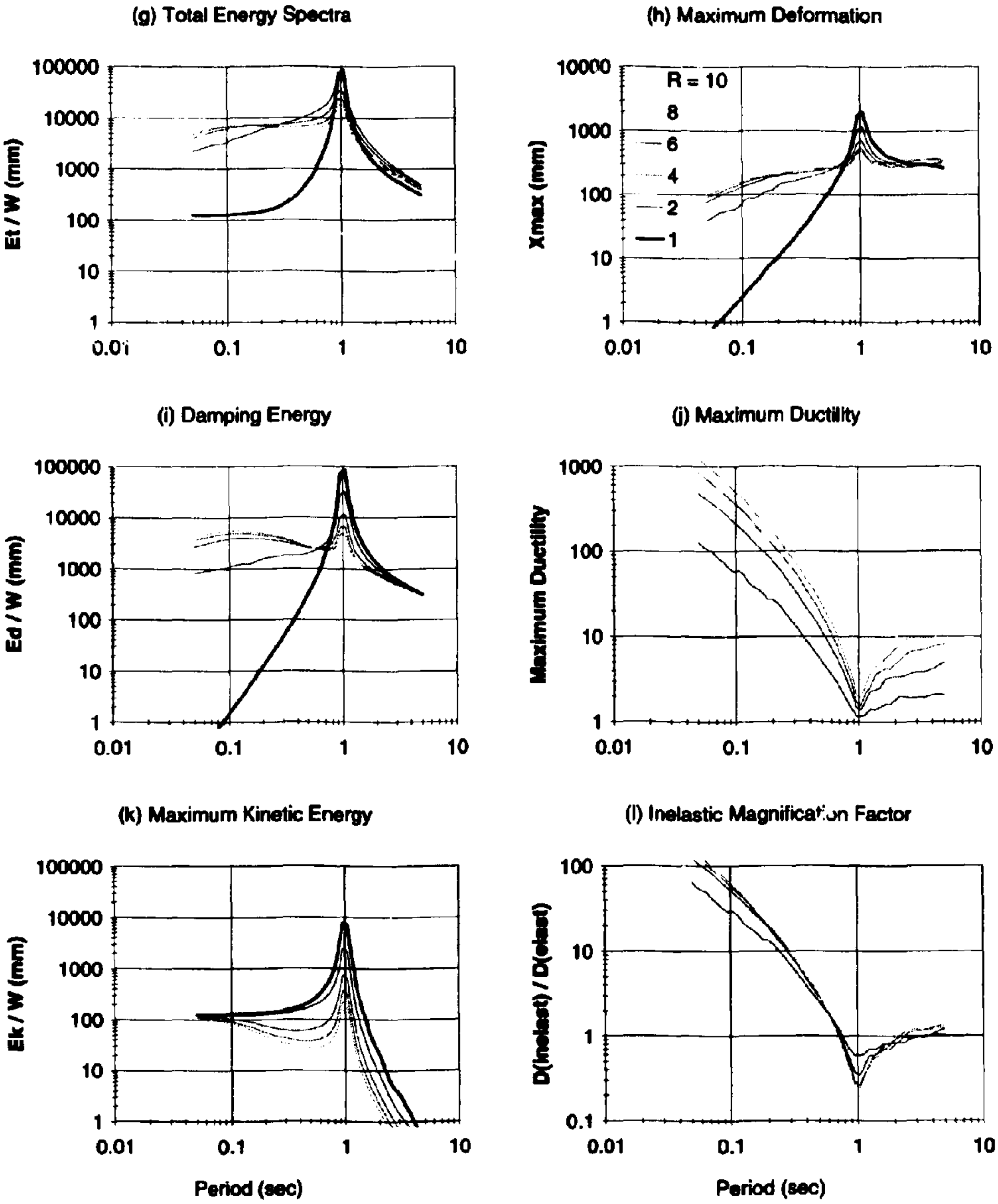

Fig. 4-17 Continued.

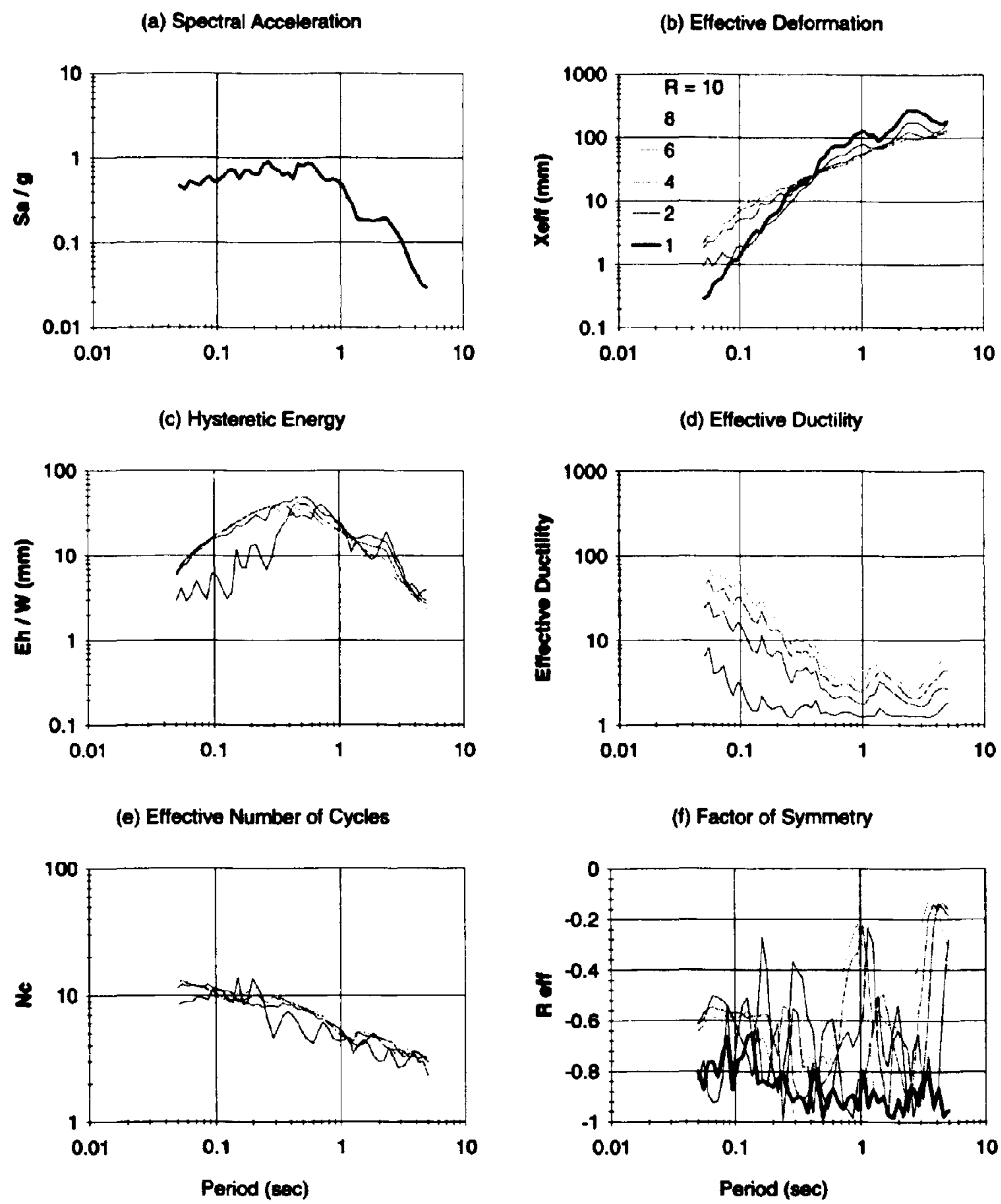

Fig. 4-18 Energy, Ductility and Low-Cycle Fatigue Demand Spectra for El Centro (1940) N-S, with 5% Viscous Damping Ratio and PGA = 0.348 g. (Modified Takeda Model)

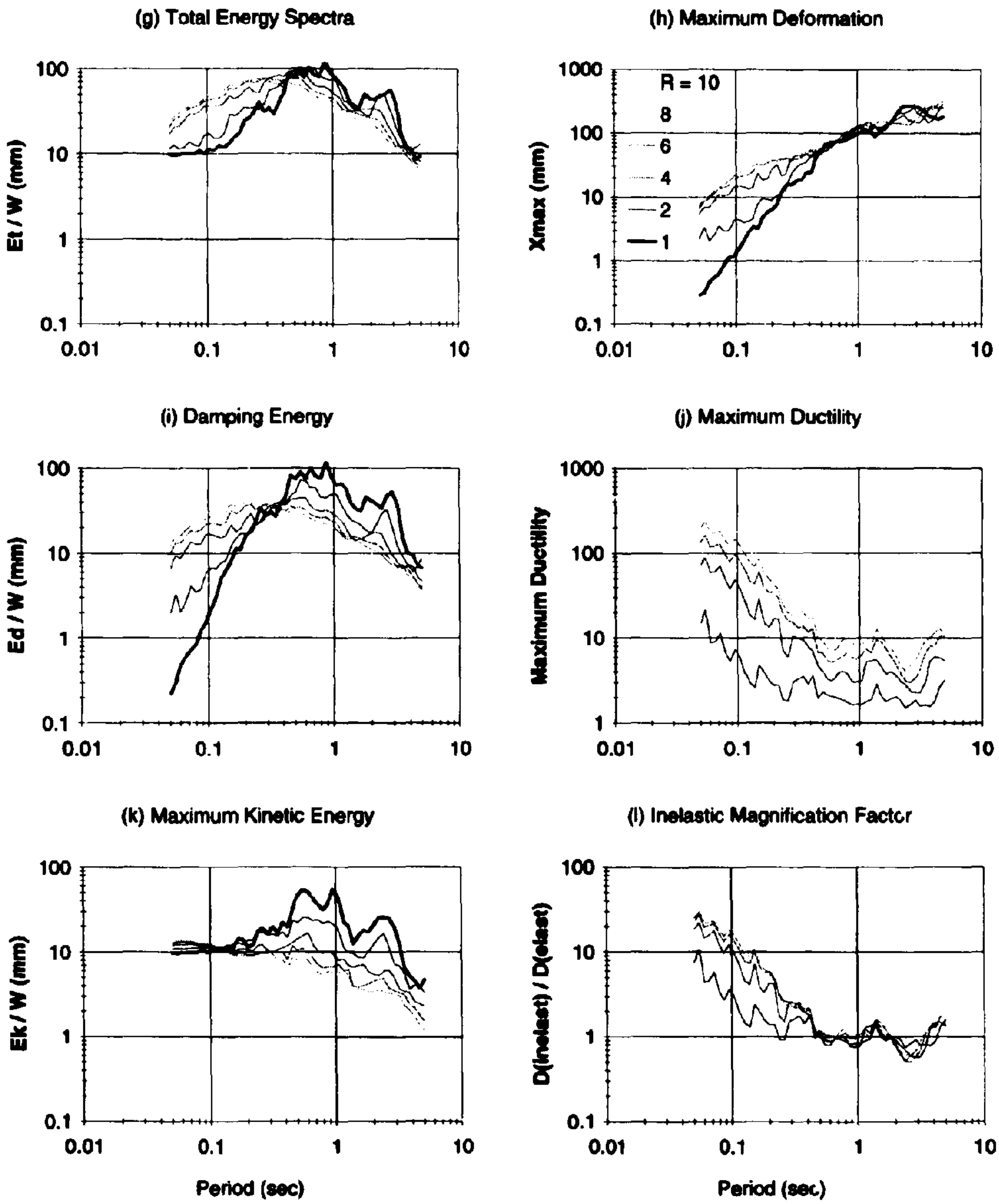

Fig. 4-18 Continued.

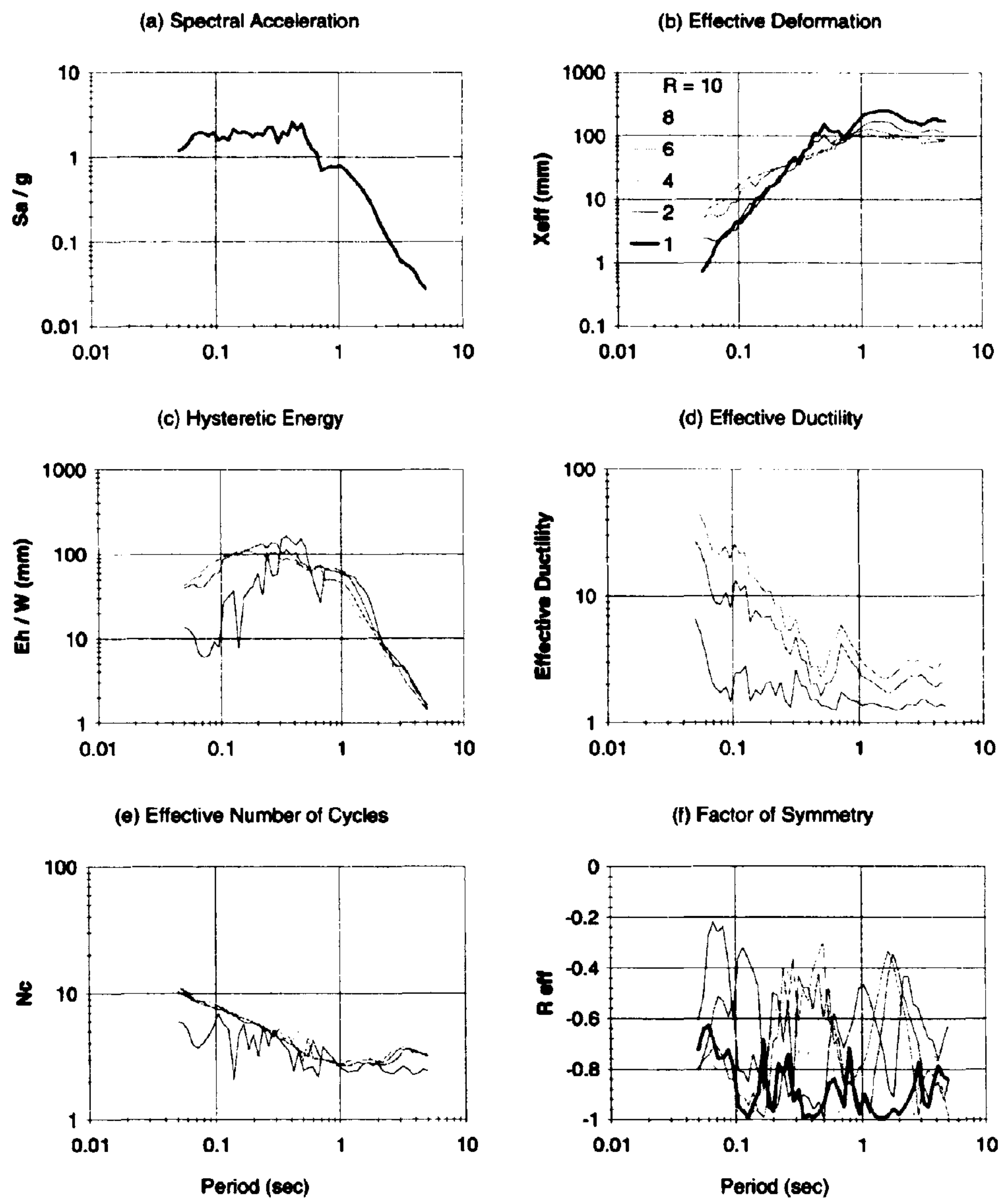

Fig. 4-19 Energy, Ductility and Low-Cycle Fatigue Demand Spectra for Pacoima Dam (1971), with 5% Viscous Damping Ratio and PGA = 1.17 g. (Modified Takeda Model)

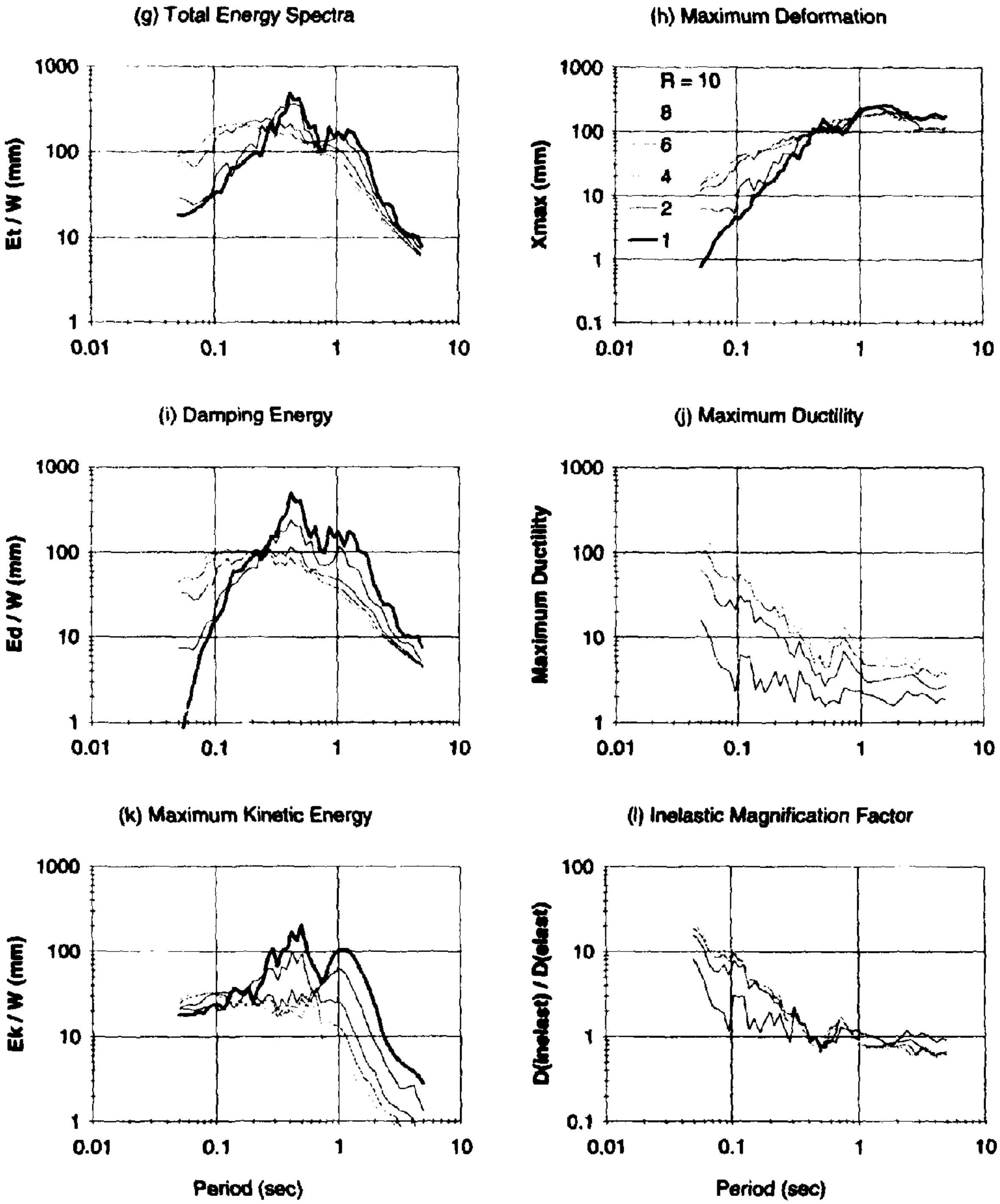

Fig. 4-19 Continued.

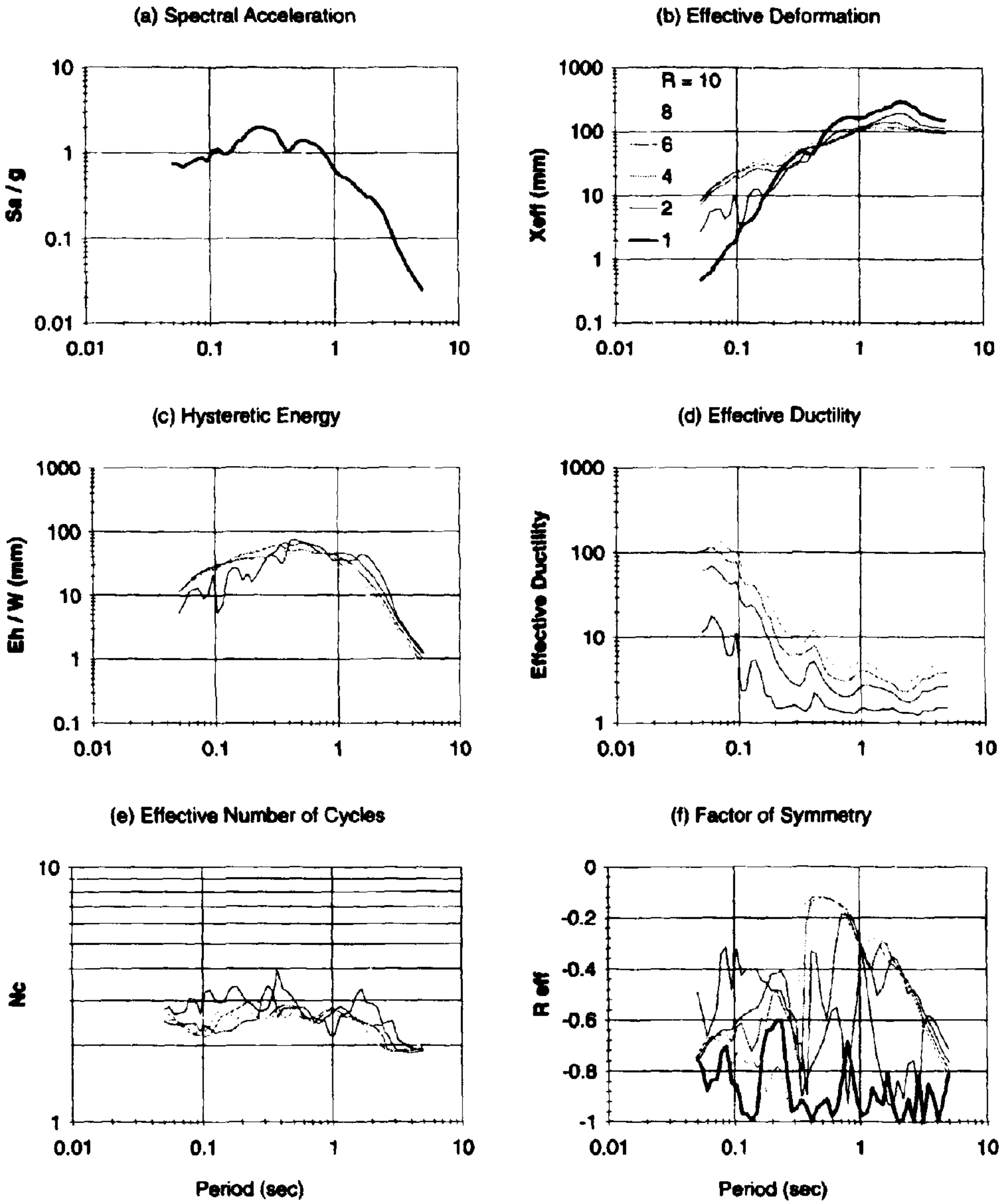

Fig. 4-20 Energy, Ductility and Low-Cycle Fatigue Demand Spectra for San Salvador (1986), with 5% Viscous Damping Ratio and PGA = 0.695 g. (Modified Takeda Model)

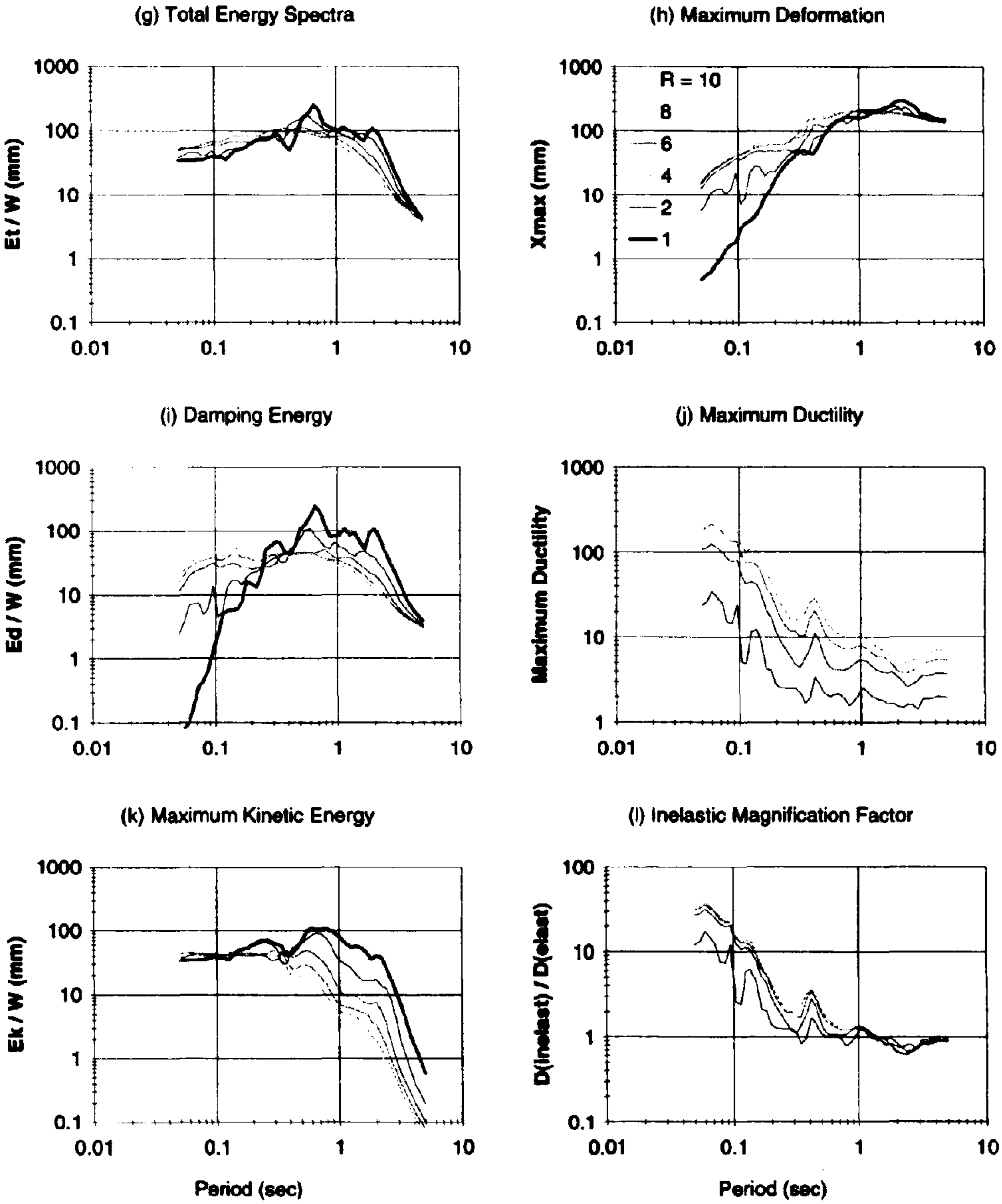

Fig. 4-20 Continued.

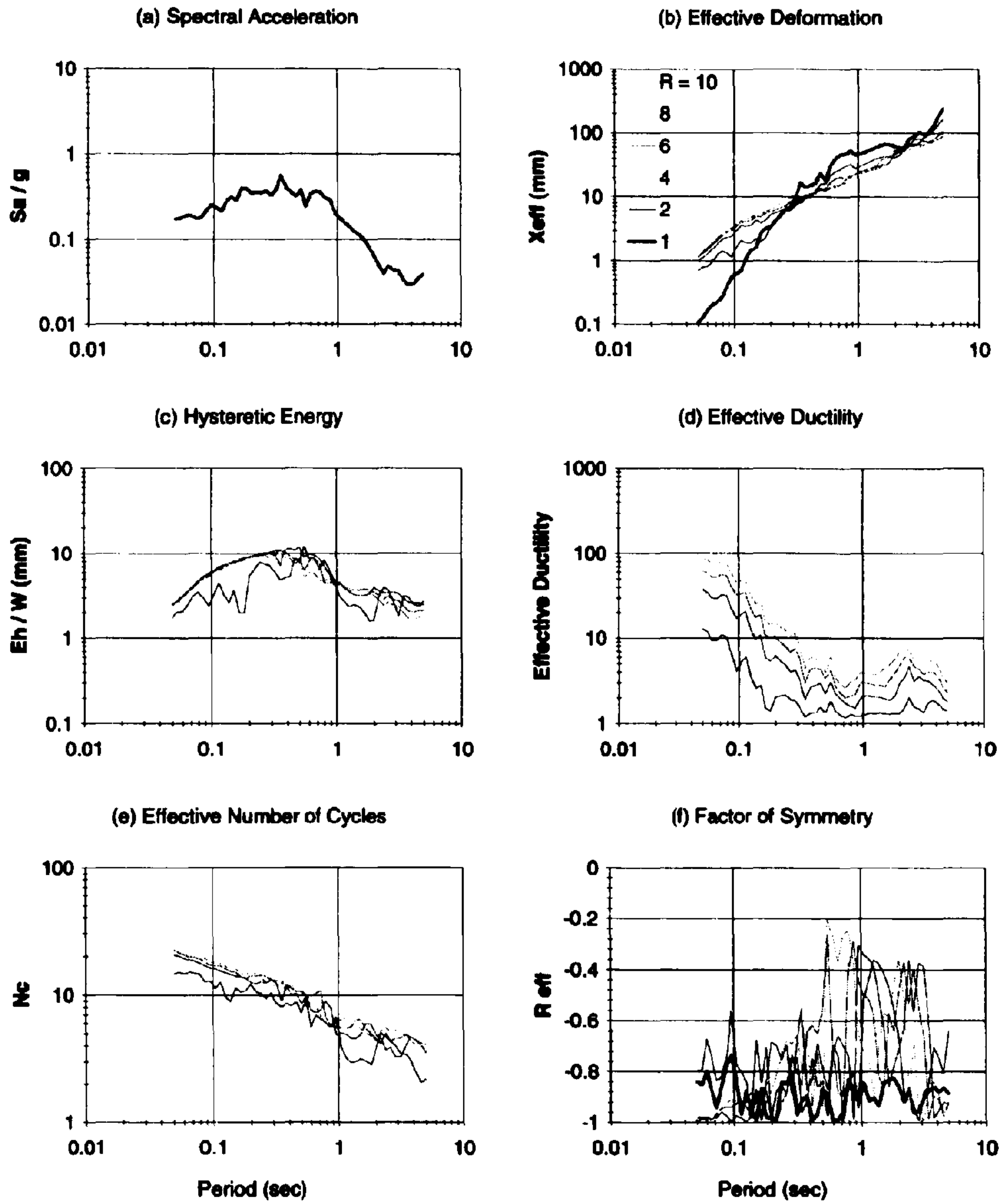

Fig. 4-21 Energy, Ductility and Low-Cycle Fatigue Demand Spectra for Taft (1952) N21E, with 5% Viscous Damping Ratio and PGA = 0.156 g. (Modified Takeda Model)

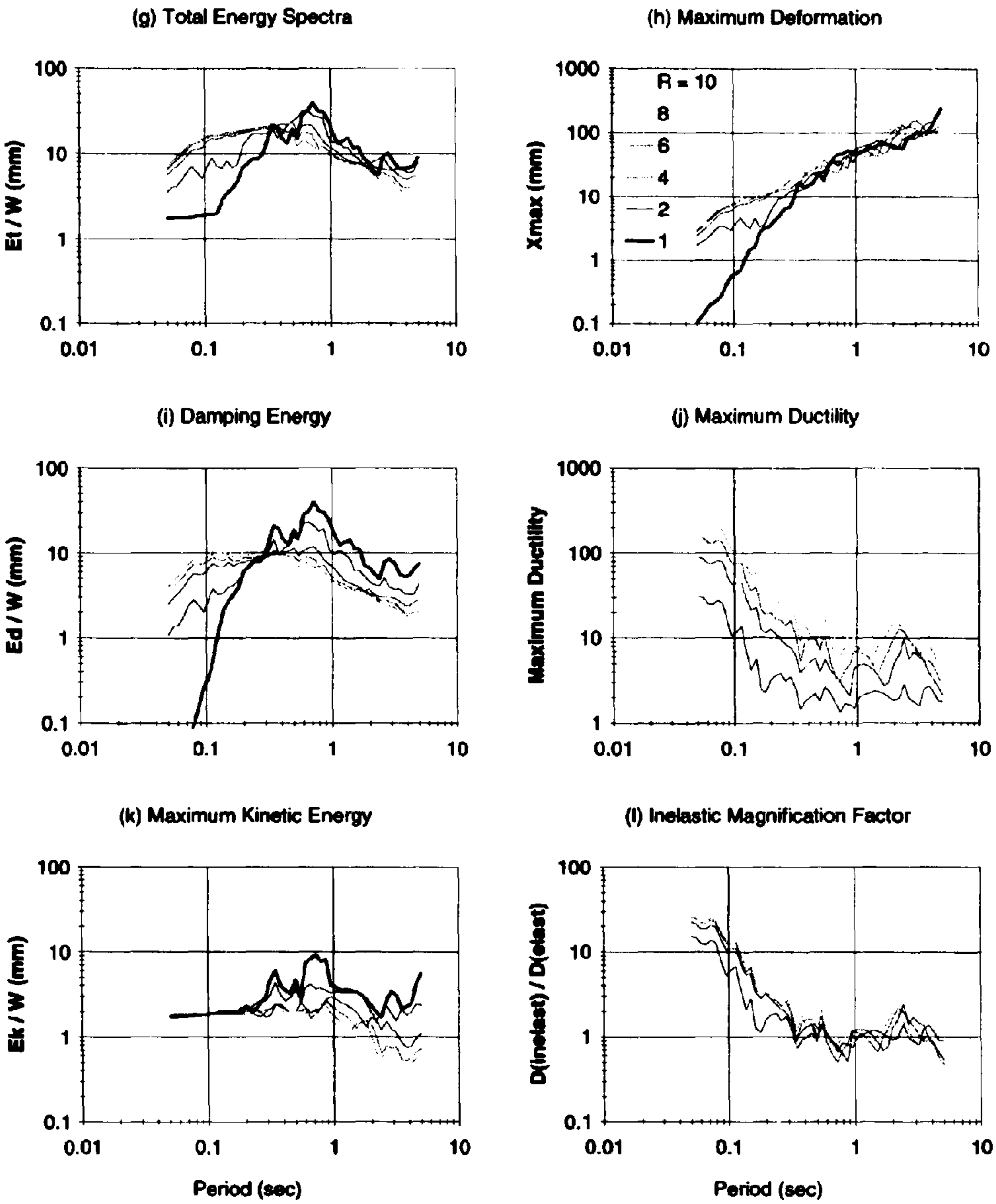

Fig. 4-21 Continued.

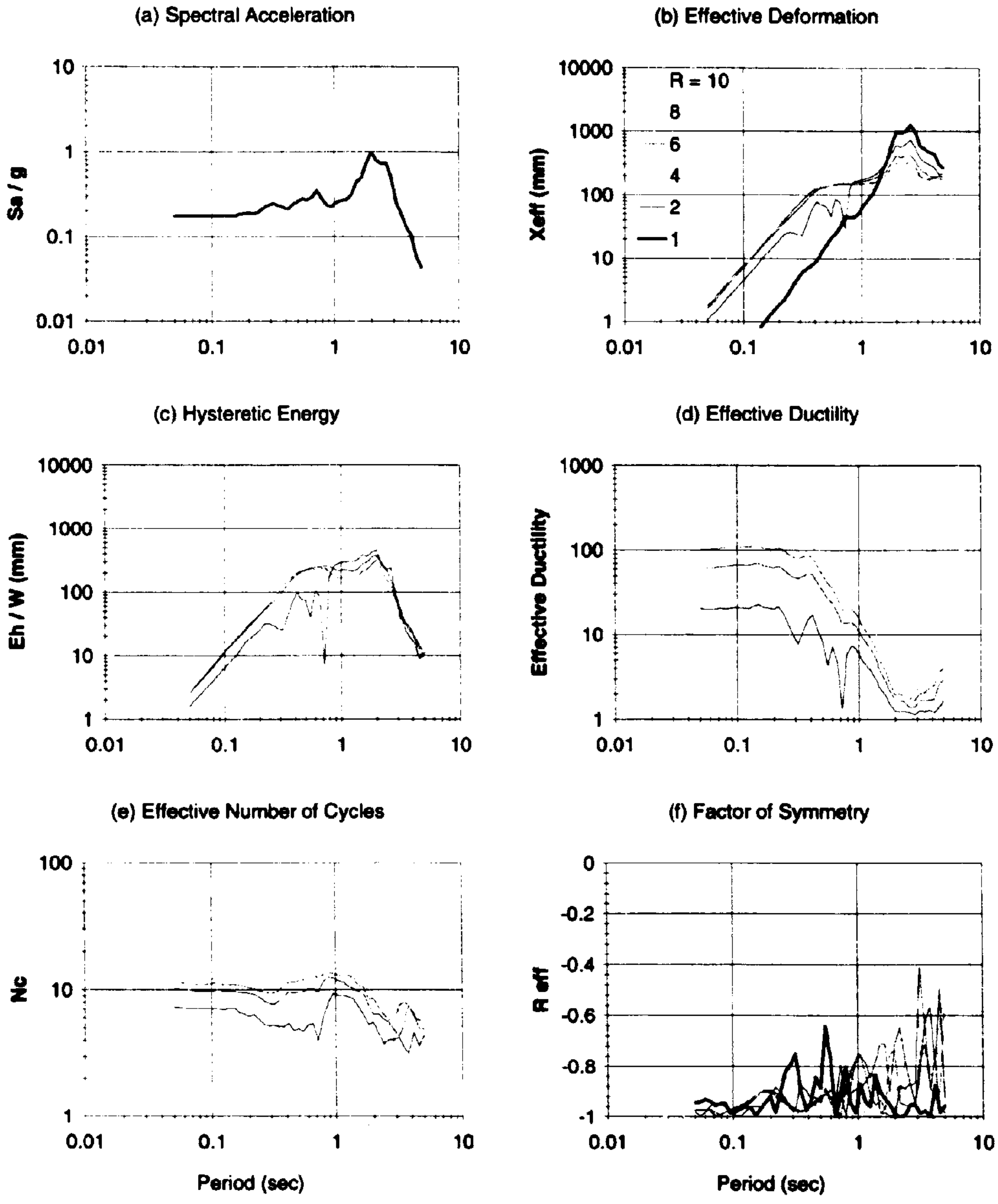

Fig. 4-22 Energy, Ductility and Low-Cycle Fatigue Demand Spectra for Mexico City (1985), with 5% Viscous Damping Ratio and PGA = 0.171 g. (Modified Takeda Model)

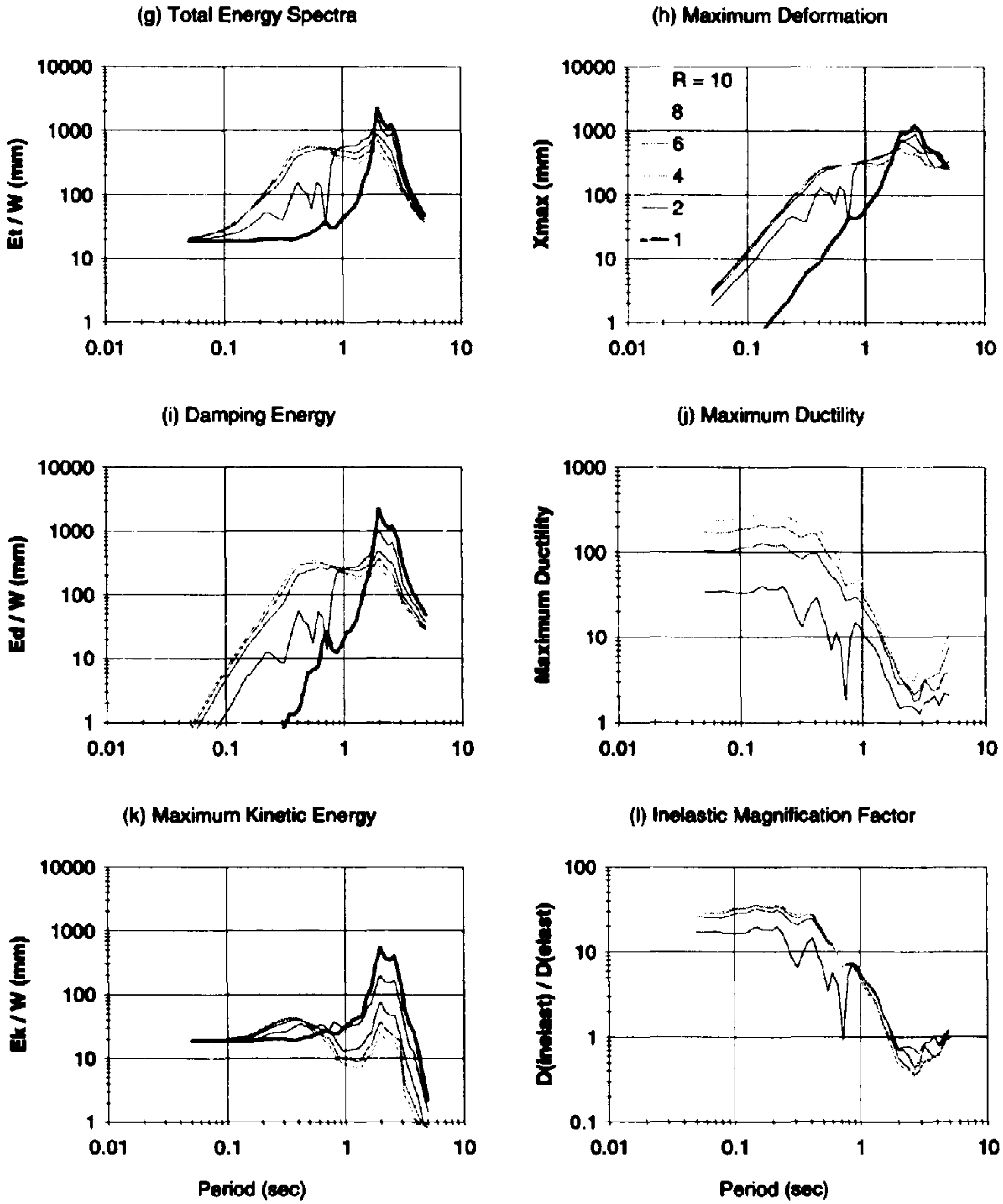

Fig. 4-22 Continued.

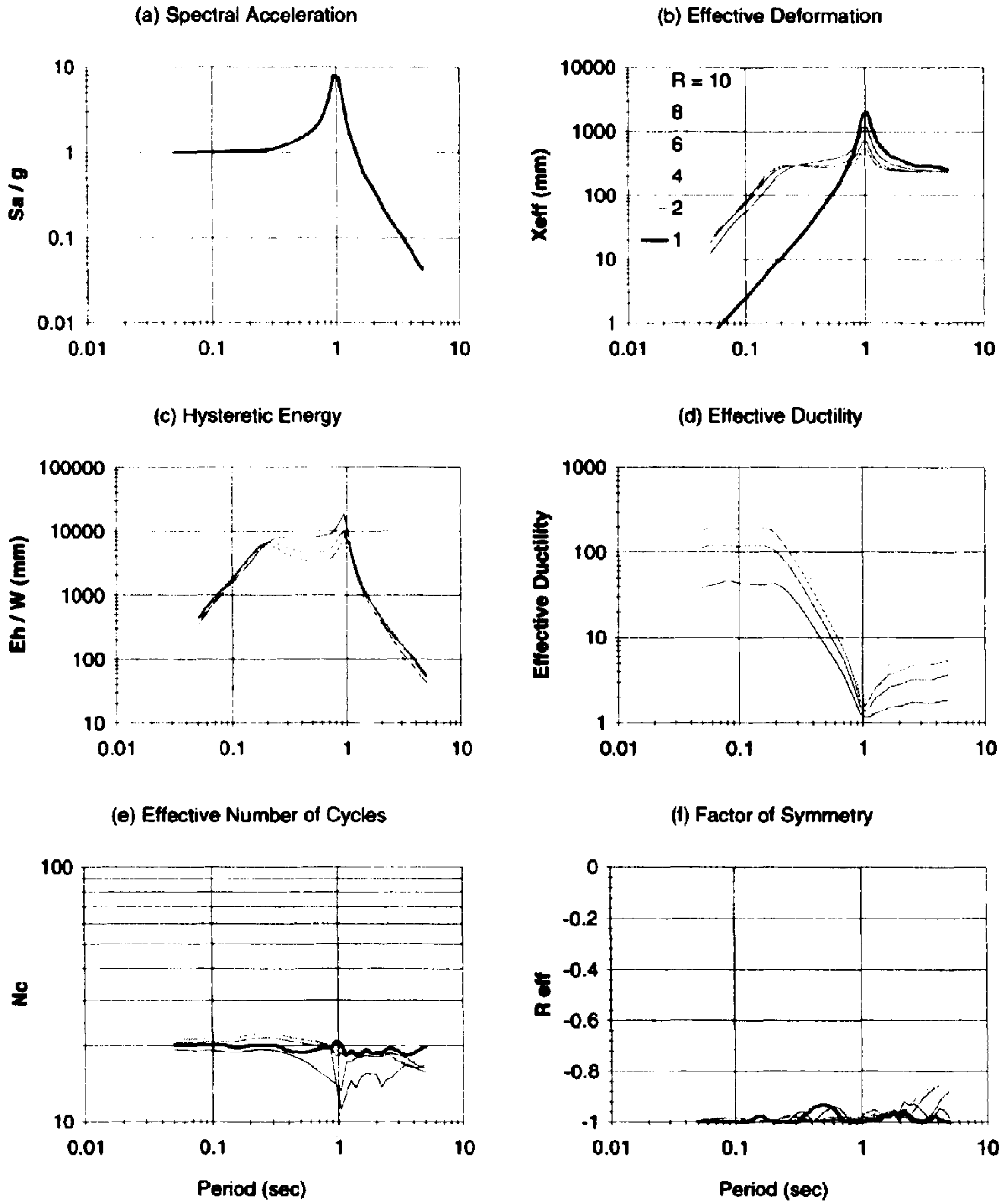

Fig. 4-23 Energy, Ductility and Low-Cycle Fatigue Demand Spectra for Sinusoidal Input, with 5% Viscous Damping Ratio and PGA = 1.0 g. (Modified Takeda Model)

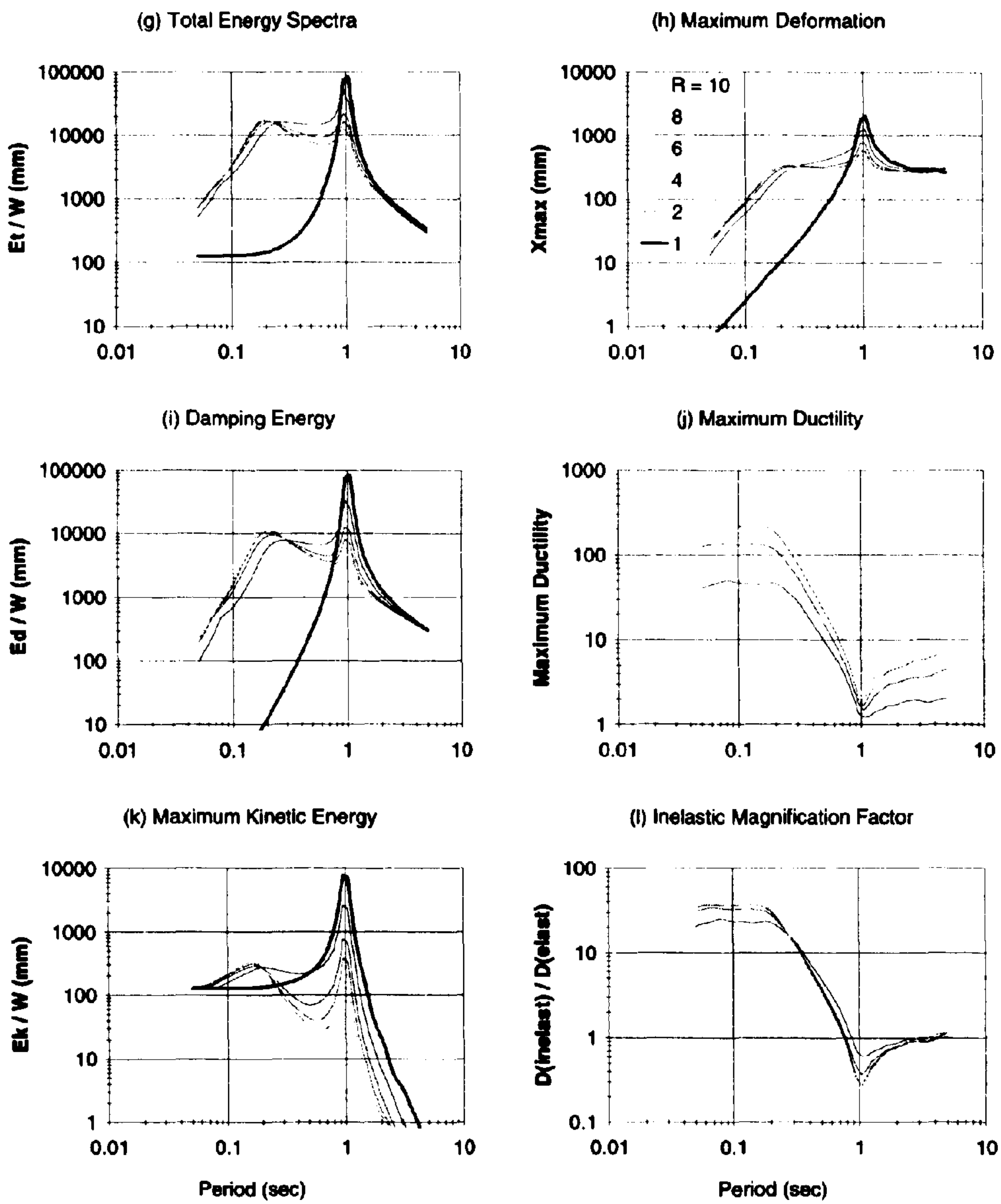

Fig. 4-23 Continued.

Section 5

Seismic Analysis and Design Recommendations

5.1 Introduction

The high design forces required to ensure that a structure will behave elastically during a strong seismic event makes such a design uneconomical. In practice the elastic force demands are reduced by a strength reduction factor (R_μ) with the acceptance of some inelastic response. Thus suitable detailing of members is required to ensure ductile behavior of the structural components. As manifested in the previous section, the inelastic effects are a function of the strength reduction factor, peak ground acceleration (PGA), duration of strong shaking, frequency content, natural period and damping of the structure, detailing and hysteretic characteristics of the structural members.

In this study the problem of energy demand has been addressed. The seismic analysis and design implications of taking into consideration the energy demand and capacity will now be presented. The energy demand is related to the low cycle fatigue of concrete, longitudinal column steel and transverse hoop steel (Mander et al., 1988a, b), while the ductility demand is related to the overall structural stability as a result of P-Δ effects.

5.2 Analysis of Results

Based on analytical studies, Mander et al. (1984) proposed an inelastic dynamic magnification factor D_m which relates the maximum inelastic displacement (X_u) to the elastic spectral displacement (S_d) and is given by:

$$D_m = \frac{X_u}{S_d} = \frac{1}{R_\mu}\left[1 + \left(\frac{T_o}{T}\right)(R_\mu - 1)\right] \geq 1 \qquad \textbf{(5-1)}$$

in which D_m = inelastic dynamic magnification factor, T = natural period of the structure, R_μ = strength reduction factor and T_o = period that separates "long" period structures from "medium" and "short" period structures. Based on an envelop to a series of maximum credible earthquakes,

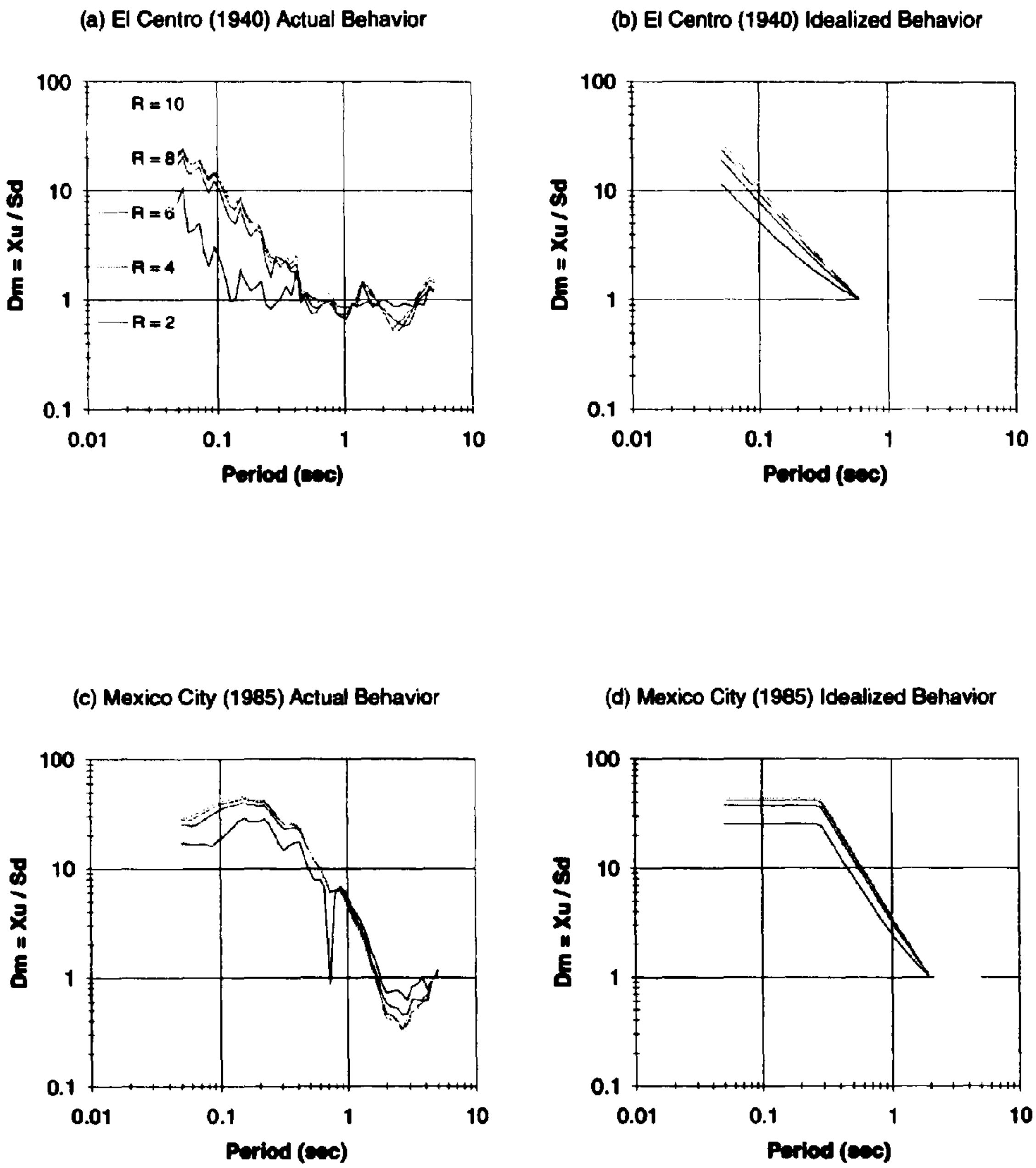

Fig. 5-1 Inelastic Dynamic Magnification Factor Idealization

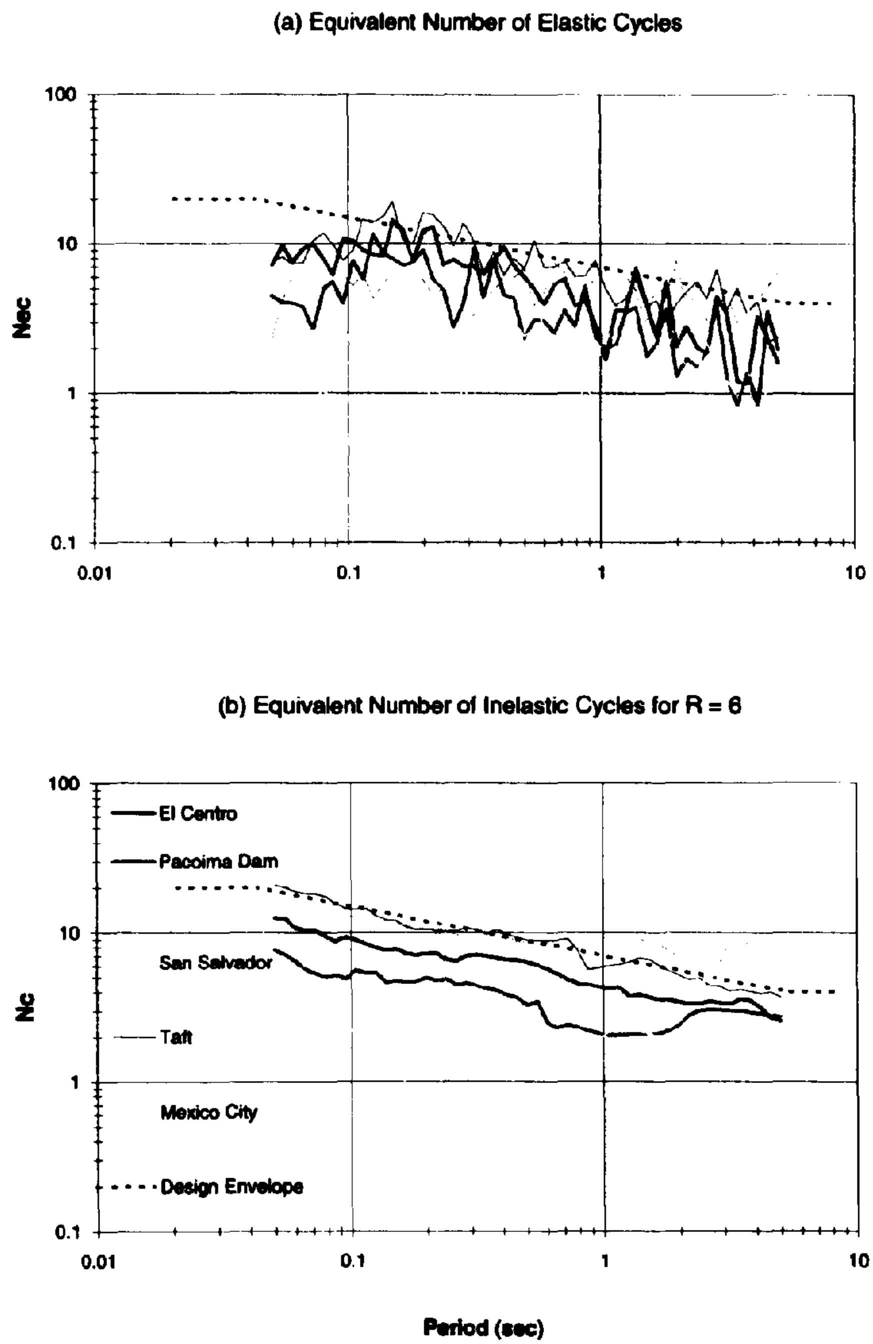

Fig. 5-2 Equivalent Number of Elastic and Inelastic Fully Reversed Cycles

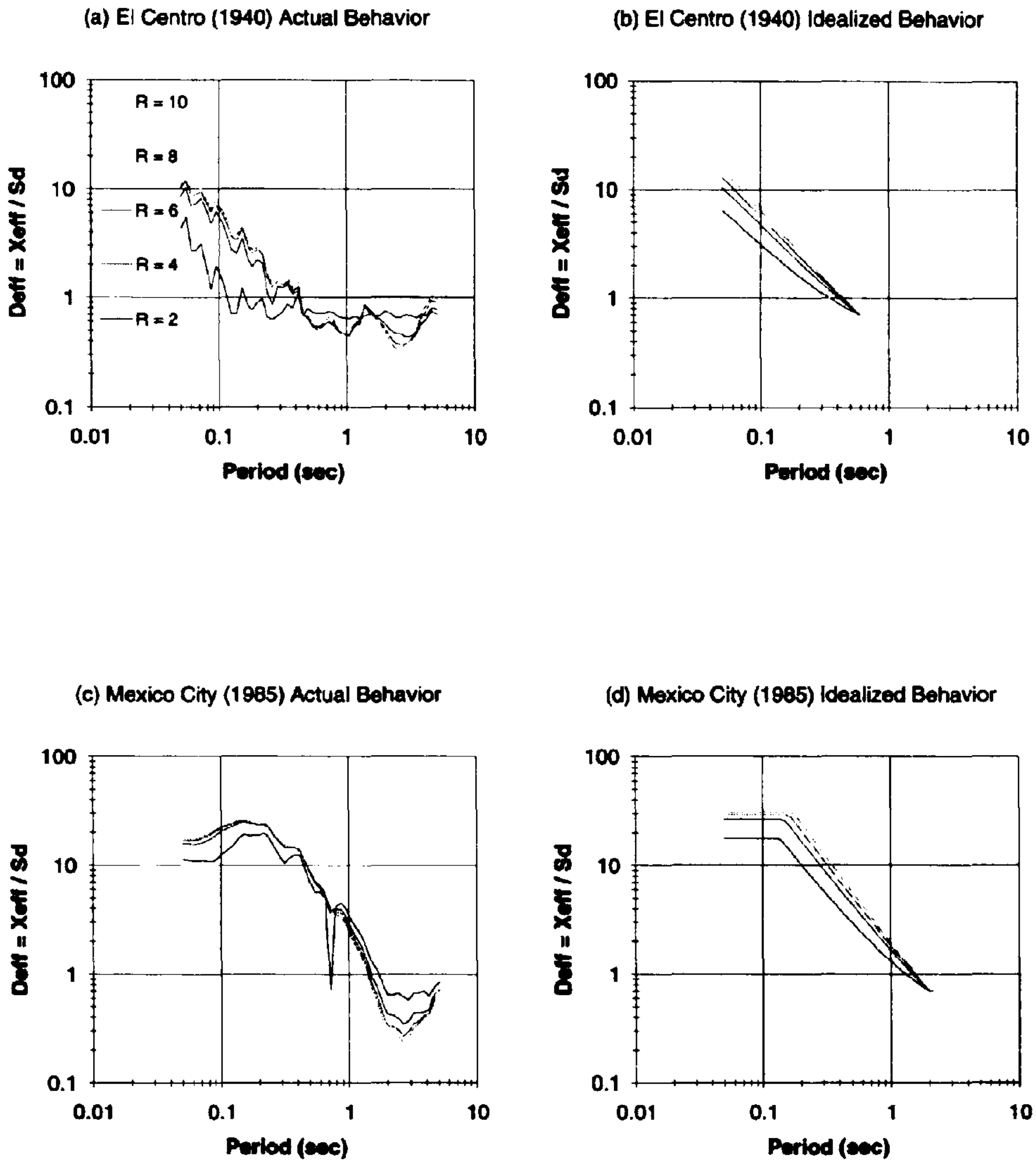

Fig. 5-3 Effective Inelastic Dynamic Magnification Factor Idealization

Eq. (5-4) is shown in Fig. 5-3. Comparing Eqs. (5-4) and (5-2) it is evident that in general the equivalent effective displacement amplitude is 70% of the maximum displacement, $X_{eff} \approx 0.7X_u$.

5.3 Design Recommendations

In earlier studies, it has been shown that the low cycle fatigue of reinforcing and prestressing bars may be expressed in the form of a single universal fatigue equation (Kasalanati, 1993; Mander et al., 1992)

$$\varepsilon_{ap} = \varepsilon_f^{\prime} (2N_f)^b \tag{5-5}$$

in which ε_{ap} = plastic strain amplitude, N_f = number of cycles to failure and $\varepsilon_f^{\prime}$ and b = fatigue strain and exponent coefficient respectively. Panthaki (1992) found experimentally that the following equation holds for both reinforcing and high strength prestressing bars

$$\varepsilon_{ap} = 0.08(2N_f)^{-0.5} \tag{5-6}$$

As shown in Fig. 5-2, the number of cycles demand is given by Eq. 5-3. Thus replacing Eq. 5-3 into Eq. 5-6 gives,

$$\varepsilon_{ap}(c) = 0.021\, T^{1/6} \tag{5-7}$$

This equation describes the limiting effective plastic strain amplitude <u>capacity</u> of the longitudinal reinforcement as a function of the structure's natural period. Thus, the effective plastic strain amplitude should be kept below this limit, if a low cycle fatigue failure is to be avoided.

The plastic curvature is related to the plastic strain amplitude in the longitudinal bars by:

$$\phi_p = \frac{2\varepsilon_{ap}}{d-d'} \tag{5-8}$$

where ϕ_p = average plastic hinge curvature, $d-d'$ = distance between outermost longitudinal bars, and $2\varepsilon_{ap}$ = total plastic strain amplitude. When the plastic hinge is subjected to one completely reversed cycle at a plastic curvature amplitude of $\pm\phi_p$, the outermost longitudinal bars are subjected to a total plastic strain amplitude of $2\varepsilon_{ap}$, as shown in Fig. 5-4.

The plastic rotation at the plastic hinge is given by,

$$\theta_p = \phi_p L_p = 2\varepsilon_{ap} \frac{L_p}{d-d'} \tag{5-9}$$

where θ_p = plastic hinge rotation and L_p = equivalent plastic hinge length. By replacing Eq. 5-7 into Eq. 5-9, the plastic rotation capacity (or column drift) is given as,

$$\theta_p(c) = 0.042\, T^{1/6} \frac{L_p}{d-d'} \qquad \textbf{(5-10)}$$

It is also possible to define an equivalent yield rotation for a cantilever column as follows. The displacement of an elastic cantilever column, Fig. 5-5, is given by:

$$\Delta_y = \frac{F_y L}{3EI} = \phi_y \frac{L^2}{3} \qquad \textbf{(5-11)}$$

Thus, an equivalent average rotation (The yield drift) may be expressed as,

$$\theta_y = \frac{\Delta_y}{L} = \phi_y \frac{L}{3} \qquad \textbf{(5-12)}$$

The yield curvature can also be expressed approximately in terms of yield strain, similarly to Eq. 5-8, as:

$$\phi_y = \frac{2\varepsilon_y}{d-d'} \qquad \textbf{(5-13)}$$

Thus, replacing Eq. (5-13) into Eq. (5-12) the equivalent yield rotation is given by:

$$\theta_y = \frac{2}{3}\varepsilon_y \frac{L}{d-d'} \qquad \textbf{(5-14)}$$

Thus, the effective displacement capacity is expressed by,

$$X_{eff}(c) = D_{eff} S_d = X_{p\,eff} + X_y = [\theta_p(c) + \theta_y]\, L \qquad \textbf{(5-15)}$$

Dividing this equation by the yield displacement, X_y, gives

$$\frac{X_{eff}}{X_y} = D_{eff}\frac{S_d}{X_y} = \frac{[\theta_p + \theta_y]L}{X_y} = \frac{\theta_p}{\theta_y} + 1 \qquad \textbf{(5-16)}$$

By definition,

$$X_y = \frac{S_d}{R_\mu} \qquad \textbf{(5-17)}$$

Replacing Eqs. (5-10), (5-14) and (5-17) into Eq. (5-16), gives

$$D_{eff} R_\mu = \frac{0.063}{\varepsilon_y} T^{1/6} \left(\frac{L_p}{L}\right) + 1 \qquad \textbf{(5-18)}$$

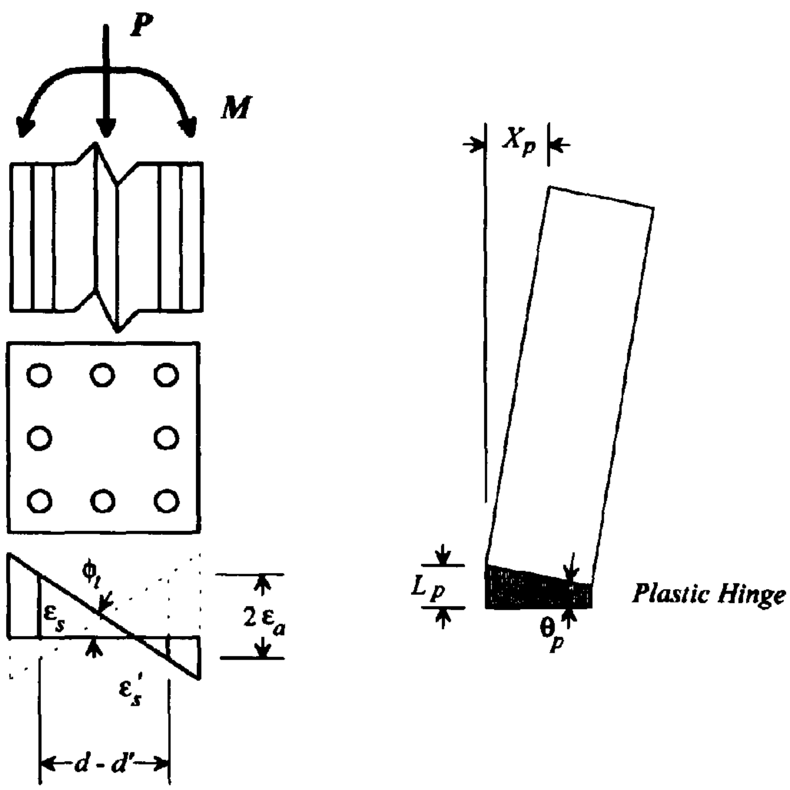

Fig. 5-4 Plastic Curvature, Plastic Rotation, Plastic Deformation and Plastic Strain Amplitude.

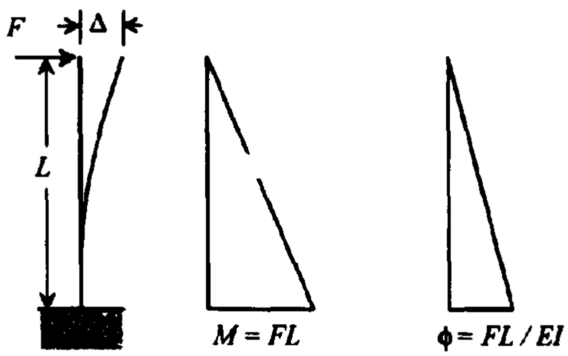

Fig. 5-5 Elastic Column Behavior

The equivalent plastic hinge length given by Paulay and Priestley (1992) can be given as:

$$L_p = 0.08L + 4350\varepsilon_y d_b \tag{5-19}$$

where L= column length (M / V), d_b= diameter of the longitudinal steel and ε_y = yield strain of that steel.

A conservative value for in Eq. (5-4) is 0.7 sec. Thus,

$$\begin{aligned} D_{eff} &= \frac{0.7}{R_\mu}\left[1 + (R_\mu - 1)\left(\frac{0.7}{T}\right)^{1.1+R_\mu/40}\right] & T < 0.7 \text{ sec} \\ D_{eff} &= 0.7 & T \geq 0.7 \text{ sec} \end{aligned} \tag{5-20}$$

now, replacing Eq. (5-20) into (5-18),

$$R_\mu = 1 + \left[\frac{0.09}{\varepsilon_y} T^{1/6}\left(\frac{L_p}{L}\right) + \frac{3}{7}\right]\left(\frac{T}{0.7}\right)^{1.1+R_\mu/40} \qquad T < 0.7 \text{ sec} \tag{5-21a}$$

$$R_\mu = 45T^{1/6}\left(\frac{L_p}{L}\right) + 1.43 \qquad T \geq 0.7 \text{ sec} \tag{5-21b}$$

A yield strain of $\varepsilon_y = 0.002$ may be conservatively adopted, thus by applying Eq. (5-19) to (5-21)

$$R_\mu = 1 + \left[\left(3.6 + 400\frac{d_b}{L}\right)T^{1/6} + 0.43\right]\left(\frac{T}{0.7}\right)^{1.1+R_\mu/40} \qquad T < 0.7 \text{ sec} \tag{5-22a}$$

$$R_\mu = \left(3.6 + 400\frac{d_b}{L}\right)T^{1/6} + 1.43 \qquad T \geq 0.7 \text{ sec} \tag{5-22b}$$

As Eq. (5-22a) is in implicit form, a simple fixed-point iteration procedure can be used to find R_μ.

Typical values of the fatigue limiting force reduction factor are presented as a function of the natural period in Fig. 5-6. Different bar diameter to column length ratios of $\frac{d_b}{L}$ = 1/300, 1/100 and 1/50 are shown to be representative of large box columns, typical bridge columns and squat shear-critical columns, respectively (Mander et al., 1984).

The strength reduction factor, shown in Fig. 5-6, can be directly applied to an elastic design spectral acceleration envelope to obtain the inelastic base shear coefficient. AASHTO (1989) recommends an elastic design envelope in the form:

$$\frac{S_a}{PGA} = cT^{-2/3} \leq 2.5 \tag{5-24}$$

in which S_a = spectral acceleration, PGA = peak ground acceleration and c = a constant varying from 1.25 for stiff soil to 2.5 for soft soil. The PGA is defined according to the seismic zone of design. In Fig. 5-7 the limiting inelastic design spectra for fatigue is presented.

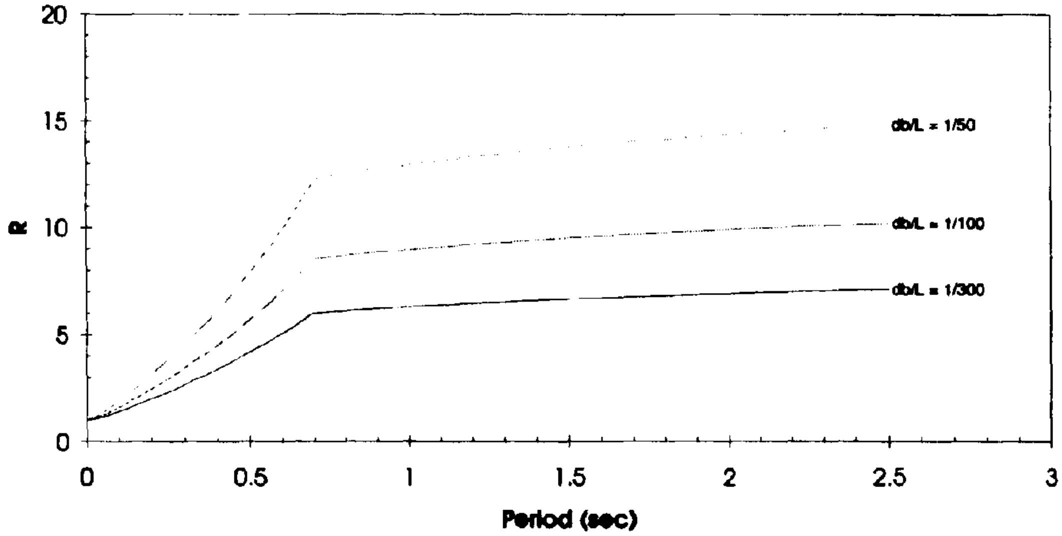

Fig. 5-6 Fatigue Limiting Force Reduction Factors

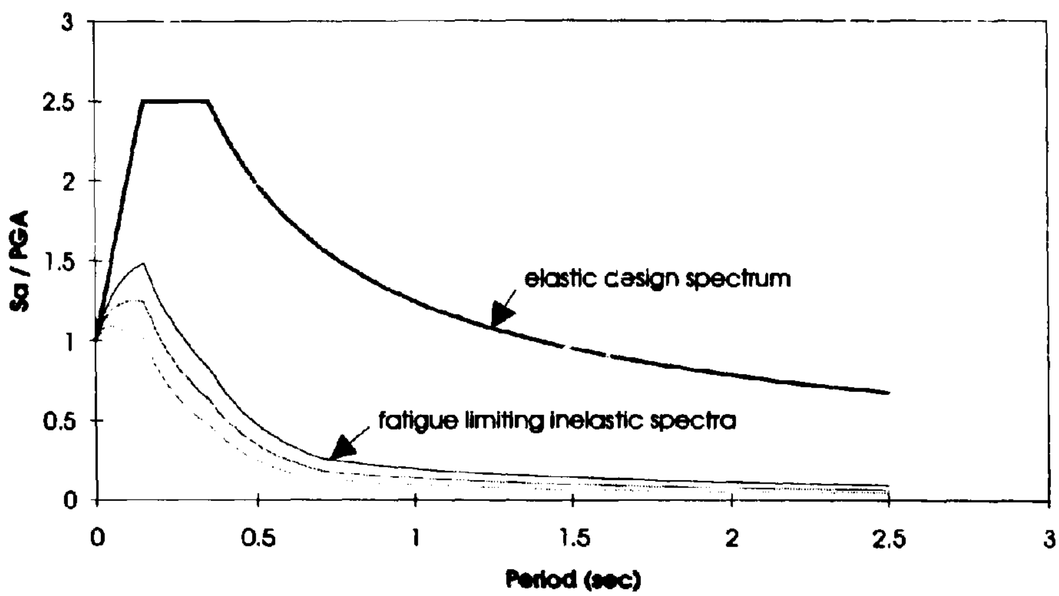

Fig. 5-7 Inelastic Design Spectra Limited by Low Cycle Fatigue

5.4 Seismic Evaluation

The steps in the proposed seismic evaluation methodology (Fig. 4-1) will now be summarized

Step 1. Determine the <u>strength demand</u> C(d) by choosing a value of A, the normalized peak ground acceleration coefficient.

Step 2. Determine the <u>strength capacity</u> C(c) by using a seismic limit (plastic) analysis or incremental pushover analysis.

Step 3. Determine the strength reduction factor

$$R_\mu = \frac{C(d)}{C(c)}$$

<u>First Order Ductility Based Analysis</u>

Step 4.1 Determine the <u>ductility demand</u>

$$\mu(d) = D_m R_\mu = 1 + \left(\frac{0.7}{T}\right)^n (R_\mu - 1)$$

but $\mu(d) \geq R_\mu$

with $n = 1.2 + 0.025 R_\mu$

Step 5.1 Determine the ductility capacity $\mu(c)$

This is based on an ultimate compression strain of $\varepsilon_{cu} = 0.008$ for unconfined concrete. For confined concrete the ultimate strain may be based on the energy balance recommendation of Mander et al. (1988a). Paulay and Priestley (1992) suggest a conservative estimate for the confined ultimate compression strain be taken as

$$\varepsilon_{cu} = 0.004 + 1.4 \rho_s f_{yh} \varepsilon_{sm} / f'_{cc}$$

where ε_{sm} = the maximum steel strain at the ultimate steel stress, f_{yh} = yield stress of the transverse hoop steel, ρ_s = volumetric ration of the transverse reinforcement and f'_{cc} = confined concrete strength (Mander et al., 1988a) which in lieu of a more precise analysis may be taken as $1.5f'_c$.

Step. 6.1 Determine the ductility based Capacity / Demand ratio

$$r_\mu = \frac{\mu(c)}{\mu(d)}$$

<u>Second Order Energy Based Fatigue Demand Analysis</u>

Step 4.2 Determine the cyclic loading demand from

$$N(d) = 7\,T^{-1/3}$$

but,

$$4 \le N(d) \le 20$$

Step 5.2 Determine the <u>cyclic loading capacity</u>

$$N(c) = \frac{0.0128}{\theta_p^2}\left(\frac{L_p}{d-d'}\right)$$

where $L_p = 0.08L + 4350\,\varepsilon_y\,d_b$

and $\theta_p = (0.7R_\mu - 1)\theta_y$ for $T > T_{PV} = 0.7\,\text{sec}$

and for $T \le 0.7$ sec, $\theta_p = \left[0.7\left(\frac{0.7}{T}\right)^n (R_\mu - 1) - 0.3\right]\theta_y$

where $n = 1.1 + 0.025R_\mu$

Step 6.2 Determine the cyclic loading Capacity / Demand ratio

$$r_N = \frac{N(c)}{N(d)}$$

The values of r_μ and r_N corresponding to several values of A are determined. Thus by interpolation it is possible to ascertain the maximum peak ground acceleration for which either stability or low cycle fatigue is critical.

5.4.1 Illustrative Example

Consider the bridge pier studied experimentally and analytically by Mander et al. (1993). Model and prototype specimens were tested and the following data was obtained:

Base shear capacity	$C_n(c) = 0.9$
Natural period	$T = 0.09$ sec
Yield drift	$\theta_y = 0.0025$ radians
Maximum ductility capacity	$\mu(c) = 15$

Step 1. Choose a peak ground acceleration of 0.5g. The maximum demand for short period structures when $T < 0.33$ sec is given by

$$C(d) = 3.25A = 1.625$$

Step 2. $C_n(c) = 0.90$, from analysis and experiment (Mander et al., 1993)

Step 3. Force reduction factor

$$R_\mu = \frac{C(d)}{C(c)} = \frac{1.625}{0.9} = 1.806$$

Step 4.1 Ductility demand

$$\mu(d) = 1 + \left(\frac{0.7}{T}\right)^{1.2+0.025R_\mu}(R_\mu - 1)$$

$$\mu(d) = 1 + \left(\frac{0.7}{0.09}\right)^{1.2+0.025\times1.806}(1.806 - 1) = 11.36$$

Step 5.1 $\mu(c) = 15$, given by experiment/analysis (Mander et al., 1993)

Step 6.1 Ductility based C/D ratio

$$r(\mu) = \frac{\mu(c)}{\mu(d)} = \frac{15}{11.36} = 1.32$$

Step 4.2 Cyclic demand

$$N(d) = 7\,T^{-1/3} = 15.6 \text{ cycles}$$

Step 5.2 Plastic rotation amplitude

$$\theta_p = \left[0.7\left(\frac{0.7}{T}\right)^{1.1+0.025R_\mu}(R_\mu - 1) - 0.3\right]\theta_y$$

$$\theta_p = \left[0.7\left(\frac{0.7}{0.09}\right)^{1.1+0.025\times1.806}(1.806 - 1) - 0.3\right]0.0025$$

$$\theta_p = 0.014 \text{ radians}$$

assuming $\dfrac{L_p}{d-d'} = 0.5$

$$N(c) = \frac{0.0128}{\theta_p^2}\left(\frac{L_p}{d-d'}\right)^2$$

$$N(c) = \frac{0.0128}{0.014^2}0.5^2$$

$$N(c) = 16.3 \text{ cycles}$$

Step 6.2 Cyclic loading C/D ratio

$$r_N = \frac{N(c)}{N(d)} = \frac{16.3}{15.6} = 1.04$$

This procedure has been repeated for a number of different peak ground acceleration (A) values. The results are plotted in Fig. 5-8. It is evident from this graph that inelastic response occurs when $A > 0.277$. The maximum sustainable peak ground acceleration is governed by low cycle fatigue when $A = 0.504$.

It will be noted that this result is quite different from that previously obtained using the ATC 6-2 methodology (Mander et al., 1993). In that approach it is implicitly assumed that the equal displacement principle holds at all times such that $\mu(d) = R_\mu$. The present results show, however, that due to the short period nature of the structure $\mu(d) >> R_\mu$. Clearly the ATC 6-2 methodology is inappropriate for short period structures, when $T < T_{PV} = 0.7$ sec. Unfortunately, this comprises the vast majority of bridges, particularly those with frame type pier bents.

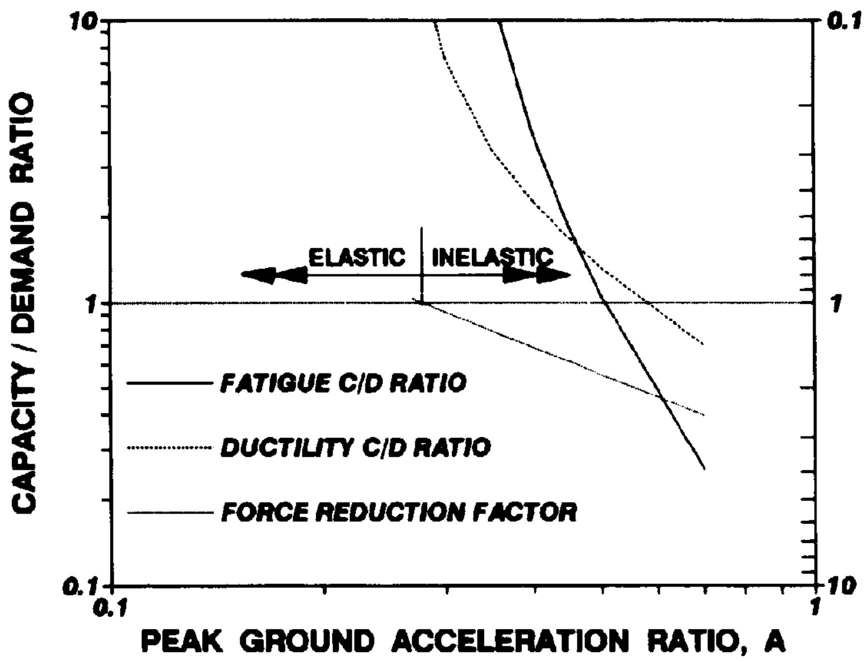

Fig. 5-8 Results of C/D Analysis for Example Problem

5.5 Discussion and Conclusions

It is of interest to compare the results obtained in this study with a recently published state-of-the-art paper on the evaluation of strength reduction factors for earthquake resistant design (Miranda and Bertero, 1994). In that paper a summary has been made of previous studies that investigated strength reduction factors and proposed empirical expressions to estimate R_μ. As observed in the present study, Miranda and Bertero demonstrate that there is generally a bilinear type of relationship between R_μ and natural period of vibration alluvium and rock. For soft soil sites, however, they present an outcome that is similar to the results computed herein for both the Mexico City (1985) and sinusoidal excitations. Miranda and Bertero conclude that the magnitude of the strength reduction factors is primarily a function of displacement ductility demand, the natural period of the system, and the soil conditions of the site. Other factors (such as the hysteretic behavior, damping of the structure, and distance to the epicenter of the earthquake) may affect the strength reduction factors, but to a much lesser degree.

Present bridge design codes assume a constant force reduction factor for all natural period. A maximum value $R_\mu = 5$ has been adopted in the AASHTO code. An exception to the constant force reduction factor is the New Zealand seismic design recommendations for bridges (Berrill et al., 1981). In that code Eq. 5-1 is implicitly adopted with T_o =0.7 sec. Certain building codes now explicitly describe period-dependent strength reduction factors. These include Mexico City Building Code (1976) and the CIRSOC 103 Argentine Code (Sonzognia et al., 1984). More recently, bilinear expressions for R_μ (with $T_0 = 0.5$ sec.) were suggested by Tso and Naumoski (1991) to improve the national building code of Canada. Hidalgo and Arias (1990) have also proposed period-dependent R_μ factors for the new version on Chilean seismic code. It should be noted, however, that none of these studies have used fatigue failure as a basis for determining the appropriate strength reduction factors.

This section has demonstrated the importance of having a reliable assessment of displacement ductility demand for short period structures. This impacts on the design of new structures when the period is less than that of the peak spectral velocity, T_{PV}. For such cases it is recommended that the force reduction factors should be reduced by no more than the values shown in Fig. 5-6, if fatigue failure is to be avoided. For simplicity a conservative fatigue based force reduction factor could be recommended for new design as:

$$R_{\mu} = 10T\,; \qquad 1 \leq R_{\mu} \leq 7$$

This section has also demonstrated the need for more rigorous fatigue based seismic analysis for the evaluation of existing bridge structures. Existing methodologies do not account for the possibility of low cycle fatigue failure. This study has also shown that such a failure is possible and may be critical where ductility based stability concerns do not govern.

Section 6

Summary, Conclusions and Recommendations

6.1 Summary

This study has been concerned with the computational modeling of energy absorption (fatigue) capacity of reinforced concrete bridge columns by using a cyclic dynamic Fiber Element computational model that was presented in the Part I of this report series. The results were used with a smooth hysteretic rule to generate seismic energy demand. By comparing the ratio of energy demand to capacity, inferences of column damageability or fatigue resistance are made.

Starting from the basic principles of nonlinear mechanics of materials, the first report gives a complete analysis methodology for bridge columns. The hysteretic behavior of steel reinforcement is dealt with in detailed: stability, degradation and consistency of cyclic behavior is explained. An energy based universally applicable low cycle fatigue model for steel was proposed. A hysteretic model for confined and unconfined concrete subjected to tension or compression cyclic loading was advanced, which is also capable for simulating gradual crack closure. A Cyclic Inelastic Strut-Tie (CIST) model was developed, in which the comprehensive concrete model proved to be suitable. The CIST model was shown to be capable of assessing inelastic shear deformations with a high degree of accuracy, within the context of a Fiber Element (FIBE) program. The FIBE approach was validated by comparing the results with a variety of columns.

In this second report, a smooth model was presented which can accurately simulate the macro behavior of reinforced concrete columns. The model parameters are determine through a system identification procedure that eliminates the need for parameter guessing. This approach permits a more rational approach as the parameters are determine by calibrating actual experimental hysteretic results or simulated experiments. Of particular importance is the accuracy with which the behavior of a full-size bridge pier was simulated both by using a Fiber

3. Fatigue Based Force Reduction Factors

Fatigue limiting force reduction factors have been derived in this study. It is now well recognized that for short period structures a uniform value of the force reduction factor leads to a large increase in the displacement ductility amplitude. This study has demonstrated that a similar increase results in the fatigue demand. It is therefore recommended that the equations developed herein for R_μ be used for fatigue based seismic analysis and design. A conservative value of the force reduction factor used to prevent fatigue failure may be adopted such that

$$R_\mu = 10\,T \qquad 1 \leq R_\mu \leq 7$$

where T = natural period of the structure.

6.3 Recommendations for Future Research

(1) Parametric studies to measure the influence of model parameters, may clarify the range and validity of the various proposed model parameters.

(2) A study on the interaction between the orthogonal cracking and yielding on biaxial flexure is needed.

(3) A modified shear model for the assessment of shear deformation on biaxial shear needs to be developed.

(4) The macro model needs to be integrated into a general purpose nonlinear dynamic analysis program as IDARC or DRAIN-2DX to study the effect of having realistically calibrated models in a multi-degree of freedom system.

(5) Inelastic Energy Spectra need to be generated for different types of structures, where a realistic modeling of hysteretic behavior are implemented by following the general guidelines given in this investigation.

(6) The effect of site dependent earthquake excitation needs to be addressed, to define its effect on fatigue and energy demands.

SEISMIC EVALUATION METHODOLOGY

Step 1. Strength Demand, C(d)

Step 2. Strength Capacity C(c) (Limit Analysis)

Step 3. $r_{ec} = \dfrac{C(d)}{C(c)} = \dfrac{1}{R_\mu}$ [If $r_{ec} \geq 1.5$ STOP]

1st Order Ductility Based Damage Analysis (SDOF)

Step 4.1 Ductility Demand $\mu(d)$

Step 5.1 Ductility Capacity $\mu(c)$ per ATC 6-2

Step 6.1 $r_\mu = \dfrac{\mu(c)}{\mu(d)}$ [If $r_\mu \geq 1.5$ STOP]

2nd Order Energy Based Damage Analysis (SDOF)

Step 4.2 Rotational Demand

$\theta_p(d), N(d) = f(R_\mu, EQ, Hyst.model)$

Step 5.2 Rotational Capacity $\theta_p(c), N(c)$

Step 6.2 $r_N = \dfrac{N(c)}{N(d)}$ [If $r_N \geq 1.5$ STOP]

3rd Order Time History Damage Analysis (MDOF)

Step 7. Generate Member Specific Hysteretic Models (From Steps 4.2 and 5.2)

Step 8. Perform Time History Analysis (IDARC or DRAIN-2DX)

Step 9. Examine Critical Members Performance. Use Fiber-Element to predict detailed behavior based on member time-history.

Fig. 6-1 Summary of Research Significance of this Study in the Context of a Seismic Evaluation Methodology.

Section 7

References

References - Section 1

____ ATC 6-2 (1983), *Seismic Retrofitting Guidelines for Highway Bridges*, Applied Technology Council, 220 pp.

Collins, P.M. and Mitchell, D., (1991), *Prestressed Concrete Structures*, Prentice Hall, New Jersey, 1991.

Hsu, T.T.C., (1993), *Unified Theory of Reinforced Concrete*, CRC Press, Boca Raton, 1993.

Mander, J.B., Priestley, M.J.N. and Park, R., (1984), *Seismic Design of Bridge Piers*, Department of Civil Engineering, University of Canterbury, Report 84-2, Feb-84, 483 pp.

Mander, J.B., Priestley, M.J.N. and Park, R., (1988a), *Theoretical Stress-Strain Model for Confined Concrete*, Journal of Structural Engineering, Vol. 114, No. 8, Aug-88, pp. 1804-1826.

Mander, J.B., Priestley, M.J.N. and Park, R., (1988b), *Observed Stress-Strain Behavior of Confined Concrete*, Journal of Structural Engineering, Vol. 114, No. 8, Aug-88, pp. 1827-1849.

Saiidi, M., (1982), *Hysteresis Models for Reinforced Concrete*, Journal of the Structural Division, Vol. 108, No. ST5, May 1982, pp. 1077-1087.

Vecchio, F.J. and Collins, M.P., (1986), *The Modified Compression-Field Theory of Reinforced Concrete Elements Subjected to Shear*, ACI Structural Journal, March-April 1986, pp. 219-231.

Zahn, F.A. Park, R. and Priestley, M.J.N., (1990), *Flexural Strength and Ductility of Circular Hollow Reinforced Concrete Columns without Confinement on Inside Face*, ACI Structural Journal, Vol. 87, No.2 March-April 1990, pp.156-166.

References - Section 2

Allahabadi, R. and Powell, G.H., (1988), *DRAIN-2DX User's Guide*, Report No. UCB/EERC-88-06, University of California, Berkeley, 1988.

Ang, B.G., Priestley, M.J.N. and Paulay, T., (1989), *Seismic Shear Strength of Circular Reinforced Concrete Columns*, ACI Structural Journal, Jan-Feb 1989, pp. 45-59.

Bannantine, J.A.; Comer, J.J. and Handrock, J.L., (1990), *Fundamentals of Metal Fatigue Analysis*, Prentice-Hall, New Jersey, 1990, 273 pp.

Bouc, R., (1967), *Forced Vibration of Mechanical System with Hysteresis*, Proceedings of 4th Conference on Nonlinear Oscillation, Prague, 1967.

Bouc, R., (1971), *Modele Mathematique D'Hysteresis*, ACUSTICA, Vol. 24, No. 1, 1971, pp. 16-25.

Clough, R.W., (1966), *Effect of Stiffness Degradation on Earthquake Ductility Requirements*, Report No. 66-16, Structural Engineering Laboratory, Berkeley, University of California, October 1966.

Glinka, G. and Kam, J.C.P., (1987), *Rainflow Counting Algorithm for Very Long Stress Histories*, International Journal of Fatigue, Vol. 9, October 1987, pp. 223-228.

Hong, N., (1991), *A Modified Rainflow Counting Method*, International Journal of Fatigue, Vol. 13, Nov. 1991, pp. 465-469.

Iwan, W.D. and Gates, N.C., (1979), *Estimating Earthquake Response of Simple Hysteretic Structures*, Journal of the Engineering Mechanics Division, Vol. 105, No. EM3, June-1979, pp. 391-405.

Kunnath, S.K., Reinhorn, A.M. and Lobo, R.F., (1992), *IDARC 3.0: A Program for the Inelastic Damage Analysis of Reinforced Concrete Structures*, Technical Report NCEER-92-0022, State University of New York at Buffalo.

Mander, J.B., Priestley, M.J.N. and Park, R., (1984), *Seismic Design of Bridge Piers*, Department of Civil Engineering, University of Canterbury, Report 84-2, Feb-84, 483 pp.

Mander J.B., (1991), *Damage Assessment of Existing Bridges in Low to Medium Seismic Risk Zones*, Proceedings of the 7th U.S.-Japan Bridge Engineering Workshop, May 8 and 9, 1991, Public Works Research Institute, Tsukube, Japan.

Matsuishi, M. and Endo, T. (1968), *Fatigue of Metals Subjected to Varying Stress*, Paper presented to japan Society of Mechanical Engineers, Jukvoka, Japan, 1968.

Park, Y.J., Reinhorn, A.M. and Kunnath, S.K., (1987), *IDARC: Inelastic Damage Analysis of Reinforced Concrete Frame - Shear-Wall Structures*, National Center for Earthquake Engineering Research, State University of New York at Buffalo, Technical Report NCEER-87-0008, July 1987.

Ramberg W. and Osgood, W. R., (1943), *Description of Stress-Strain Curves by Three Parameters*, Technical Note 902, National Advisory Committee for Aeronautics, July 1943.

Rychlik, I., (1987), *A New Definition of the Rainflow Cycle Counting Method,* International Journal of Fatigue, Vol. 9, April 1987, pp. 119-121.

Saiidi, M., (1982), *Hysteresis Models for Reinforced Concrete*, Journal of the Structural Division, ASCE, Vol. 108, No. ST5, May 1982, pp. 1077-1087.

Takeda, T., Sozen, M.A. and Nielsen, N.N., (1970), *Reinforced Concrete Response to Simulated Earthquakes*, Journal of the Structural Division, Vol. 96, No. ST12, Dec. 1970, pp. 2557-2573.

Wen, Y.K., (1975), *Approximate Method for Nonlinear Random Vibration*, Journal of Engineering Mechanics Division, ASCE, Vol. 101, EM4, 1975.

Wen, Y.K., (1976), *Method for Random Vibration of Hysteretic Systems,* Journal of the Engineering Mechanics Division, ASCE, Vol. 102, No.EM2, Apr. 1976, pp. 249-263.

Xiulin, Z. and Baotong, L. (1987), *On a Fatigue Formula Under Stress Cycling,* International Journal of Fatigue, Vol. 9, July 1987, pp. 169-174.

References - Section 3

Aycardi, L.E., Mander, J.B. and Reinhorn, A.M., (1992), *Seismic Resistance of Reinforced Concrete Frame Structures Designed Only for Gravity Loads: Part II - Experimental Performance of Subassemblages*, National Center for Earthquake Engineering Research, State University of New York at Buffalo, Dec-1992.

Aycardi, L.E., (1991), *The Experimental Behavior of Gravity Load Designed Reinforced Concrete Subassemblages Under Reversal Cyclic Lateral Load,* M.S. Thesis, Department of Civil Engineering, SUNY at Buffalo, 1991.

Clough, R.W. and Penzien, J., (1993), *Dynamics of Structures*, Second Edition, McGraw-Hill, 1993, 738 pp.

Mander, J.B., Priestley, M.J.N. and Park, R., (1984), *Seismic Design of Bridge Piers*, Department of Civil Engineering, University of Canterbury, Report 84-2, Feb-84, 483 pp.

Mander, J.B., Waheed, S.M., Chaudary, M.T.A. and Chen, S.S., (1993), *Seismic Performance of Shear-Critical Reinforced Concrete Bridge Piers*, April 1993, Technical Report NCEER-93-0010.

Otani, S. and Sozen, M.A., (1974), *Simulated Earthquake Tests of R/C Frames*, Journal of the Structural Division, Vol. 100, No. ST3, May 1982, pp. 687-701.

Park, Y.J., Reinhorn, A.M. and Kunnath, S.K., (1987), *IDARC: Inelastic Damage Analysis of Reinforced Concrete Frame - Shear-Wall Structures*, National Center for Earthquake Engineering Research, State University of New York at Buffalo, Technical Report NCEER-87-0008, July 1987.

Press, W.H., Flannery, B.P., Teukolsky, S.A. and Vetterling, W.T., (1989), *Numerical Recipes: The Art of Scientific Computing (FORTRAN Version)*, Cambrdige University Press, Cambridge, 1989, 702 pp.

Saiidi, M., (1982), *Hysteresis Models for Reinforced Concrete*, Journal of the Structural Division, Vol. 108, No. ST5, May 1982, pp. 1077-1087.

Takeda, T., Sozen, M.A. and Nielsen, N.N., (1970), *Reinforced Concrete Response to Simulated Earthquakes*, Journal of the Structural Division, Vol. 96, No. ST12, Dec. 1970, pp. 2557-2573.

Wen, Y.K., (1975), *Approximate Method for Nonlinear Random Vibration*, Journal of Engineering Mechanics Division, ASCE, Vol. 101, EM4, 1975.

Wen, Y.K., (1976), *Method for Random Vibration of Hysteretic Systems*, Journal of the Engineering Mechanics Division, ASCE, Vol. 102, No.EM2, Apr. 1976, pp. 249-263.

References - Section 4

____ ATC 6-2 (1983), *Seismic Retrofitting Guidelines for Highway Bridges*, Applied Technology Council, 220 pp.

Allahabadi, R. and Powell, G.H., (1988), *DRAIN-2DX User's Guide*, Report No. UCB/EERC-88-06, University of California, Berkeley, 1988.

Chen, C.C. and Robinson, A.R., (1993), *Improved Time-History Analysis for Structural Dynamics. I: Treatment of Rapid Variation or Excitation and Material Nonlinearity*, Journal of Engineering Mechanics, Vol. 119, No. 12, Dec.1993, pp. 2496-2513.

Clough, R.W. and Penzien, J., (1993), *Dynamics of Structures*, Second Edition, McGraw-Hill, 1993, 738 pp.

Craig, R.R. Jr., (1981), *Structural Dynamics "An Introduction to Computational Methods"*, John Wiley and Sons, New York, 1981.

Fertis, D.G. and Lee, C.T., (1992), *Inelastic Response of Variable Stiffness Members Under Cyclic Loading*, Journal of Engineering Mechanics, Vol. 118, No. 7 , July 1992, pp. 1406-1422.

Iwan, W.D. and Gates, N.C., (1979), *Estimating Earthquake Response of Simple Hysteretic Structures*, Journal of the Engineering Mechanics Division, Vol. 105, No. EM3, June-1979, pp. 391-405.

Kunnath, S.K., Reinhorn, A.M. and Lobo, R.F., (1992), *IDARC 3.0: A Program for the Inelastic Damage Analysis of Reinforced Concrete Structures*, Technical Report NCEER-92-0022, State University of New York at Buffalo.

Mander, J.B., Waheed, S.M., Chaudary, M.T.A. and Chen, S.S., (1993), *Seismic Performance of Shear-Critical Reinforced Concrete Bridge Piers*, April 1993, Technical Report NCEER-93-0010.

McCabe, S.L. and Hall, W.J., (1989), *Assessment of Seismic Structural Damage*, Journal of Structural Engineering, Vol. 115, No. 9, Sept-1989, pp. 2166-2183.

Miranda, E., (1993), *Evaluation of Seismic Design Criteria for Highway Bridges*, Earthquake Spectra, Vol. 9, No. 2, 1993, pp. 233-250.

Miranda, E., (1993), *Evaluation of Site-Dependent Inelastic Seismic Design Spectra*, Journal of Structural Engineering, Vol. 119, No. 5, May 1993, pp. 1319-1338.

Miranda, E., (1993), *Site-Dependent Strength-Reduction Factors*, Journal of Structural Engineering, Vol. 119, No. 12, Dec. 1993, pp. 3503-3519.

Park, Y.J., Wen, Y.K. and Ang, H-S., (1986), *Random Vibration of Hysteretic Systems Under bi-directional Ground Motions*, Earthquake Engineering and Structural Dynamics, Vol. 14, 1986, pp. 543-557.

Seible, F. and Priestley, M.N.J., (1991), *Performance Assessment of Damaged Bridge Bents after Loma Prieta Earthquake*, Pacific Conference on Earthquake Engineering, Auckland, New Zealand, 1991, Proceeding: Vol. 3, pp. 323-333.

Uang, C. and Bertero, V.V., (1990), *Evaluation of Seismic Energy in Structures*, Journal of Earthquake Engineering and Structural Dynamics, Vol. 19, 1990, pp. 77-90.

References - Section 5

_____AASHTO, (1983), *Guide Specifications for Seismic Design of Highway Bridges*, American Association of State Highway and Transportation Officials, Washington D.C., 106 pp.

_____AASHTO, (1989), *Standard Specifications for Highway Bridges*, American Association of State Highway and Transportation Officials, Washington D.C., 426 pp.

Hidalgo, P.A. and Arias, A. (1990), *New Chilean Code for Earthquake-Resistant Design of Buildings*, Proc. 4th U.S. Nat. Conf. Earthquake Engrg., Palm Springs, California, Vol. 2, pp. 927-936.

Kasalanati, A., (1993), *Variable Amplitude Low Cycle Fatigue Behavior of Reinforcing Steel*, M.S. Thesis, Department of Civil Engineering, SUNY at Buffalo, 1993.

Mander, J.B., Priestley, M.J.N. and Park, R., (1984), *Seismic Design of Bridge Piers*, Department of Civil Engineering, University of Canterbury, Report 84-2, Feb-84, 483 pp.

Mander, J.B., Priestley, M.J.N. and Park, R., (1988a), *Theoretical Stress-Strain Model for Confined Concrete*, Journal of Structural Engineering, Vol. 114, No. 8, Aug-88, pp. 1804-1826.

Mander, J.B., Priestley, M.J.N. and Park, R., (1988b), *Observed Stress-Strain Behavior of Confined Concrete*, Journal of Structural Engineering, Vol. 114, No. 8, Aug-88, pp. 1827-1849.

Mander, J.B., Panthaki, F.D. and Chaudhary, M.T., (1992), *Evaluation of Seismic Vulnerability of Highway Bridges in the Eastern United States*, September 1992, Technical Council on Lifeline Earthquake Engineering, ASCE National Convention in New York, Monograph No. 5, pp. 72-86.

Mander, J.B., Waheed, S.M., Chaudary, M.T.A. and Chen, S.S., (1993), *Seismic Performance of Shear-Critical Reinforced Concrete Bridge Piers*, April 1993, Technical Report NCEER-93-0010.

Miranda, E. and Bertero, V.V. (1994), *Evaluation of Strength Reduction Factors for Earthquake-Resistant Design,* Earthquake Spectra, Vol. 10, No. 2, pp. 357-379.

Panthaki, F.D., (1992), *Low Cycle Fatigue Behavior of High Strength and Ordinary Reinforcing Steels*, MS-Thesis, SUNY at PBuffalo, 1992.

Paulay, T. and Priestley, M.J.N., (1992), *Seismic Design of Reinforced Concrete and Masonry Buildings*, John Wiley and Sons, New York, 1992.

Tso, W.K. and Naumoski, N. (1991), *Period-Dependent Seismic Force Reduction Factors for Short-Period Structures*, Can. J. Civ. Engrg., Vol. 18, pp. 568-574.

References - Section 6

____ ATC 6-2 (1983), *Seismic Retrofitting Guidelines for Highway Bridges*, Applied Technology Council, 220 pp.

Allahabadi, R. and Powell, G.H., (1988), *DRAIN-2DX User's Guide*, Report No. UCB/EERC-88-06, University of California, Berkeley, 1988.

Aycardi, L.E., Mander, J.B. and Reinhorn, A.M., (1992), *Seismic Resistance of Reinforced Concrete Frame Structures Designed Only for Gravity Loads: Part II - Experimental Performance of Subassemblages*, National Center for Earthquake Engineering Research, State University of New York at Buffalo, Dec-1992.

Berrill, J.B., Priestley, M.J.N. and Peek, R., (1981), *Further Comments on Seismic Design Loads for Bridges*, Bulletin of the N.Z. National Society of Earthquake Engineering, Vol. 14, No. 1, March 1981, pp. 3-11.

Collins, P.M. and Mitchell, D., (1991), *Prestressed Concrete Structures*, Prentice Hall, New Jersey, 1991.

Hsu, T.T.C., (1988), *Softened Truss Model Theory for Shear and Torsion*, ACI Structural Journal, Vol. 85, No. 6, Nov-Dec 1988, pp. 624-635.

Hsu, T.T.C., (1993), *Unified Theory of Reinforced Concrete*, CRC Press, Boca Raton, 1993.

Kanaan, A.E. and Powell, G.H., (1973), *DRAIN-2D A General Purpose Computer Program for Dynamic Analysis of Inelastic Plane Structures*, Report No. UCB/EERC/73/06 and 73/22, University of California, Berkeley, 1973.

Mander, J.B., Waheed, S.M., Chaudary, M.T.A. and Chen, S.S., (1993), *Seismic Performance of Shear-Critical Reinforced Concrete Bridge Piers*, April 1993, Technical Report NCEER-93-0010.

Menegotto, M. and Pinto, (1973), P.E., *Method of Analysis for Cyclically Loaded Reinforced Concrete Plane Frames Including Changes in Geometry and Non-elastic Behavior of Elements Under Combined Normal Force and Bending.* IABSE Symposium on the Resistance and Ultimate Deformability of Structures Acted on by Well-Defined Repeated Loads, Lisbon 1973.

Panthaki, F.D., (1991), *Low Cycle Fatigue Behavior of High Strength and Ordinary Reinforcing Steels*, MS-Thesis, SUNY/Buffalo, 1991.

Takeda, T., Sozen, M.A. and Nielsen, N.N., (1970), *Reinforced Concrete Response to Simulated Earthquakes*, Journal of the Structural Division, Vol. 96, No. ST12, Dec. 1970, pp. 2557-2573.

Uang, C. and Bertero, V.V., (1990), *Evaluation of Seismic Energy in Structures*, Journal of Earthquake Engineering and Structural Dynamics, Vol. 19, 1990, pp. 77-90.

Vecchio, F.J. and Collins, M.P., (1986), *The Modified Compression-Field Theory of Reinforced Concrete Elements Subjected to Shear*, ACI Structural Journal, March-April 1986, pp. 219-231.

NATIONAL CENTER FOR EARTHQUAKE ENGINEERING RESEARCH
LIST OF TECHNICAL REPORTS

The National Center for Earthquake Engineering Research (NCEER) publishes technical reports on a variety of subjects related to earthquake engineering written by authors funded through NCEER. These reports are available from both NCEER's Publications Department and the National Technical Information Service (NTIS). Requests for reports should be directed to the Publications Department, National Center for Earthquake Engineering Research, State University of New York at Buffalo, Red Jacket Quadrangle, Buffalo, New York 14261. Reports can also be requested through NTIS, 5285 Port Royal Road, Springfield, Virginia 22161. NTIS accession numbers are shown in parenthesis, if available.

NCEER-87-0001 "First-Year Program in Research, Education and Technology Transfer," 3/5/87, (PB88-134275).

NCEER-87-0002 "Experimental Evaluation of Instantaneous Optimal Algorithms for Structural Control," by R.C. Lin, T.T. Soong and A.M. Reinhorn, 4/20/87, (PB88-134341).

NCEER-87-0003 "Experimentation Using the Earthquake Simulation Facilities at University at Buffalo," by A.M. Reinhorn and R.L. Ketter, to be published.

NCEER-87-0004 "The System Characteristics and Performance of a Shaking Table," by J.S. Hwang, K.C. Chang and G.C. Lee, 6/1/87, (PB88-134259). This report is available only through NTIS (see address given above).

NCEER-87-0005 "A Finite Element Formulation for Nonlinear Viscoplastic Material Using a Q Model," by O. Gyebi and G. Dasgupta, 11/2/87, (PB88-213764).

NCEER-87-0006 "Symbolic Manipulation Program (SMP) - Algebraic Codes for Two and Three Dimensional Finite Element Formulations," by X. Lee and G. Dasgupta, 11/9/87, (PB88-218522).

NCEER-87-0007 "Instantaneous Optimal Control Laws for Tall Buildings Under Seismic Excitations," by J.N. Yang, A. Akbarpour and P. Ghaemmaghami, 6/10/87, (PB88-134333). This report is only available through NTIS (see address given above).

NCEER-87-0008 "IDARC: Inelastic Damage Analysis of Reinforced Concrete Frame - Shear-Wall Structures," by Y.J. Park, A.M. Reinhorn and S.K. Kunnath, 7/20/87, (PB88-134325).

NCEER-87-0009 "Liquefaction Potential for New York State: A Preliminary Report on Sites in Manhattan and Buffalo," by M. Budhu, V. Vijayakumar, R.F. Giese and L. Baumgras, 8/31/87, (PB88-163704). This report is available only through NTIS (see address given above).

NCEER-87-0010 "Vertical and Torsional Vibration of Foundations in Inhomogeneous Media," by A.S. Veletsos and K.W. Dotson, 6/1/87, (PB88-134291).

NCEER-87-0011 "Seismic Probabilistic Risk Assessment and Seismic Margins Studies for Nuclear Power Plants," by Howard H.M. Hwang, 6/15/87, (PB88-134267).

NCEER-87-0012 "Parametric Studies of Frequency Response of Secondary Systems Under Ground-Acceleration Excitations," by Y. Yong and Y.K. Lin, 6/10/87, (PB88-134309).

NCEER-87-0013 "Frequency Response of Secondary Systems Under Seismic Excitation," by J.A. HoLung, J. Cai and Y.K. Lin, 7/31/87, (PB88-134317).

NCEER-87-0014 "Modelling Earthquake Ground Motions in Seismically Active Regions Using Parametric Time Series Methods," by G.W. Ellis and A.S. Cakmak, 8/25/87, (PB88-134283).

NCEER-87-0015 "Detection and Assessment of Seismic Structural Damage," by E. DiPasquale and A.S. Cakmak, 8/25/87, (PB88-163712).

NCEER-87-0016 "Pipeline Experiment at Parkfield, California," by J. Isenberg and E. Richardson, 9/15/87, (PB88-163720). This report is available only through NTIS (see address given above).

NCEER-87-0017 "Digital Simulation of Seismic Ground Motion," by M. Shinozuka, G. Deodatis and T. Harada, 8/31/87, (PB88-155197). This report is available only through NTIS (see address given above).

NCEER-87-0018 "Practical Considerations for Structural Control: System Uncertainty, System Time Delay and Truncation of Small Control Forces," J.N. Yang and A. Akbarpour, 8/10/87, (PB88-163738).

NCEER-87-0019 "Modal Analysis of Nonclassically Damped Structural Systems Using Canonical Transformation," by J.N. Yang, S. Sarkani and F.X. Long, 9/27/87, (PB88-187851).

NCEER-87-0020 "A Nonstationary Solution in Random Vibration Theory," by J.R. Red-Horse and P.D. Spanos, 11/3/87, (PB88-163746).

NCEER-87-0021 "Horizontal Impedances for Radially Inhomogeneous Viscoelastic Soil Layers," by A.S. Veletsos and K.W. Dotson, 10/15/87, (PB88-150859).

NCEER-87-0022 "Seismic Damage Assessment of Reinforced Concrete Members," by Y.S. Chung, C. Meyer and M. Shinozuka, 10/9/87, (PB88-150867). This report is available only through NTIS (see address given above).

NCEER-87-0023 "Active Structural Control in Civil Engineering," by T.T. Soong, 11/11/87, (PB88-187778).

NCEER-87-0024 "Vertical and Torsional Impedances for Radially Inhomogeneous Viscoelastic Soil Layers," by K.W. Dotson and A.S. Veletsos, 12/87, (PB88-187786).

NCEER-87-0025 "Proceedings from the Symposium on Seismic Hazards, Ground Motions, Soil-Liquefaction and Engineering Practice in Eastern North America," October 20-22, 1987, edited by K.H. Jacob, 12/87, (PB88-188115).

NCEER-87-0026 "Report on the Whittier-Narrows, California, Earthquake of October 1, 1987," by J. Pantelic and A. Reinhorn, 11/87, (PB88-187752). This report is available only through NTIS (see address given above).

NCEER-87-0027 "Design of a Modular Program for Transient Nonlinear Analysis of Large 3-D Building Structures," by S. Srivastav and J.F. Abel, 12/30/87, (PB88-187950).

NCEER-87-0028 "Second-Year Program in Research, Education and Technology Transfer," 3/8/88, (PB88-219480).

NCEER-88-0001 "Workshop on Seismic Computer Analysis and Design of Buildings With Interactive Graphics," by W. McGuire, J.F. Abel and C.H. Conley, 1/18/88, (PB88-187760).

NCEER-88-0002 "Optimal Control of Nonlinear Flexible Structures," by J.N. Yang, F.X. Long and D. Wong, 1/22/88, (PB88-213772).

NCEER-88-0003 "Substructuring Techniques in the Time Domain for Primary-Secondary Structural Systems," by G.D. Manolis and G. Juhn, 2/10/88, (PB88-213780).

NCEER-88-0004 "Iterative Seismic Analysis of Primary-Secondary Systems," by A. Singhal, L.D. Lutes and P.D. Spanos, 2/23/88, (PB88-213798).

NCEER-88-0005 "Stochastic Finite Element Expansion for Random Media," by P.D. Spanos and R. Ghanem, 3/14/88, (PB88-213806).

NCEER-88-0006 "Combining Structural Optimization and Structural Control," by F.Y. Cheng and C.P. Pantelides, 1/10/88, (PB88-213814).

NCEER-88-0007 "Seismic Performance Assessment of Code-Designed Structures," by H.H-M. Hwang, J-W. Jaw and H-J. Shau, 3/20/88, (PB88-219423).

NCEER-88-0008 "Reliability Analysis of Code-Designed Structures Under Natural Hazards," by H.H-M. Hwang, H. Ushiba and M. Shinozuka, 2/29/88, (PB88-229471).

NCEER-88-0009 "Seismic Fragility Analysis of Shear Wall Structures," by J-W Jaw and H.H-M. Hwang, 4/30/88, (PB89-102867).

NCEER-88-0010 "Base Isolation of a Multi-Story Building Under a Harmonic Ground Motion - A Comparison of Performances of Various Systems," by F-G Fan, G. Ahmadi and I.G. Tadjbakhsh, 5/18/88, (PB89-122238).

NCEER-88-0011 "Seismic Floor Response Spectra for a Combined System by Green's Functions," by F.M. Lavelle, L.A. Bergman and P.D. Spanos, 5/1/88, (PB89-102875).

NCEER-88-0012 "A New Solution Technique for Randomly Excited Hysteretic Structures," by G.Q. Cai and Y.K. Lin, 5/16/88, (PB89-102883).

NCEER-88-0013 "A Study of Radiation Damping and Soil-Structure Interaction Effects in the Centrifuge," by K. Weissman, supervised by J.H. Prevost, 5/24/88, (PB89-144703).

NCEER-88-0014 "Parameter Identification and Implementation of a Kinematic Plasticity Model for Frictional Soils," by J.H. Prevost and D.V. Griffiths, to be published.

NCEER-88-0015 "Two- and Three- Dimensional Dynamic Finite Element Analyses of the Long Valley Dam," by D.V. Griffiths and J.H. Prevost, 6/17/88, (PB89-144711).

NCEER-88-0016 "Damage Assessment of Reinforced Concrete Structures in Eastern United States," by A.M. Reinhorn, M.J. Seidel, S.K. Kunnath and Y.J. Park, 6/15/88, (PB89-122220).

NCEER-88-0017 "Dynamic Compliance of Vertically Loaded Strip Foundations in Multilayered Viscoelastic Soils," by S. Ahmad and A.S.M. Israil, 6/17/88, (PB89-102891).

NCEER-88-0018 "An Experimental Study of Seismic Structural Response With Added Viscoelastic Dampers," by R.C. Lin, Z. Liang, T.T. Soong and R.H. Zhang, 6/30/88, (PB89-122212). This report is available only through NTIS (see address given above).

NCEER-88-0019 "Experimental Investigation of Primary - Secondary System Interaction," by G.D. Manolis, G. Juhn and A.M. Reinhorn, 5/27/88, (PB89-122204).

NCEER-88-0020 "A Response Spectrum Approach For Analysis of Nonclassically Damped Structures," by J.N. Yang, S. Sarkani and F.X. Long, 4/22/88, (PB89-102909).

NCEER-88-0021 "Seismic Interaction of Structures and Soils: Stochastic Approach," by A.S. Veletsos and A.M. Prasad, 7/21/88, (PB89-122196).

NCEER-88-0022 "Identification of the Serviceability Limit State and Detection of Seismic Structural Damage," by E. DiPasquale and A.S. Cakmak, 6/15/88, (PB89-122188). This report is available only through NTIS (see address given above).

NCEER-88-0023 "Multi-Hazard Risk Analysis: Case of a Simple Offshore Structure," by B.K. Bhartia and E.H. Vanmarcke, 7/21/88, (PB89-145213).

NCEER-88-0024 "Automated Seismic Design of Reinforced Concrete Buildings," by Y.S. Chung, C. Meyer and M. Shinozuka, 7/5/88, (PB89-122170). This report is available only through NTIS (see address given above).

NCEER-88-0025 "Experimental Study of Active Control of MDOF Structures Under Seismic Excitations," by L.L. Chung, R.C. Lin, T.T. Soong and A.M. Reinhorn, 7/10/88, (PB89-122600).

NCEER-88-0026 "Earthquake Simulation Tests of a Low-Rise Metal Structure," by J.S. Hwang, K.C. Chang, G.C. Lee and R.L. Ketter, 8/1/88, (PB89-102917).

NCEER-88-0027 "Systems Study of Urban Response and Reconstruction Due to Catastrophic Earthquakes," by F. Kozin and H.K. Zhou, 9/22/88, (PB90-162348).

NCEER-88-0028 "Seismic Fragility Analysis of Plane Frame Structures," by H.H-M. Hwang and Y.K. Low, 7/31/88, (PB89-131445).

NCEER-88-0029 "Response Analysis of Stochastic Structures," by A. Kardara, C. Bucher and M. Shinozuka, 9/22/88, (PB89-174429).

NCEER-88-0030 "Nonnormal Accelerations Due to Yielding in a Primary Structure," by D.C.K. Chen and L.D. Lutes, 9/19/88, (PB89-131437).

NCEER-88-0031 "Design Approaches for Soil-Structure Interaction," by A.S. Veletsos, A.M. Prasad and Y. Tang, 12/30/88, (PB89-174437). This report is available only through NTIS (see address given above).

NCEER-88-0032 "A Re-evaluation of Design Spectra for Seismic Damage Control," by C.J. Turkstra and A.G. Tallin, 11/7/88, (PB89-145221).

NCEER-88-0033 "The Behavior and Design of Noncontact Lap Splices Subjected to Repeated Inelastic Tensile Loading," by V.E. Sagan, P. Gergely and R.N. White, 12/8/88, (PB89-163737).

NCEER-88-0034 "Seismic Response of Pile Foundations," by S.M. Mamoon, P.K. Banerjee and S. Ahmad, 11/1/88, (PB89-145239).

NCEER-88-0035 "Modeling of R/C Building Structures With Flexible Floor Diaphragms (IDARC2)," by A.M. Reinhorn, S.K. Kunnath and N. Panahshahi, 9/7/88, (PB89-207153).

NCEER-88-0036 "Solution of the Dam-Reservoir Interaction Problem Using a Combination of FEM, BEM with Particular Integrals, Modal Analysis, and Substructuring," by C-S. Tsai, G.C. Lee and R.L. Ketter, 12/31/88, (PB89-207146).

NCEER-88-0037 "Optimal Placement of Actuators for Structural Control," by F.Y. Cheng and C.P. Pantelides, 8/15/88, (PB89-162846).

NCEER-88-0038 "Teflon Bearings in Aseismic Base Isolation: Experimental Studies and Mathematical Modeling," by A. Mokha, M.C. Constantinou and A.M. Reinhorn, 12/5/88, (PB89-218457). This report is available only through NTIS (see address given above).

NCEER-88-0039 "Seismic Behavior of Flat Slab High-Rise Buildings in the New York City Area," by P. Weidlinger and M. Ettouney, 10/15/88, (PB90-145681).

NCEER-88-0040 "Evaluation of the Earthquake Resistance of Existing Buildings in New York City," by P. Weidlinger and M. Ettouney, 10/15/88, to be published.

NCEER-88-0041 "Small-Scale Modeling Techniques for Reinforced Concrete Structures Subjected to Seismic Loads," by W. Kim, A. El-Attar and R.N. White, 11/22/88, (PB89-189625).

NCEER-88-0042 "Modeling Strong Ground Motion from Multiple Event Earthquakes," by G.W. Ellis and A.S. Cakmak, 10/15/88, (PB89-174445).

NCEER-88-0043 "Nonstationary Models of Seismic Ground Acceleration," by M. Grigoriu, S.E. Ruiz and E. Rosenblueth, 7/15/88, (PB89-189617).

NCEER-88-0044 "SARCF User's Guide: Seismic Analysis of Reinforced Concrete Frames," by Y.S. Chung, C. Meyer and M. Shinozuka, 11/9/88, (PB89-174452).

NCEER-88-0045 "First Expert Panel Meeting on Disaster Research and Planning," edited by J. Pantelic and J. Stoyle, 9/15/88, (PB89-174460).

NCEER-88-0046 "Preliminary Studies of the Effect of Degrading Infill Walls on the Nonlinear Seismic Response of Steel Frames," by C.Z. Chrysostomou, P. Gergely and J.F. Abel, 12/19/88, (PB89-208383).

NCEER-88-0047 "Reinforced Concrete Frame Component Testing Facility - Design, Construction, Instrumentation and Operation," by S.P. Pessiki, C. Conley, T. Bond, P. Gergely and R.N. White, 12/16/88, (PB89-174478).

NCEER-89-0001 "Effects of Protective Cushion and Soil Compliancy on the Response of Equipment Within a Seismically Excited Building," by J.A. HoLung, 2/16/89, (PB89-207179).

NCEER-89-0002 "Statistical Evaluation of Response Modification Factors for Reinforced Concrete Structures," by H.H-M. Hwang and J-W. Jaw, 2/17/89, (PB89-207187).

NCEER-89-0003 "Hysteretic Columns Under Random Excitation," by G-Q. Cai and Y.K. Lin, 1/9/89, (PB89-196513).

NCEER-89-0004 "Experimental Study of 'Elephant Foot Bulge' Instability of Thin-Walled Metal Tanks," by Z-H. Jia and R.L. Ketter, 2/22/89, (PB89-207195).

NCEER-89-0005 "Experiment on Performance of Buried Pipelines Across San Andreas Fault," by J. Isenberg, E. Richardson and T.D. O'Rourke, 3/10/89, (PB89-218440). This report is available only through NTIS (see address given above).

NCEER-89-0006 "A Knowledge-Based Approach to Structural Design of Earthquake-Resistant Buildings," by M. Subramani, P. Gergely, C.H. Conley, J.F. Abel and A.H. Zaghw, 1/15/89, (PB89-218465).

NCEER-89-0007 "Liquefaction Hazards and Their Effects on Buried Pipelines," by T.D. O'Rourke and P.A. Lane, 2/1/89, (PB89-218481).

NCEER-89-0008 "Fundamentals of System Identification in Structural Dynamics," by H. Imai, C-B. Yun, O. Maruyama and M. Shinozuka, 1/26/89, (PB89-207211).

NCEER-89-0009 "Effects of the 1985 Michoacan Earthquake on Water Systems and Other Buried Lifelines in Mexico," by A.G. Ayala and M.J. O'Rourke, 3/8/89, (PB89-207229).

NCEER-89-R010 "NCEER Bibliography of Earthquake Education Materials," by K.E.K. Ross, Second Revision, 9/1/89, (PB90-125352).

NCEER-89-0011 "Inelastic Three-Dimensional Response Analysis of Reinforced Concrete Building Structures (IDARC-3D), Part I - Modeling," by S.K. Kunnath and A.M. Reinhorn, 4/17/89, (PB90-114612).

NCEER-89-0012 "Recommended Modifications to ATC-14," by C.D. Poland and J.O. Malley, 4/12/89, (PB90-108648).

NCEER-89-0013 "Repair and Strengthening of Beam-to-Column Connections Subjected to Earthquake Loading," by M. Corazao and A.J. Durrani, 2/28/89, (PB90-109885).

NCEER-89-0014 "Program EXKAL2 for Identification of Structural Dynamic Systems," by O. Maruyama, C-B. Yun, M. Hoshiya and M. Shinozuka, 5/19/89, (PB90-109877).

NCEER-89-0015 "Response of Frames With Bolted Semi-Rigid Connections, Part I - Experimental Study and Analytical Predictions," by P.J. DiCorso, A.M. Reinhorn, J.R. Dickerson, J.B. Radziminski and W.L. Harper, 6/1/89, to be published.

NCEER-89-0016 "ARMA Monte Carlo Simulation in Probabilistic Structural Analysis," by P.D. Spanos and M.P. Mignolet, 7/10/89, (PB90-109893).

NCEER-89-P017 "Preliminary Proceedings from the Conference on Disaster Preparedness - The Place of Earthquake Education in Our Schools," Edited by K.E.K. Ross, 6/23/89, (PB90-108606).

NCEER-89-0017 "Proceedings from the Conference on Disaster Preparedness - The Place of Earthquake Education in Our Schools," Edited by K.E.K. Ross, 12/31/89, (PB90-207895). This report is available only through NTIS (see address given above).

NCEER-89-0018 "Multidimensional Models of Hysteretic Material Behavior for Vibration Analysis of Shape Memory Energy Absorbing Devices, by E.J. Graesser and F.A. Cozzarelli, 6/7/89, (PB90-164146).

NCEER-89-0019 "Nonlinear Dynamic Analysis of Three-Dimensional Base Isolated Structures (3D-BASIS)," by S. Nagarajaiah, A.M. Reinhorn and M.C. Constantinou, 8/3/89, (PB90-161936). This report is available cnly through NTIS (see address given above).

NCEER-89-0020 "Structural Control Considering Time-Rate of Control Forces and Control Rate Constraints," by F.Y. Cheng and C.P. Pantelides, 8/3/89, (PB90-120445).

NCEER-89-0021 "Subsurface Conditions of Memphis and Shelby County," by K.W. Ng, T-S. Chang and H-H.M. Hwang, 7/26/89, (PB90-120437).

NCEER-89-0022 "Seismic Wave Propagation Effects on Straight Jointed Buried Pipelines," by K. Elhmadi and M.J. O'Rourke, 8/24/89, (PB90-162322).

NCEER-89-0023 "Workshop on Serviceability Analysis of Water Delivery Systems," edited by M. Grigoriu, 3/6/89, (PB90-127424).

NCEER-89-0024 "Shaking Table Study of a 1/5 Scale Steel Frame Composed of Tapered Members," by K.C. Chang, J.S. Hwang and G.C. Lee, 9/18/89, (PB90-160169).

NCEER-89-0025 "DYNA1D: A Computer Program for Nonlinear Seismic Site Response Analysis - Technical Documentation," by Jean H. Prevost, 9/14/89, (PB90-161944). This report is available only through NTIS (see address given above).

NCEER-89-0026 "1:4 Scale Model Studies of Active Tendon Systems and Active Mass Dampers for Aseismic Protection," by A.M. Reinhorn, T.T. Soong, R.C. Lin, Y.P. Yang, Y. Fukao, H. Abe and M. Nakai, 9/15/89, (PB90-173246).

NCEER-89-0027 "Scattering of Waves by Inclusions in a Nonhomogeneous Elastic Half Space Solved by Boundary Element Methods," by P.K. Hadley, A. Askar and A.S. Cakmak, 6/15/89, (PB90-145699).

NCEER-89-0028 "Statistical Evaluation of Deflection Amplification Factors for Reinforced Concrete Structures," by H.H.M. Hwang, J-W. Jaw and A.L. Ch'ng, 8/31/89, (PB90-164633).

NCEER-89-0029 "Bedrock Accelerations in Memphis Area Due to Large New Madrid Earthquakes," by H.H.M. Hwang, C.H.S. Chen and G. Yu, 11/7/89, (PB90-162330).

NCEER-89-0030 "Seismic Behavior and Response Sensitivity of Secondary Structural Systems," by Y.Q. Chen and T.T. Soong, 10/23/89, (PB90-164658).

NCEER-89-0031 "Random Vibration and Reliability Analysis of Primary-Secondary Structural Systems," by Y. Ibrahim, M. Grigoriu and T.T. Soong, 11/10/89, (PB90-161951).

NCEER-89-0032 "Proceedings from the Second U.S. - Japan Workshop on Liquefaction, Large Ground Deformation and Their Effects on Lifelines, September 26-29, 1989," Edited by T.D. O'Rourke and M. Hamada, 12/1/89, (PB90-209388).

NCEER-89-0033 "Deterministic Model for Seismic Damage Evaluation of Reinforced Concrete Structures," by J.M. Bracci, A.M. Reinhorn, J.B. Mander and S.K. Kunnath, 9/27/89.

NCEER-89-0034 "On the Relation Between Local and Global Damage Indices," by E. DiPasquale and A.S. Cakmak, 8/15/89, (PB90-173865).

NCEER-89-0035 "Cyclic Undrained Behavior of Nonplastic and Low Plasticity Silts," by A.J. Walker and H.E. Stewart, 7/26/89, (PB90-183518).

NCEER-89-0036 "Liquefaction Potential of Surficial Deposits in the City of Buffalo, New York," by M. Budhu, R. Giese and L. Baumgrass, 1/17/89, (PB90-208455).

NCEER-89-0037 "A Deterministic Assessment of Effects of Ground Motion Incoherence," by A.S. Veletsos and Y. Tang, 7/15/89, (PB90-164294).

NCEER-89-0038 "Workshop on Ground Motion Parameters for Seismic Hazard Mapping," July 17-18, 1989, edited by R.V. Whitman, 12/1/89, (PB90-173923).

NCEER-89-0039 "Seismic Effects on Elevated Transit Lines of the New York City Transit Authority," by C.J. Costantino, C.A. Miller and E. Heymsfield, 12/26/89, (PB90-207887).

NCEER-89-0040 "Centrifugal Modeling of Dynamic Soil-Structure Interaction," by K. Weissman, Supervised by J.H. Prevost, 5/10/89, (PB90-207879).

NCEER-89-0041 "Linearized Identification of Buildings With Cores for Seismic Vulnerability Assessment," by I-K. Ho and A.E. Aktan, 11/1/89, (PB90-251943).

NCEER-90-0001 "Geotechnical and Lifeline Aspects of the October 17, 1989 Loma Prieta Earthquake in San Francisco," by T.D. O'Rourke, H.E. Stewart, F.T. Blackburn and T.S. Dickerman, 1/90, (PB90-208596).

NCEER-90-0002 "Nonnormal Secondary Response Due to Yielding in a Primary Structure," by D.C.K. Chen and L.D. Lutes, 2/28/90, (PB90-251976).

NCEER-90-0003 "Earthquake Education Materials for Grades K-12," by K.E.K. Ross, 4/16/90, (PB91-251984).

NCEER-90-0004 "Catalog of Strong Motion Stations in Eastern North America," by R.W. Busby, 4/3/90, (PB90-251984).

NCEER-90-0005 "NCEER Strong-Motion Data Base: A User Manual for the GeoBase Release (Version 1.0 for the Sun3)," by P. Friberg and K. Jacob, 3/31/90 (PB90-258062).

NCEER-90-0006 "Seismic Hazard Along a Crude Oil Pipeline in the Event of an 1811-1812 Type New Madrid Earthquake," by H.H.M. Hwang and C-H.S. Chen, 4/16/90(PB90-258054).

NCEER-90-0007 "Site-Specific Response Spectra for Memphis Sheahan Pumping Station," by H.H.M. Hwang and C.S. Lee, 5/15/90, (PB91-108811).

NCEER-90-0008 "Pilot Study on Seismic Vulnerability of Crude Oil Transmission Systems," by T. Ariman, R. Dobry, M. Grigoriu, F. Kozin, M. O'Rourke, T. O'Rourke and M. Shinozuka, 5/25/90, (PB91-108837).

NCEER-90-0009 "A Program to Generate Site Dependent Time Histories: EQGEN," by G.W. Ellis, M. Srinivasan and A.S. Cakmak, 1/30/90, (PB91-108829).

NCEER-90-0010 "Active Isolation for Seismic Protection of Operating Rooms," by M.E. Talbott, Supervised by M. Shinozuka, 6/8/9, (PB91-110205).

NCEER-90-0011 "Program LINEARID for Identification of Linear Structural Dynamic Systems," by C-B. Yun and M. Shinozuka, 6/25/90, (PB91-110312).

NCEER-90-0012 "Two-Dimensional Two-Phase Elasto-Plastic Seismic Response of Earth Dams," by A.N. Yiagos, Supervised by J.H. Prevost, 6/20/90, (PB91-110197).

NCEER-90-0013 "Secondary Systems in Base-Isolated Structures: Experimental Investigation, Stochastic Response and Stochastic Sensitivity," by G.D. Manolis, G. Juhn, M.C. Constantinou and A.M. Reinhorn, 7/1/90, (PB91-110320).

NCEER-90-0014 "Seismic Behavior of Lightly-Reinforced Concrete Column and Beam-Column Joint Details," by S.P. Pessiki, C.H. Conley, P. Gergely and R.N. White, 8/22/90, (PB91-108795).

NCEER-90-0015 "Two Hybrid Control Systems for Building Structures Under Strong Earthquakes," by J.N. Yang and A. Danielians, 6/29/90, (PB91-125393).

NCEER-90-0016 "Instantaneous Optimal Control with Acceleration and Velocity Feedback," by J.N. Yang and Z. Li, 6/29/90, (PB91-125401).

NCEER-90-0017 "Reconnaissance Report on the Northern Iran Earthquake of June 21, 1990," by M. Mehrain, 10/4/90, (PB91-125377).

NCEER-90-0018 "Evaluation of Liquefaction Potential in Memphis and Shelby County," by T.S. Chang, P.S. Tang, C.S. Lee and H. Hwang, 8/10/90, (PB91-125427).

NCEER-90-0019 "Experimental and Analytical Study of a Combined Sliding Disc Bearing and Helical Steel Spring Isolation System," by M.C. Constantinou, A.S. Mokha and A.M. Reinhorn, 10/4/90, (PB91-125385).

NCEER-90-0020 "Experimental Study and Analytical Prediction of Earthquake Response of a Sliding Isolation System with a Spherical Surface," by A.S. Mokha, M.C. Constantinou and A.M. Reinhorn, 10/11/90, (PB91-125419).

NCEER-90-0021 "Dynamic Interaction Factors for Floating Pile Groups," by G. Gazetas, K. Fan, A. Kaynia and E. Kausel, 9/10/90, (PB91-170381).

NCEER-90-0022 "Evaluation of Seismic Damage Indices for Reinforced Concrete Structures," by S. Rodriguez-Gomez and A.S. Cakmak, 9/30/90, PB91-171322).

NCEER-90-0023 "Study of Site Response at a Selected Memphis Site," by H. Desai, S. Ahmad, E.S. Gazetas and M.R. Oh, 10/11/90, (PB91-196857).

NCEER-90-0024 "A User's Guide to Strongmo: Version 1.0 of NCEER's Strong-Motion Data Access Tool for PCs and Terminals," by P.A. Friberg and C.A.T. Susch, 11/15/90, (PB91-171272).

NCEER-90-0025 "A Three-Dimensional Analytical Study of Spatial Variability of Seismic Ground Motions," by L.-L. Hong and A.H.-S. Ang, 10/30/90, (PB91-170399).

NCEER-90-0026 "MUMOID User's Guide - A Program for the Identification of Modal Parameters," by S. Rodriguez-Gomez and E. DiPasquale, 9/30/90, (PB91-171298).

NCEER-90-0027 "SARCF-II User's Guide - Seismic Analysis of Reinforced Concrete Frames," by S. Rodriguez-Gomez, Y.S. Chung and C. Meyer, 9/30/90, (PB91-171280).

NCEER-90-0028 "Viscous Dampers: Testing, Modeling and Application in Vibration and Seismic Isolation," by N. Makris and M.C. Constantinou, 12/20/90 (PB91-190561).

NCEER-90-0029 "Soil Effects on Earthquake Ground Motions in the Memphis Area," by H. Hwang, C.S. Lee, K.W. Ng and T.S. Chang, 8/2/90, (PB91-190751).

NCEER-91-0001 "Proceedings from the Third Japan-U.S. Workshop on Earthquake Resistant Design of Lifeline Facilities and Countermeasures for Soil Liquefaction, December 17-19, 1990," edited by T.D. O'Rourke and M. Hamada, 2/1/91, (PB91-179259).

NCEER-91-0002 "Physical Space Solutions of Non-Proportionally Damped Systems," by M. Tong, Z. Liang and G.C. Lee, 1/15/91, (PB91-179242).

NCEER-91-0003 "Seismic Response of Single Piles and Pile Groups," by K. Fan and G. Gazetas, 1/10/91, (PB92-174994).

NCEER-91-0004 "Damping of Structures: Part 1 - Theory of Complex Damping," by Z. Liang and G. Lee, 10/10/91, (PB92-197235).

NCEER-91-0005 "3D-BASIS - Nonlinear Dynamic Analysis of Three Dimensional Base Isolated Structures: Part II," by S. Nagarajaiah, A.M. Reinhorn and M.C. Constantinou, 2/28/91, (PB91-190553).

NCEER-91-0006 "A Multidimensional Hysteretic Model for Plasticity Deforming Metals in Energy Absorbing Devices," by E.J. Graesser and F.A. Cozzarelli, 4/9/91, (PB92-108364).

NCEER-91-0007 "A Framework for Customizable Knowledge-Based Expert Systems with an Application to a KBES for Evaluating the Seismic Resistance of Existing Buildings," by E.G. Ibarra-Anaya and S.J. Fenves, 4/9/91, (PB91-210930).

NCEER-91-0008 "Nonlinear Analysis of Steel Frames with Semi-Rigid Connections Using the Capacity Spectrum Method," by G.G. Deierlein, S-H. Hsieh, Y-J. Shen and J.F. Abel, 7/2/91, (PB92-113828).

NCEER-91-0009 "Earthquake Education Materials for Grades K-12," by K.E.K. Ross, 4/30/91, (PB91-212142).

NCEER-91-0010 "Phase Wave Velocities and Displacement Phase Differences in a Harmonically Oscillating Pile," by N. Makris and G. Gazetas, 7/8/91, (PB92-108356).

NCEER-91-0011 "Dynamic Characteristics of a Full-Size Five-Story Steel Structure and a 2/5 Scale Model," by K.C. Chang, G.C. Yao, G.C. Lee, D.S. Hao and Y.C. Yeh," 7/2/91, (PB93-116648).

NCEER-91-0012 "Seismic Response of a 2/5 Scale Steel Structure with Added Viscoelastic Dampers," by K.C. Chang, T.T. Soong, S-T. Oh and M.L. Lai, 5/17/91, (PB92-110816).

NCEER-91-0013 "Earthquake Response of Retaining Walls; Full-Scale Testing and Computational Modeling," by S. Alampalli and A-W.M. Elgamal, 6/20/91, to be published.

NCEER-91-0014 "3D-BASIS-M: Nonlinear Dynamic Analysis of Multiple Building Base Isolated Structures," by P.C. Tsopelas, S. Nagarajaiah, M.C. Constantinou and A.M. Reinhorn, 5/28/91, (PB92-113885).

NCEER-91-0015 "Evaluation of SEAOC Design Requirements for Sliding Isolated Structures," by D. Theodossiou and M.C. Constantinou, 6/10/91, (PB92-114602).

NCEER-91-0016 "Closed-Loop Modal Testing of a 27-Story Reinforced Concrete Flat Plate-Core Building," by H.R. Somaprasad, T. Toksoy, H. Yoshiyuki and A.E. Aktan, 7/15/91, (PB92-129980).

NCEER-91-0017 "Shake Table Test of a 1/6 Scale Two-Story Lightly Reinforced Concrete Building," by A.G. El-Attar, R.N. White and P. Gergely, 2/28/91, (PB92-222447).

NCEER-91-0018 "Shake Table Test of a 1/8 Scale Three-Story Lightly Reinforced Concrete Building," by A.G. El-Attar, R.N. White and P. Gergely, 2/28/91, (PB93-116630).

NCEER-91-0019 "Transfer Functions for Rigid Rectangular Foundations," by A.S. Veletsos, A.M. Prasad and W.H. Wu, 7/31/91.

NCEER-91-0020 "Hybrid Control of Seismic-Excited Nonlinear and Inelastic Structural Systems," by J.N. Yang, Z. Li and A. Danielians, 8/1/91, (PB92-143171).

NCEER-91-0021 "The NCEER-91 Earthquake Catalog: Improved Intensity-Based Magnitudes and Recurrence Relations for U.S. Earthquakes East of New Madrid," by L. Seeber and J.G. Armbruster, 8/28/91, (PB92-176742).

NCEER-91-0022 "Proceedings from the Implementation of Earthquake Planning and Education in Schools: The Need for Change - The Roles of the Changemakers," by K.E.K. Ross and F. Winslow, 7/23/91, (PB92-129998).

NCEER-91-0023 "A Study of Reliability-Based Criteria for Seismic Design of Reinforced Concrete Frame Buildings," by H.H.M. Hwang and H-M. Hsu, 8/10/91, (PB92-140235).

NCEER-91-0024 "Experimental Verification of a Number of Structural System Identification Algorithms," by R.G. Ghanem, H. Gavin and M. Shinozuka, 9/18/91, (PB92-176577).

NCEER-91-0025 "Probabilistic Evaluation of Liquefaction Potential," by H.H.M. Hwang and C.S. Lee," 11/25/91, (PB92-143429).

NCEER-91-0026 "Instantaneous Optimal Control for Linear, Nonlinear and Hysteretic Structures - Stable Controllers," by J.N. Yang and Z. Li, 11/15/91, (PB92-163807).

NCEER-91-0027 "Experimental and Theoretical Study of a Sliding Isolation System for Bridges," by M.C. Constantinou, A. Kartoum, A.M. Reinhorn and P. Bradford, 11/15/91, (PB92-176973).

NCEER-92-0001 "Case Studies of Liquefaction and Lifeline Performance During Past Earthquakes, Volume 1: Japanese Case Studies," Edited by M. Hamada and T. O'Rourke, 2/17/92, (PB92-197243).

NCEER-92-0002 "Case Studies of Liquefaction and Lifeline Performance During Past Earthquakes, Volume 2: United States Case Studies," Edited by T. O'Rourke and M. Hamada, 2/17/92, (PB92-197250).

NCEER-92-0003 "Issues in Earthquake Education," Edited by K. Ross, 2/3/92, (PB92-222389).

NCEER-92-0004 "Proceedings from the First U.S. - Japan Workshop on Earthquake Protective Systems for Bridges," Edited by I.G. Buckle, 2/4/92, (PB94-142239, A99, MF-A06).

NCEER-92-0005 "Seismic Ground Motion from a Haskell-Type Source in a Multiple-Layered Half-Space," A.P. Theoharis, G. Deodatis and M. Shinozuka, 1/2/92, to be published.

NCEER-92-0006 "Proceedings from the Site Effects Workshop," Edited by R. Whitman, 2/29/92, (PB92-197201).

NCEER-92-0007 "Engineering Evaluation of Permanent Ground Deformations Due to Seismically-Induced Liquefaction," by M.H. Baziar, R. Dobry and A-W.M. Elgamal, 3/24/92, (PB92-222421).

NCEER-92-0008 "A Procedure for the Seismic Evaluation of Buildings in the Central and Eastern United States," by C.D. Poland and J.O. Malley, 4/2/92, (PB92-222439).

NCEER-92-0009 "Experimental and Analytical Study of a Hybrid Isolation System Using Friction Controllable Sliding Bearings," by M.Q. Feng, S. Fujii and M. Shinozuka, 5/15/92, (PB93-150282).

NCEER-92-0010 "Seismic Resistance of Slab-Column Connections in Existing Non-Ductile Flat-Plate Buildings," by A.J. Durrani and Y. Du, 5/18/92.

NCEER-92-0011 "The Hysteretic and Dynamic Behavior of Brick Masonry Walls Upgraded by Ferrocement Coatings Under Cyclic Loading and Strong Simulated Ground Motion," by H. Lee and S.P. Prawel, 5/11/92, to be published.

NCEER-92-0012 "Study of Wire Rope Systems for Seismic Protection of Equipment in Buildings," by G.F. Demetriades, M.C. Constantinou and A.M. Reinhorn, 5/20/92.

NCEER-92-0013 "Shape Memory Structural Dampers: Material Properties, Design and Seismic Testing," by P.R. Witting and F.A. Cozzarelli, 5/26/92.

NCEER-92-0014 "Longitudinal Permanent Ground Deformation Effects on Buried Continuous Pipelines," by M.J. O'Rourke, and C. Nordberg, 6/15/92.

NCEER-92-0015 "A Simulation Method for Stationary Gaussian Random Functions Based on the Sampling Theorem," by M. Grigoriu and S. Balopoulou, 6/11/92, (PB93-127496).

NCEER-92-0016 "Gravity-Load-Designed Reinforced Concrete Buildings: Seismic Evaluation of Existing Construction and Detailing Strategies for Improved Seismic Resistance," by G.W. Hoffmann, S.K. Kunnath, A.M. Reinhorn and J.B. Mander, 7/15/92, (PB94-142007, A08, MF-A02).

NCEER-92-0017 "Observations on Water System and Pip line Performance in the Limón Area of Costa Rica Due to the April 22, 1991 Earthquake," by M. O'Rourke and D. Ballantyne, 6/30/92, (PB93-126811).

NCEER-92-0018 "Fourth Edition of Earthquake Education Materials for Grades K-12," Edited by K.E.K. Ross, 8/10/92.

NCEER-92-0019 "Proceedings from the Fourth Japan-U.S. Workshop on Earthquake Resistant Design of Lifeline Facilities and Countermeasures for Soil Liquefaction," Edited by M. Hamada and T.D. O'Rourke, 8/12/92, (PB93-163939).

NCEER-92-0020 "Active Bracing System: A Full Scale Implementation of Active Control," by A.M. Reinhorn, T.T. Soong, R.C. Lin, M.A. Riley, Y.P. Wang, S. Aizawa and M. Higashino, 8/14/92, (PB93-127512).

NCEER-92-0021 "Empirical Analysis of Horizontal Ground Displacement Generated by Liquefaction-Induced Lateral Spreads," by S.F. Bartlett and T.L. Youd, 8/17/92, (PB93-188241).

NCEER-92-0022 "IDARC Version 3.0: Inelastic Damage Analysis of Reinforced Concrete Structures," by S.K. Kunnath, A.M. Reinhorn and R.F. Lobo, 8/31/92, (PB93-227502, A07, MF-A02).

NCEER-92-0023 "A Semi-Empirical Analysis of Strong-Motion Peaks in Terms of Seismic Source, Propagation Path and Local Site Conditions, by M. Kamiyama, M.J. O'Rourke and R. Flores-Berrones, 9/9/92, (PB93-150266).

NCEER-92-0024 "Seismic Behavior of Reinforced Concrete Frame Structures with Nonductile Details, Part I: Summary of Experimental Findings of Full Scale Beam-Column Joint Tests," by A. Beres, R.N. White and P. Gergely, 9/30/92, (PB93-227783, A05, MF-A01).

NCEER-92-0025 "Experimental Results of Repaired and Retrofitted Beam-Column Joint Tests in Lightly Reinforced Concrete Frame Buildings," by A. Beres, S. El-Borgi, R.N. White and P. Gergely, 10/29/92, (PB93-227791, A05, MF-A01).

NCEER-92-0026 "A Generalization of Optimal Control Theory: Linear and Nonlinear Structures," by J.N. Yang, Z. Li and S. Vongchavalitkul, 11/2/92, (PB93-188621).

NCEER-92-0027 "Seismic Resistance of Reinforced Concrete Frame Structures Designed Only for Gravity Loads: Part I - Design and Properties of a One-Third Scale Model Structure," by J.M. Bracci, A.M. Reinhorn and J.B. Mander, 12/1/92, (PB94-104502, A08, MF-A02).

NCEER-92-0028 "Seismic Resistance of Reinforced Concrete Frame Structures Designed Only for Gravity Loads: Part II - Experimental Performance of Subassemblages," by L.E. Aycardi, J.B. Mander and A.M. Reinhorn, 12/1/92, (PB94-104510, A08, MF-A02).

NCEER-92-0029 "Seismic Resistance of Reinforced Concrete Frame Structures Designed Only for Gravity Loads: Part III - Experimental Performance and Analytical Study of a Structural Model," by J.M. Bracci, A.M. Reinhorn and J.B. Mander, 12/1/92, (PB93-227528, A09, MF-A01).

NCEER-92-0030 "Evaluation of Seismic Retrofit of Reinforced Concrete Frame Structures: Part I - Experimental Performance of Retrofitted Subassemblages," by D. Choudhuri, J.B. Mander and A.M. Reinhorn, 12/8/92, (PB93-198307, A07, MF-A02).

NCEER-92-0031 "Evaluation of Seismic Retrofit of Reinforced Concrete Frame Structures: Part II - Experimental Performance and Analytical Study of a Retrofitted Structural Model," by J.M. Bracci, A.M. Reinhorn and J.B. Mander, 12/8/92, (PB93-198315, A09, MF-A03).

NCEER-92-0032 "Experimental and Analytical Investigation of Seismic Response of Structures with Supplemental Fluid Viscous Dampers," by M.C. Constantinou and M.D. Symans, 12/21/92, (PB93-191435).

NCEER-92-0033 "Reconnaissance Report on the Cairo, Egypt Earthquake of October 12, 1992," by M. Khater, 12/23/92, (PB93-188621).

NCEER-92-0034 "Low-Level Dynamic Characteristics of Four Tall Flat-Plate Buildings in New York City," by H. Gavin, S. Yuan, J. Grossman, E. Pekelis and K. Jacob, 12/28/92, (PB93-188217).

NCEER-93-0001 "An Experimental Study on the Seismic Performance of Brick-Infilled Steel Frames With and Without Retrofit," by J.B. Mander, B. Nair, K. Wojtkowski and J. Ma, 1/29/93, (PB93-227510, A07, MF-A02).

NCEER-93-0002 "Social Accounting for Disaster Preparedness and Recovery Planning," by S. Cole, E. Pantoja and V. Razak, 2/22/93, (PB94-142114, A12, MF-A03).

NCEER-93-0003 "Assessment of 1991 NEHRP Provisions for Nonstructural Components and Recommended Revisions," by T.T. Soong, G. Chen, Z. Wu, R-H. Zhang and M. Grigoriu, 3/1/93, (PB93-188639).

NCEER-93-0004 "Evaluation of Static and Response Spectrum Analysis Procedures of SEAOC/UBC for Seismic Isolated Structures," by C.W. Winters and M.C. Constantinou, 3/23/93, (PB93-198299).

NCEER-93-0005 "Earthquakes in the Northeast - Are We Ignoring the Hazard? A Workshop on Earthquake Science and Safety for Educators," edited by K.E.K. Ross, 4/2/93, (PB94-103066, A09, MF-A02).

NCEER-93-0006 "Inelastic Response of Reinforced Concrete Structures with Viscoelastic Braces," by R.F. Lobo, J.M. Bracci, K.L. Shen, A.M. Reinhorn and T.T. Soong, 4/5/93, (PB93-227486, A05, MF-A02).

NCEER-93-0007 "Seismic Testing of Installation Methods for Computers and Data Processing Equipment," by K. Kosar, T.T. Soong, K.L. Shen, J.A. HoLung and Y.K. Lin, 4/12/93, (PB93-198299).

NCEER-93-0008 "Retrofit of Reinforced Concrete Frames Using Added Dampers," by A. Reinhorn, M. Constantinou and C. Li, to be published.

NCEER-93-0009 "Seismic Behavior and Design Guidelines for Steel Frame Structures with Added Viscoelastic Dampers," by K.C. Chang, M.L. Lai, T.T. Soong, D.S. Hao and Y.C. Yeh, 5/1/93, (PB94-141959, A07, MF-A02).

NCEER-93-0010 "Seismic Performance of Shear-Critical Reinforced Concrete Bridge Piers," by J.B. Mander, S.M. Waheed, M.T.A. Chaudhary and S.S. Chen, 5/12/93, (PB93-227494, A08, MF-A02).

NCEER-93-0011 "3D-BASIS-TABS: Computer Program for Nonlinear Dynamic Analysis of Three Dimensional Base Isolated Structures," by S. Nagarajaiah, C. Li, A.M. Reinhorn and M.C. Constantinou, 8/2/93, (PB94-141819, A09, MF-A02).

NCEER-93-0012 "Effects of Hydrocarbon Spills from an Oil Pipeline Break on Ground Water," by O.J. Helweg and H.H.M. Hwang, 8/3/93, (PB94-141942, A06, MF-A02).

NCEER-93-0013 "Simplified Procedures for Seismic Design of Nonstructural Components and Assessment of Current Code Provisions," by M.P. Singh, L.E. Suarez, E.E. Matheu and G.O. Maldonado, 8/4/93, (PB94-141827, A09, MF-A02).

NCEER-93-0014 "An Energy Approach to Seismic Analysis and Design of Secondary Systems," by G. Chen and T.T. Soong, 8/6/93, (PB94-142767, A11, MF-A03).

NCEER-93-0015 "Proceedings from School Sites: Becoming Prepared for Earthquakes - Commemorating the Third Anniversary of the Loma Prieta Earthquake," Edited by F.E. Winslow and K.E.K. Ross, 8/16/93.

NCEER-93-0016 "Reconnaissance Report of Damage to Historic Monuments in Cairo, Egypt Following the October 12, 1992 Dahshur Earthquake," by D. Sykora, D. Look, G. Croci, E. Karaesmen and E. Karaesmen, 8/19/93, (PB94-142221, A08, MF-A02).

NCEER-93-0017 "The Island of Guam Earthquake of August 8, 1993," by S.W. Swan and S.K. Harris, 9/30/93, (PB94-141843, A04, MF-A01).

NCEER-93-0018 "Engineering Aspects of the October 12, 1992 Egyptian Earthquake," by A.W. Elgamal, M. Amer, K. Adalier and A. Abul-Fadl, 10/7/93, (PB94-141983, A05, MF-A01).

NCEER-93-0019 "Development of an Earthquake Motion Simulator and its Application in Dynamic Centrifuge Testing," by I. Krstelj, Supervised by J.H. Prevost, 10/23/93.

NCEER-93-0020 "NCEER-Taisei Corporation Research Program on Sliding Seismic Isolation Systems for Bridges: Experimental and Analytical Study of a Friction Pendulum System (FPS)," by M.C. Constantinou, P. Tsopelas, Y-S. Kim and S. Okamoto, 11/1/93, (PB94-142775, A08, MF-A02).

NCEER-93-0021 "Finite Element Modeling of Elastomeric Seismic Isolation Bearings," by L.J. Billings, Supervised by R. Shepherd, 11/8/93, to be published.

NCEER-93-0022 "Seismic Vulnerability of Equipment in Critical Facilities: Life-Safety and Operational Consequences," by K. Porter, G.S. Johnson, M.M. Zadeh, C. Scawthorn and S. Eder, 11/24/93.

NCEER-93-0023 "Hokkaido Nansei-oki, Japan Earthquake of July 12, 1993, by P.I. Yanev and C.R. Scawthorn, 12/23/93.

NCEER-94-0001 "An Evaluation of Seismic Serviceability of Water Supply Networks with Application to the San Francisco Auxiliary Water Supply System," by I. Markov, Supervised by M. Grigoriu and T. O'Rourke, 1/21/94.

NCEER-94-0002 "NCEER-Taisei Corporation Research Program on Sliding Seismic Isolation Systems for Bridges: Experimental and Analytical Study of Systems Consisting of Sliding Bearings, Rubber Restoring Force Devices and Fluid Dampers," Volumes I and II, by P. Tsopelas, S. Okamoto, M.C. Constantinou, D. Ozaki and S. Fujii, 2/4/94.

NCEER-94-0003 "A Markov Model for Local and Global Damage Indices in Seismic Analysis," by S. Rahman and M. Grigoriu, 2/18/94.

NCEER-94-0004 "Proceedings from the NCEER Workshop on Seismic Response of Masonry Infills," edited by D.P. Abrams, 3/1/94.

NCEER-94-0005 "The Northridge, California Earthquake of January 17, 1994: General Reconnaissance Report," edited by J.D. Goltz, 3/11/94.

NCEER-94-0006 "Seismic Energy Based Fatigue Damage Analysis of Bridge Columns: Part I - Evaluation of Seismic Capacity," by G.A. Chang and J.B. Mander, 3/14/94.

NCEER-94-0007 "Seismic Isolation of Multi-Story Frame Structures Using Spherical Sliding Isolation Systems," by T.M. Al-Hussaini, V.A. Zayas and M.C. Constantinou, 3/17/94.

NCEER-94-0008 "The Northridge, California Earthquake of January 17, 1994: Performance of Highway Bridges," edited by I.G. Buckle, 3/24/94.

NCEER-94-0009 "Proceedings of the Third U.S.-Japan Workshop on Earthquake Protective Systems for Bridges," edited by I.G. Buckle and I. Friedland, 3/31/94.

NCEER-94-0010 "3D-BASIS-ME: Computer Program for Nonlinear Dynamic Analysis of Seismically Isolated Single and Multiple Structures and Liquid Storage Tanks," by P.C. Tsopelas, M.C. Constantinou and A.M. Reinhorn, 4/12/94.

NCEER-94-0011 "The Northridge, California Earthquake of January 17, 1994: Performance of Gas Transmission Pipelines," by T.D. O'Rourke and M.C. Palmer, 5/16/94.

NCEER-94-0012 "Feasibility Study of Replacement Procedures and Earthquake Performance Related to Gas Transmission Pipelines," by T.D. O'Rourke and M.C. Palmer, 5/25/94.

NCEER-94-0013 "Seismic Energy Based Fatigue Damage Analysis of Bridge Columns: Part II - Evaluation of Seismic Demand," by G.A. Chang and J.B. Mander, 6/1/94, to be published.